RECOMMENDATION ITU-R P.372-7

Radio noise*

(Question ITU-R 214/3)

(1951-1953-1956-1959-1963-1974-1978-1982-1986-1990-1994-2001)

The ITU Radiocommunication Assembly,

considering

a) that radio noise sets a limit to the performance of radio systems;

b) that the effective antenna noise figure, or antenna noise temperature, together with the amplitude probability distribution of the received noise envelope, are suitable parameters (almost always necessary, but sometimes not sufficient) for use in system performance determinations and design;

c) that it is generally inappropriate to use receiving systems with noise figures less than those specified by the minimum external noise;

d) that knowledge of radio emission from natural sources is required in

– evaluation of the effects of the atmosphere on radiowaves;

– allocation of frequencies to remote sensing of the Earth's environment,

recommends

that the following information should be used where appropriate in radio system design and analysis:

1 Sources of radio noise

Radio noise external to the radio receiving system derives from the following causes:

– radiation from lightning discharges (atmospheric noise due to lightning);

– unintended radiation from electrical machinery, electrical and electronic equipments, power transmission lines, or from internal combustion engine ignition (man-made noise);

– emissions from atmospheric gases and hydrometeors;

– the ground or other obstructions within the antenna beam;

– radiation from celestial radio sources.

---

* A computer program associated with the characteristics and applications of atmospheric noise due to lightning, of man-made noise and of galactic noise (at frequencies below about 100 MHz), described in this Recommendation, is available from that part of the ITU-R website dealing with Radiocommunication Study Group 3.

Note that noise or signals due to unwanted co-channel transmissions or due to spurious emissions from individual transmitting or receiving systems are not considered in this Recommendation.

2 Terms for the specification of noise intensity and their interrelationship

The noise factor, f, for a receiving system is composed of a number of noise sources at the receiving terminal of the system. Both internal and external noise must be considered. The only appropriate reference point for the overall operating noise factor for a radio receiving system is the input of an equivalent loss-free receiving antenna. (The terminals of this lossless antenna do not exist physically.) For receivers free from spurious responses, the system noise factor is given by:

$$f = f_a + (f_c - 1) + l_c\,(f_t - 1) + l_c\,l_t\,(f_r - 1) \tag{1}$$

where:

f_a: the external noise factor defined as:

$$f_a = \frac{p_n}{k\,t_0\,b} \tag{2}$$

NOTE 1 – F_a is the external noise figure defined as:

$$F_a = 10 \log f_a \qquad \text{dB}$$

p_n: available noise power from an equivalent lossless antenna

k: Boltzmann's constant = 1.38×10^{-23} J/K

t_0: reference temperature (K) taken as 290 K

b: noise power bandwidth of the receiving system (Hz)

l_c: antenna circuit loss (available input power/available output power)

l_t: transmission line loss (available input power/available output power)

f_r: noise factor of the receiver.

NOTE 2 – F_r is the receiver noise figure defined as:

$$F_r = 10 \log f_r \qquad \text{dB}$$

f_c is the noise factor associated with the antenna circuit losses,

$$f_c = 1 + (l_c - 1)\left(\frac{t_c}{t_0}\right) \tag{3}$$

f_t is the noise factor associated with the transmission line losses,

$$f_t = 1 + (l_t - 1)\left(\frac{t_t}{t_0}\right) \tag{4}$$

where:

t_c: actual temperature (K) of the antenna and nearby ground

and

t_t: actual temperature (K) of the transmission line.

If $t_c = t_t = t_0$, equation (1) becomes

$$f = f_a - 1 + f_c f_t f_r \tag{5}$$

Equation (2) can be written:

$$P_n = F_a + B - 204 \qquad \text{dBW} \tag{6}$$

where:

$P_n =$ 10 log p_n: available power (W)

$B =$ 10 log b, and –204 = 10 log $k\, t_0$.

For a short ($h << \lambda$) vertical monopole above a perfect ground plane, the vertical component of the r.m.s. field strength is given by:

$$E_n = F_a + 20 \log f_{\text{MHz}} + B - 95.5 \qquad \text{dB}(\mu\text{V/m}) \tag{7}$$

where:

E_n: field strength in bandwidth b, and

f_{MHz}: centre frequency (MHz).

Similarly for a half-wave dipole in free space:

$$E_n = F_a + 20 \log f_{\text{MHz}} + B - 99.0 \qquad \text{dB}(\mu\text{V/m}) \tag{8}$$

The external noise factor is also commonly expressed as a temperature, t_a, where, by definition of f_a:

$$f_a = \frac{t_a}{t_0} \tag{9}$$

t_a is the effective antenna temperature due to external noise.

From estimates of F_a the corresponding values of E_n may be determined using equations such as (7) and (8) appropriate to the type of antenna employed.

The noise power above, while needed in determining the signal-to-noise ratio, for example, is seldom sufficient to determine system performance (white Gaussian background noise being the only exception). Appropriate probabilistic descriptions of the received random noise waveform are required. Since for the types of noise of concern in this Recommendation, the phase of the received envelope is usually uniformly distributed, the amplitude probability distribution (APD) (exceedance probability) of the received envelope is specified. For impulsive noise processes at the higher frequencies (i.e., > about 1 GHz), F_a values are quite low and only the higher magnitude pulses appear above the receiver's noise threshold. Descriptions here can take the form of peak value for a given time period, exceedance probabilities at these higher levels, pulse count at a specified level, etc.

3 Noise levels as a function of frequency

The following three figures and related discussion specify the expected values of F_a in the frequency range 0.1 Hz to 100 GHz along with other noise levels of interest. The three figures display the relative magnitude of the noise types specified in § 1. Additional details for the various noise types are given in later sections of this Recommendation.

Figure 1 covers the frequency range 0.1 Hz to 10 kHz. The solid curve is the minimum expected hourly median values of F_a based on measurements (taking into account the entire Earth's surface, all seasons and times of day) and the dashed curve gives the maximum expected values. Note that in this frequency range there is very little seasonal, diurnal, or geographic variation. The larger variability in the 100-10 000 Hz range is due to the variability of the Earth-ionosphere wave-guide cutoff.

FIGURE 1

F_a, minimum and maximum, versus frequency (0.1 to 10^4 Hz)

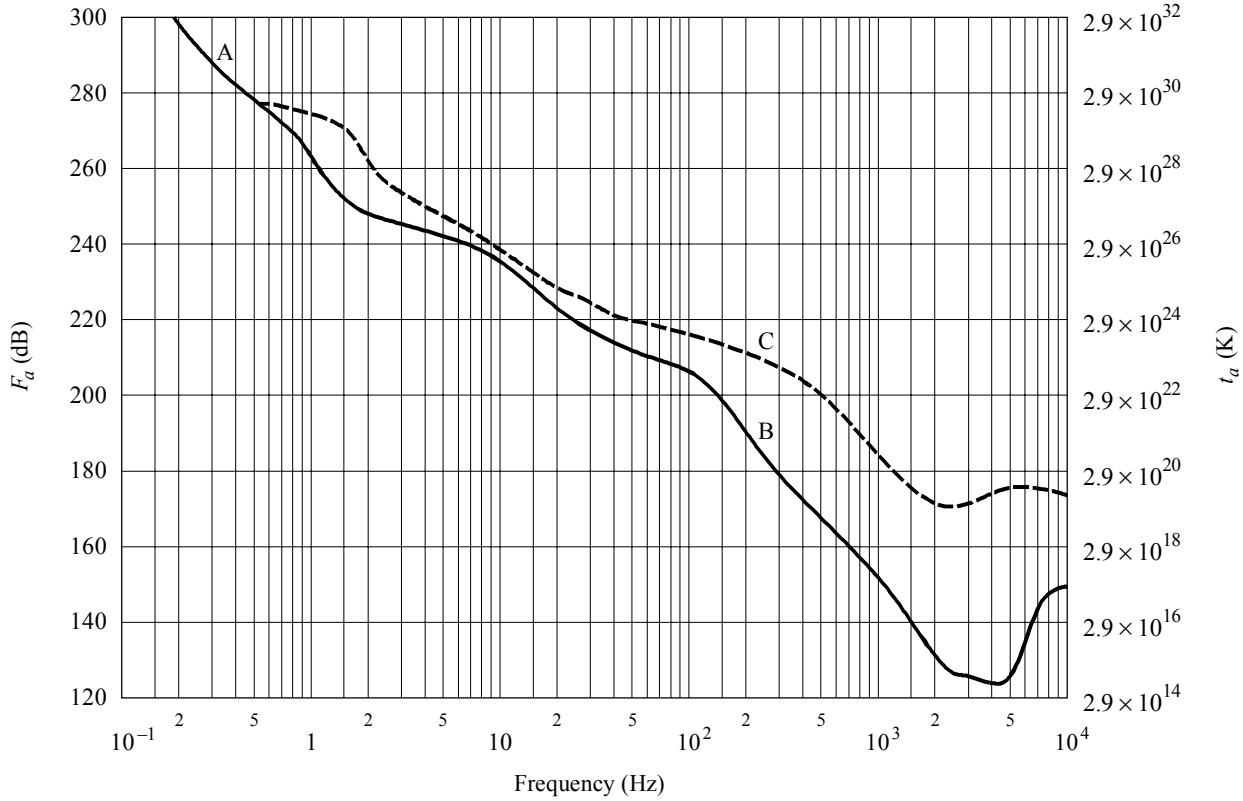

A: micropulsations
B: minimum value expected of atmospheric noise
C: maximum value expected of atmospheric noise

0372-01

Figure 2 covers the frequency range 10^4 to 10^8 Hz, i.e., 10 kHz to 100 MHz for various categories of noise. The minimum expected noise is shown by the solid curves. For atmospheric noise, the minimum values of the hourly medians expected are taken to be those values exceeded 99.5% of the hours and the maximum values are those exceeded 0.5% of the hours. For the atmospheric noise curves, all times of day, seasons, and the entire Earth's surface have been taken into account.

Figure 3 covers the frequency range 10^8 to 10^{11} Hz i.e., 100 MHz to 100 GHz. Again the minimum noise is given by solid curves, while some other noises of interest are given by dashed curves.

FIGURE 2

F_a versus frequency (10^4 to 10^8 Hz)

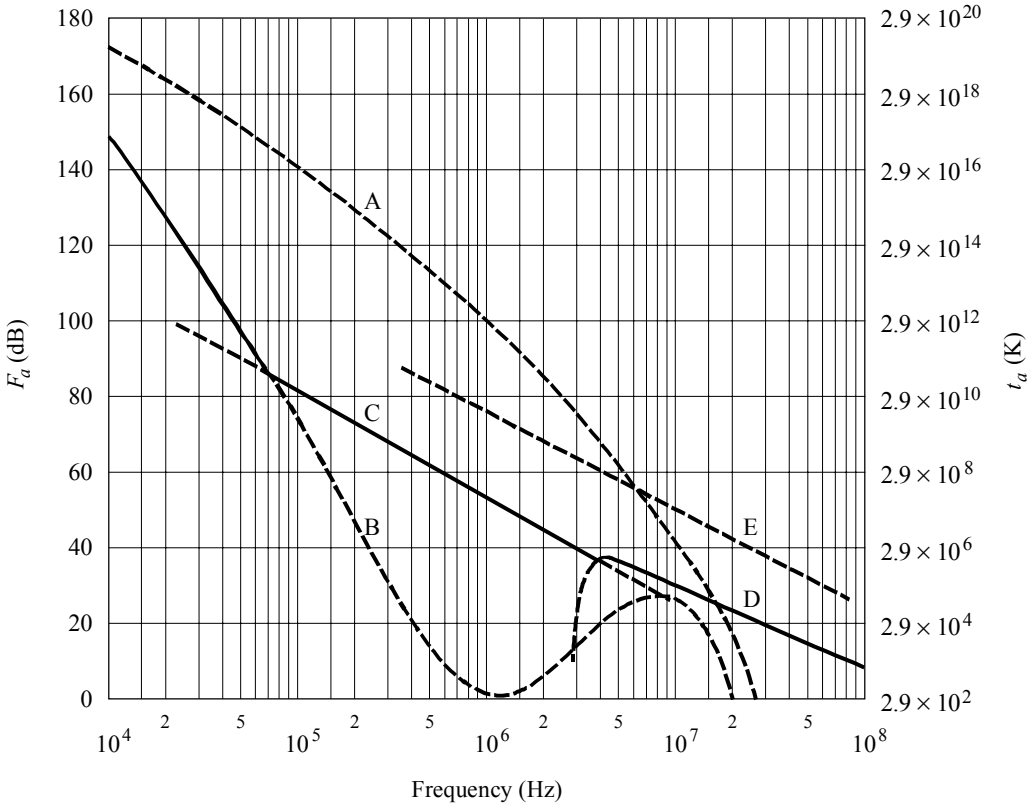

A : atmospheric noise, value exceeded 0.5% of time
B : atmospheric noise, value exceeded 99.5% of time
C : man-made noise, quiet receiving site
D : galactic noise
E : median business area man-made noise
minimum noise level expected

0372-02

The majority of the results shown in the three figures are for omni-directional antennas (except as noted on the figures). For directional antennas, however, studies have indicated that at HF (for example), for atmospheric noise from lightning for very narrow beam antennas, there can be as much as 10 dB variation (5 dB above to 5 dB below the average F_a value shown) depending on antenna pointing direction, frequency and geographical location.

For galactic noise, the average value (over the entire sky) is given by the solid curve labelled galactic noise (Figs. 2 and 3). Measurements indicate a ±2 dB variation about this curve, neglecting ionospheric shielding. The minimum galactic noise (narrow beam antenna towards galactic pole) is 3 dB below the solid galactic noise curve shown on Fig. 3. The maximum galactic noise for narrow beam antennas is shown via a dashed curve in Fig. 3.

4 Noise from atmospheric gases and the Earth's surface

Noise from individual sources such as the Sun, atmospheric gases, the Earth's surface, etc., are usually given in terms of a brightness temperature, t_b. The antenna temperature, t_a, is the convolution of the antenna pattern and the brightness temperature of the sky and ground. For antennas whose patterns encompass a single source, the antenna temperature and brightness temperature are the same (curves C, D and E of Fig. 3, for example).

FIGURE 3

F_a versus frequency (10^8 to 10^{11} Hz)

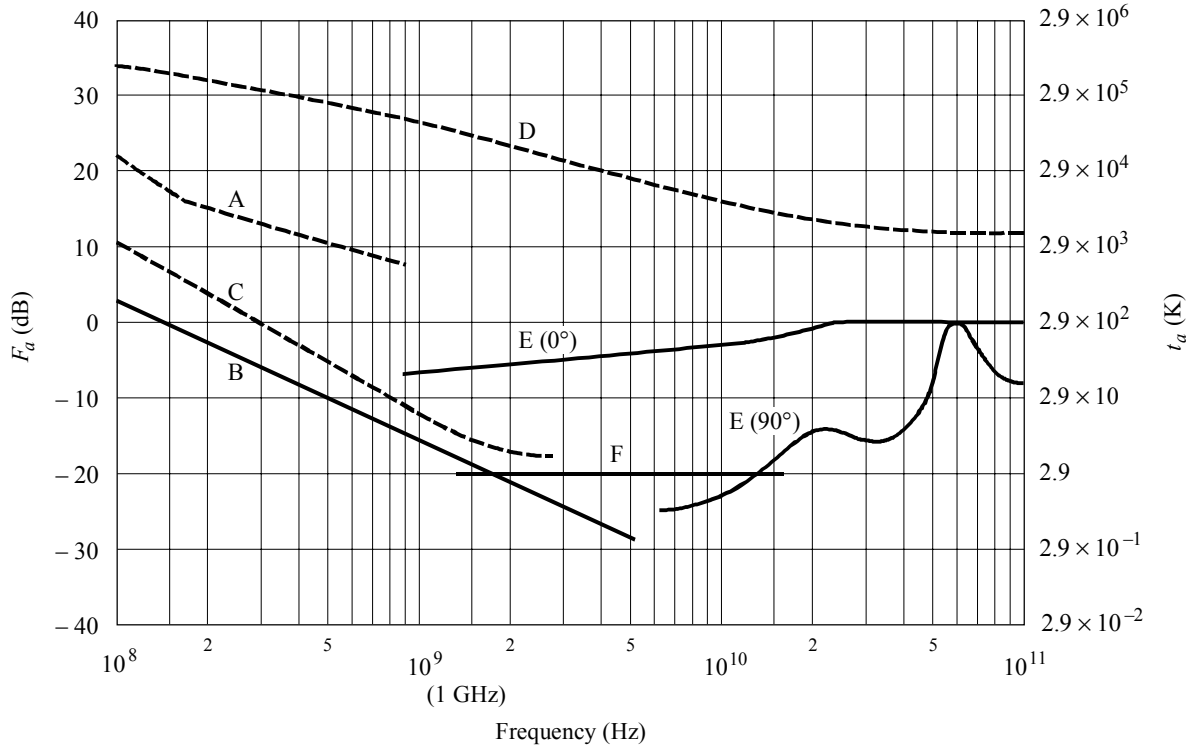

A: estimated median business area man-made noise
B: galactic noise
C: galactic noise (toward galactic centre with infinitely narrow beamwidth)
D: quiet Sun (½° beamwidth directed at Sun)
E: sky noise due to oxygen and water vapour (very narrow beam antenna); upper curve, 0° elevation angle; lower curve, 90° elevation angle
F: black body (cosmic background), 2.7 K
minimum noise level expected

0372-03

Figures 4 and 5 show the brightness temperature of the atmosphere for a ground-based receiver excluding the cosmic noise contribution of 2.7 K or other extra-terrestrial sources for frequencies between 1 and 340 GHz in the first instance and 1 and 60 GHz in the second. The curves are calculated using a radiative transfer program for seven different elevation angles and an average atmosphere (7.5 g surface water vapour density, surface temperature of 288 K, and a scale height of 2 km for water vapour). The 1976 United States Standard Atmosphere is used for the dry atmosphere. A typical water vapour contribution is added above the tropopause.

In Earth-space communication, if the attenuation of the signal from a spacecraft transmitter is known, a good estimate of the brightness temperature for frequencies between 2 and 30 GHz in that direction can be obtained from the following formula:

$$t_b = t_e (1 - e^{-d}) + 2.7 \quad \text{K} \tag{10}$$

where:

d: optical depth = attenuation (dB/4.343)

t_e: effective temperature, usually taken to be around 275 K.

FIGURE 4

Brightness temperature (clear air) for 7.5 g/m³ water vapour concentration (surface temperature and pressure equal to 15° C and 1 023 mb); θ is the elevation angle

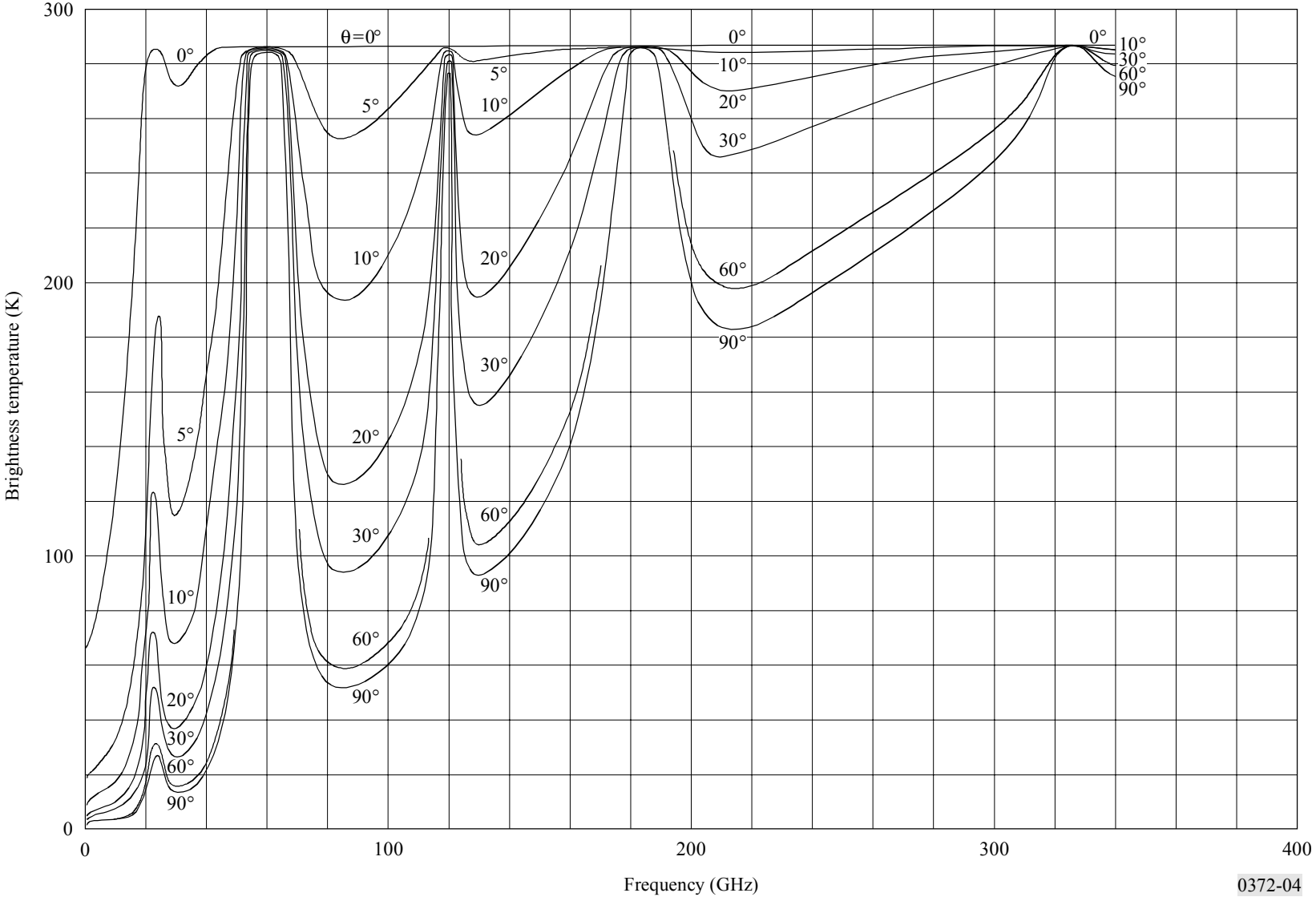

FIGURE 5

Brightness temperature for clear air for 7.5 g/m³ of water vapour concentration (expansion of abscissa scale of Fig. 4); θ is the elevation angle

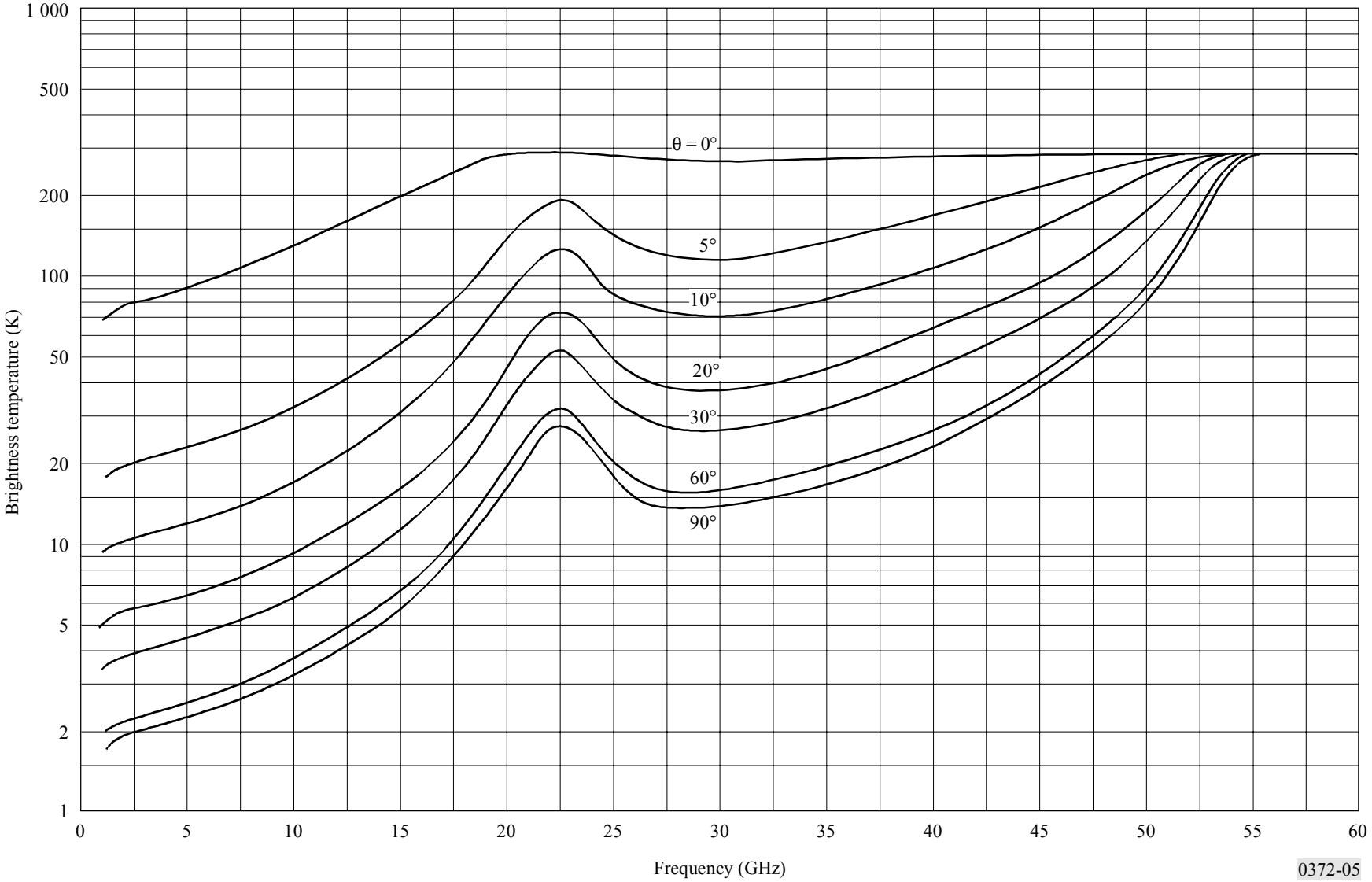

The above relation will give results to an accuracy of about 0.1 dB below 30 GHz. Above that frequency, a scattering component enters into the attenuation and the brightness temperature estimate will be too high. The above relationship can be used to include attenuation by rain.

A radiative transfer study including cloud effects has been carried out in the United States of America. Zenith brightness temperatures have been computed from meteorological data for a typical year selected from a database of 15 years for each of 15 locations. Results from two United States locations, Yuma, Arizona (5.5 cm annual rainfall) and New York City (98.5 cm annual rainfall) are given in Figs. 6a) and 6b) for five different frequencies. It can be seen from the curves that the noise temperature at zenith for 90 GHz may be lower than for 44 GHz. This is the case for very low zenith brightness temperatures, which means that the water vapour content is very low (lower than about 3 g/m^3). From Fig. 4 (7.5 g/m^2 water vapour), however, it can be seen that the brightness temperatures for 90 GHz and 44 GHz are nearly the same.

The brightness temperature of the Earth's surface as seen from a particular nadir angle may be calculated using the radiative transfer equation describing the reflection of downwelling atmospheric radiation and the emission of radiation by the Earth's surface.

This calculation involves integration of downwelling radiation over all angles and includes atmospheric attenuation.

It may be simplified as:

$$T = \in T_{surf} + \rho T_{atm}$$

where:

$\in$: effective emissivity of the surface

ρ: effective reflection coefficient

T_{surf}: physical temperature (K) of the Earth's surface

T_{atm}: weighted average of the sky brightness temperature.

Up to about 100 GHz, but particularly below 10 GHz, the reflection coefficient ρ is generally high and the emissivity $\in$ low.

In Fig. 7a) the emissivity and the brightness temperature of a smooth water surface are given for vertical and horizontal polarizations and for two angles of incidence. It should be noted that fresh and salted water are indistinguishable for frequencies greater than 5 GHz.

Figure 7b) shows the nadir brightness temperature of the sea surface at three frequencies as a function of the sea surface physical temperature, for a salinity of 36 parts per thousand.

The increase in brightness temperature of the sea surface with wind speed is given in Figs. 7c) and 7d), which also provides a useful tool for storm detection.

FIGURE 6

Fraction of the time the zenith sky noise (brightness) temperature is equal to or less than the abscissa value for a typical year

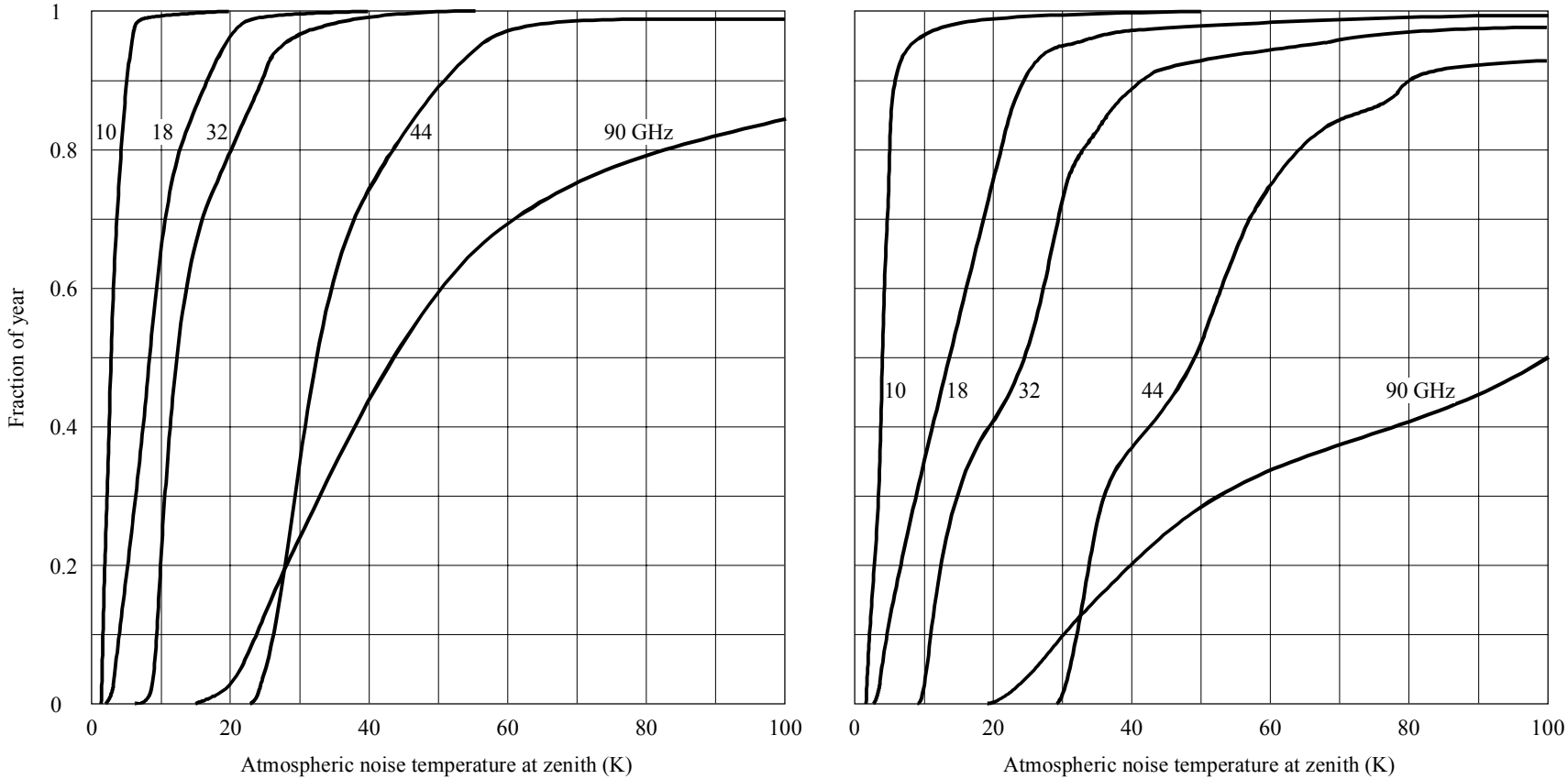

a) Yuma, Arizona, USA (1961; total rainfall: 55 mm)

b) New York, NY, USA (1959; total rainfall: 985 mm)

0372-06

FIGURE 7

Emissivity and brightness temperature variations of the sea surface

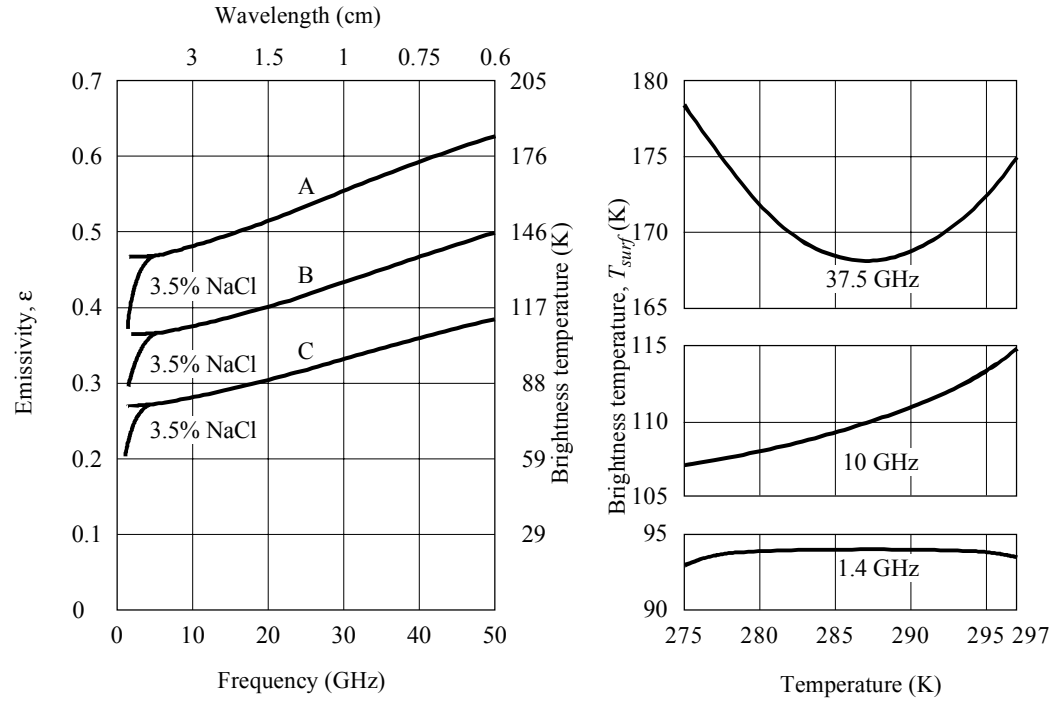

a) Emissivity of a smooth water surface

A: vertical polarization
B: incidence angles of 45° and 0°
C: horizontal polarization

b) Brightness temperature of the sea surface as a function of sea surface temperature (nadir) for a salinity of 36 parts per thousand

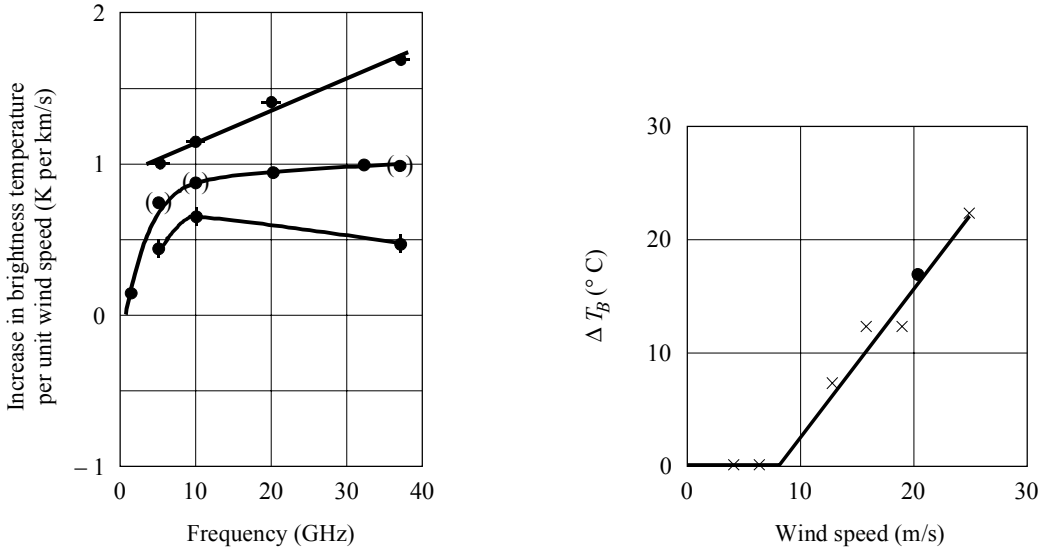

c) Spectrum of increase in brightness temperature caused by wind at the ocean surface

● Nadir
Vertical polarization (38°)
Horizontal polarization (38°)
(●) Inferred

d) Increase in brightness temperature of the ocean surface at 19.35 GHz due to wind speed

× Atlantic, North Sea
● Salton Sea

0372-07

The emissivities (and hence the brightness temperatures) of land surfaces are higher than those of water surfaces due to the lower dielectric constants of land. In Fig. 8a) the brightness temperature of a smooth field for different moisture contents is shown; in Fig. 8b) the brightness temperature for different degrees of roughness is presented. The curves are given for vertical, horizontal and circular polarization. If the moisture content increases, the brightness temperature decreases; if the roughness is higher, the brightness temperature increases.

Figure 9 shows calculations of brightness temperature as seen from geostationary orbit by a satellite using an Earth-coverage beam (Earth fills the main beam between 3 dB points). As the satellite moves around its orbit, one can see the effect of the African land mass (hot) at 30° E longitude and of the Pacific Ocean (cold) at 180° W to 150° W longitude. Brightness temperature increases with increasing frequency, largely due to gaseous absorption. Curves are for US Standard Atmosphere with 2.5 g/m^3 water vapour and 50% cloud cover. The Earth-coverage antenna pattern is given by $G(\varphi) = -3(\varphi/8.715)^2$ dB for $0 \le \varphi \le 8.715$ where φ is the angle off boresight.

5 Man-made noise

Median values of man-made noise power for a number of environments are shown in Fig. 10. The Figure also includes a curve for galactic noise (see § 6).

In all cases results are consistent with a linear variation of the median value, F_{am}, with frequency f of the form:

$$F_{am} = c - d \log f \qquad (11)$$

With f expressed in MHz, c and d take the values given in Table 1. Note that equation (11) is valid in the range 0.3 to 250 MHz for all the environmental categories except those of curves D and E as indicated on the Figure.

TABLE 1

Values of the constants *c* and *d*

Environmental category	*c*	*d*
Business (curve A)	76.8	27.7
Residential (curve B)	72.5	27.7
Rural (curve C)	67.2	27.7
Quiet rural (curve D)	53.6	28.6
Galactic noise (curve E)	52.0	23.0

FIGURE 8

Brightness temperature at 1 430 MHz of the ground as a function of elevation angle

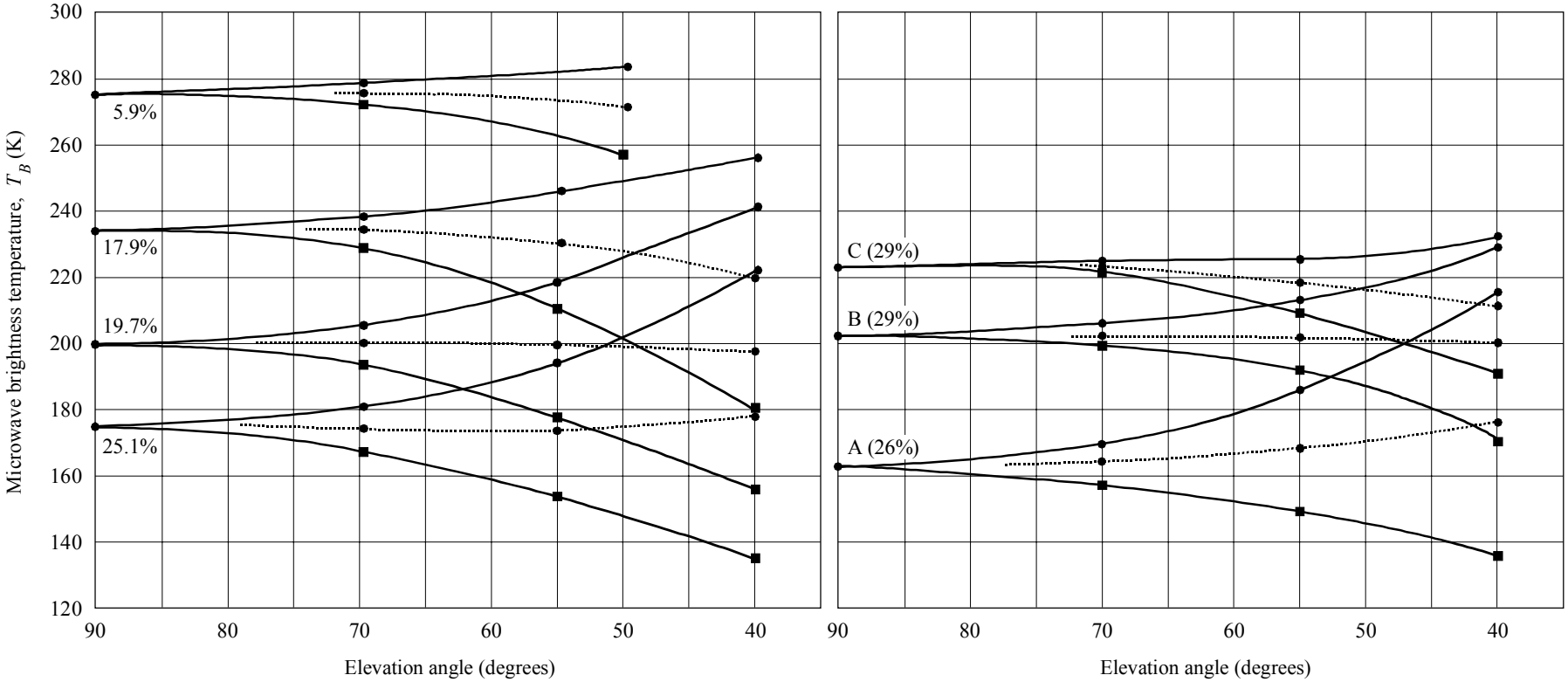

a) Moisture content from 5.9% to 25.1% for a bare, smooth field

b) For (A) smooth field (B) medium roughness and (C) rough (deeply ploughed) field with percentage water content as indicated

Vertical polarization, T_{BV}

Horizontal polarization, T_{BH}

Circular polarization, 1/2 ($T_{BV} + T_{BH}$)

0372-08

FIGURE 9

Weighted brightness temperature of the Earth as a function of longitude viewed from geostationary orbit at frequencies between 1 and 51 GHz

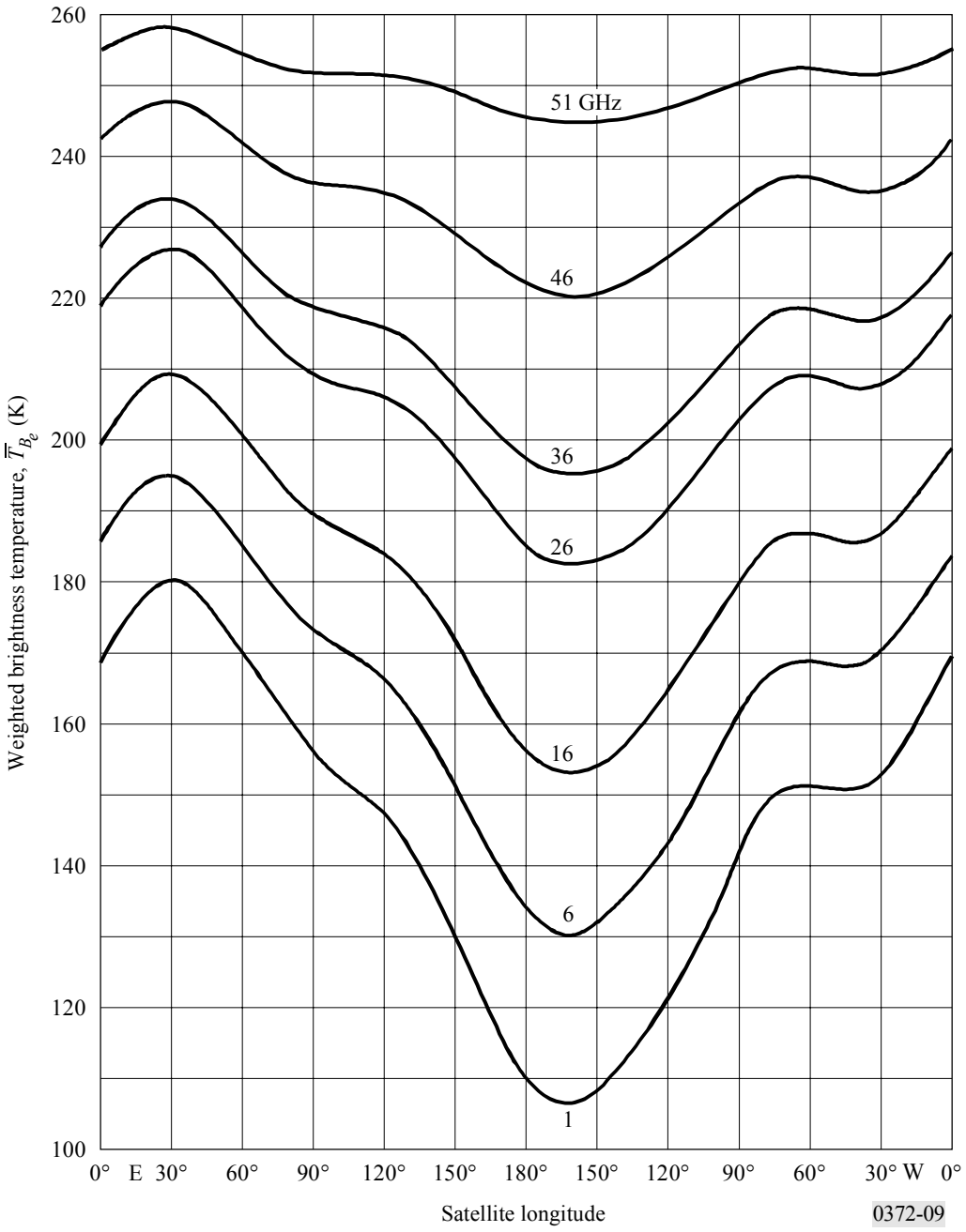

FIGURE 10

Median values of man-made noise power for a short vertical lossless grounded monopole antenna

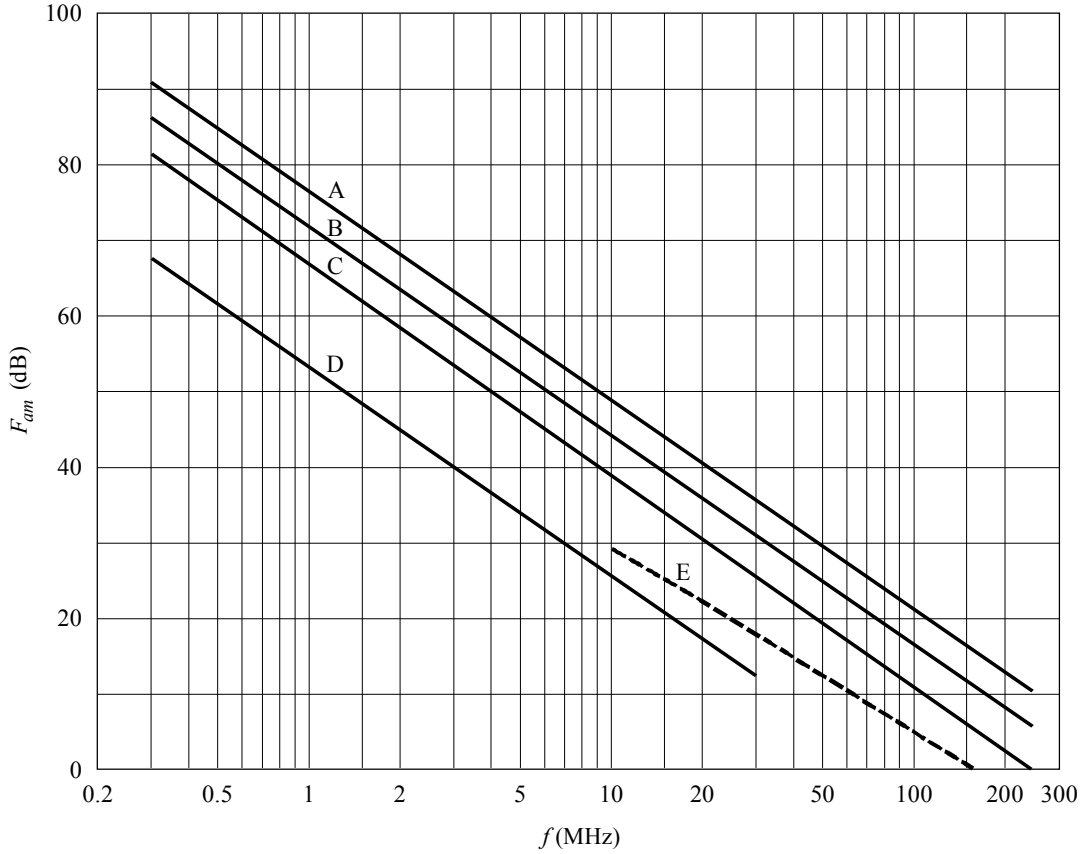

Environmental category:

Curves A: business
B: residential
C: rural
D: quiet rural
E: galactic (see § 6)

0372-10

For the business, residential and rural categories, the average over the above frequency range of the decile deviations of noise power with time, D_u and D_l, is given in Table 2. This Table also provides values of the deviation with location. It may be assumed that these variations are uncorrelated and that log-normal half distributions each side of the median are appropriate. These values were measured in the 1970s and may change with time, dependent on the activities which may generate man-made noise.

TABLE 2

Values of decile deviations of man-made noise

Category	Decile	Variation with time (dB)	Variation with location (dB)
Business	Upper Lower	11.0 6.7	8.4 8.4
Residential	Upper Lower	10.6 5.3	5.8 5.8
Rural	Upper Lower	9.2 4.6	6.8 6.8

An analysis of available measurement data for business areas (essentially the only area for which data are available) in the frequency range 200 MHz to 900 MHz also shows a linear variation with the logarithm of frequency, but with a more gradual slope. The result is, with f in MHz,

$$F_{am} = 44.3 - 12.3 \log f \qquad \text{for } 200 \text{ MHz} < f < 900 \text{ MHz} \tag{12}$$

There are not enough data available to obtain reasonable estimates of variations of F_a about F_{am} (D_u and D_l, say).

At VHF a significant component of man-made noise is due to ignition impulses from motor vehicles. For this contribution noise may be presented as an impulsive noise amplitude distribution (NAD) (the impulsive noise spectrum amplitude as a function of impulse rate). Figure 11 is an example of the noise amplitude distribution at 150 MHz for three categories of motor vehicle density. The NAD for other frequencies may be determined from the relationship:

$$A = C + 10 \log V - 28 \log f \qquad \text{dB}(\mu\text{V/MHz}) \tag{13}$$

where:

C: 106 dB(μV/MHz)

V: traffic density (vehicles/km^2)

f: frequency (MHz).

FIGURE 11

Noise amplitude distribution at base station (150 MHz)

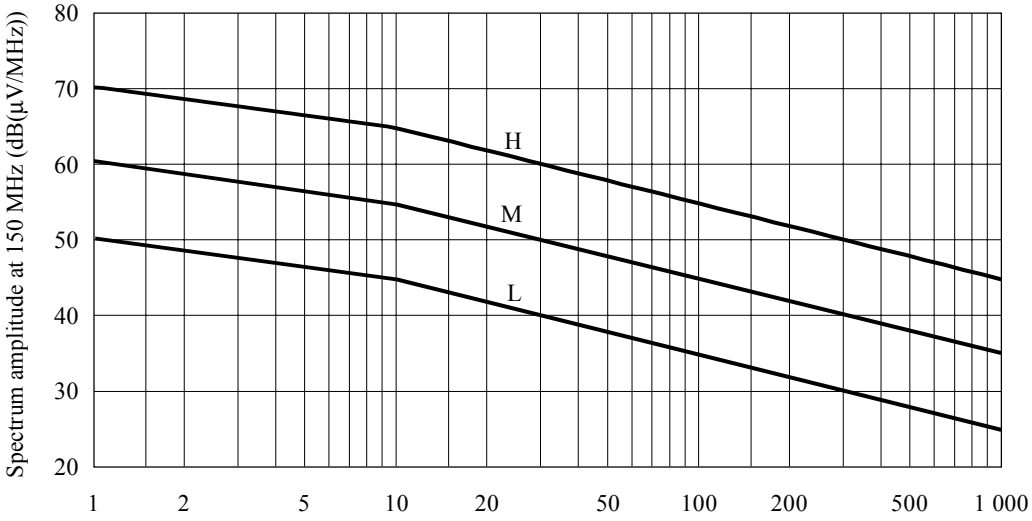

For frequencies other than 150 MHz, raise or lower curves H, M, and L in accordance with the formula below:

$$A = C + 10 \log V - 28 \log f$$

where A = dB(μV/MHz) at 10 pps.

Curves H: high noise location (V = 100)
M: moderate noise location (V = 10)
L: low noise location (V = 1)

0372-11

6 Brightness temperature due to extra-terrestrial sources

As a general rule, for communications below 2 GHz, one needs to be concerned with the Sun and the galaxy (the Milky Way), which appears as a broad belt of strong emission. For frequencies up to about 100 MHz, the median noise figure for galactic noise, neglecting ionospheric shielding, is given by:

$$F_{am} = 52 - 23 \log f \quad (14)$$

where:

f: frequency (MHz).

Above 2 GHz, one need consider only the Sun and a few very strong non-thermal sources such as Cassiopeia A, Cygnus A and X and the Crab nebula since the cosmic background contributes 2.7 K only and the Milky Way appears as a narrow zone of somewhat enhanced intensity. The brightness temperature range for the common extra-terrestrial noise sources in the frequency range 0.1 to 100 GHz is illustrated in Fig. 12.

FIGURE 12

Extra-terrestrial noise sources

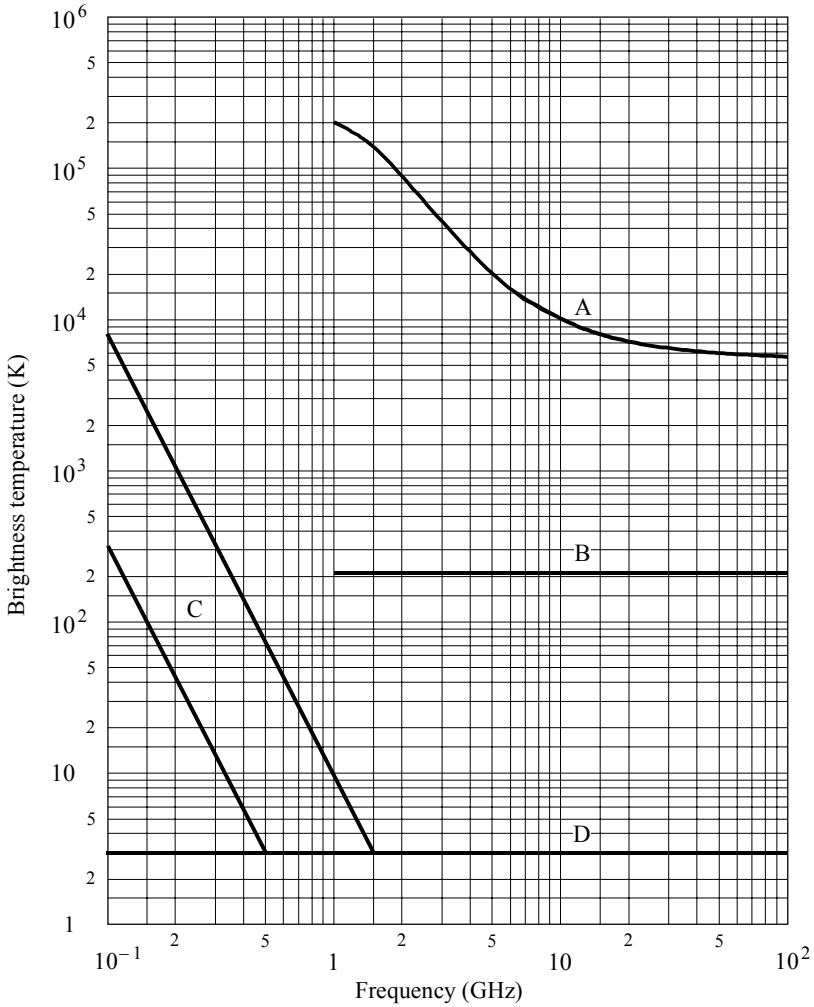

A: quiet Sun
B: Moon
} diameter ~ 0.5°
C: range of galactic noise
D: cosmic background

0372-12

Figures 13a, 13b, 13c and 13d plot the total radio sky temperature at 408 MHz smoothed to 5° angular resolution. Figures 13 are given in equatorial coordinates, declination δ (latitude) and right ascension α (hours eastward around equator from vernal equinox). The contours are directly in K above 2.7 K. The accuracy is 1 K. The contour intervals are:

– 2 K below 60 K,

– 4 K from 60 K to 100 K,

– 10 K from 100 K to 200 K,

– 20 K above 200 K.

Arrows on unlabelled contour lines point clockwise around a minimum in the brightness distribution.

The dashed sinusoidal curve between ±23.5° in Figs. 13a and 13d defines the ecliptic which crosses the Milky Way close to the galactic centre. This means that, if one observes a spacecraft in interplanetary space, it might be necessary to take this into account. The strongest point sources are indicated by narrow peaks of the temperature distribution, while weaker sources are less apparent owing to the limited angular resolution.

The radiation of the galactic background varies with frequency. To obtain brightness temperatures at other frequencies f_i for background radiation use

$$t_b(f_i) = t_b(f_0)\,(f_i/f_0)^{-2.75} + 2.7 \qquad \text{K} \tag{15}$$

Thus for $t_b = 200$ K, $f_0 = 408$ MHz and $f_i = 1$ GHz, this extrapolation would yield:

$$t_b = 19.7 \qquad \text{K}$$

More precise extrapolation using this formula needs to take into account variations of the exponent over the frequency range and over the sky. For point sources, the variation of the intensity with frequency depends on their different physical conditions.

For telecommunication using satellites in geostationary orbit, a limited part of the sky is of special interest, as illustrated in Fig. 14a). The corresponding range of declinations (±8.7°) is shown in Fig. 14b), indicating the strongest sources.

FIGURE 13a

Radio sky temperature at 408 MHz

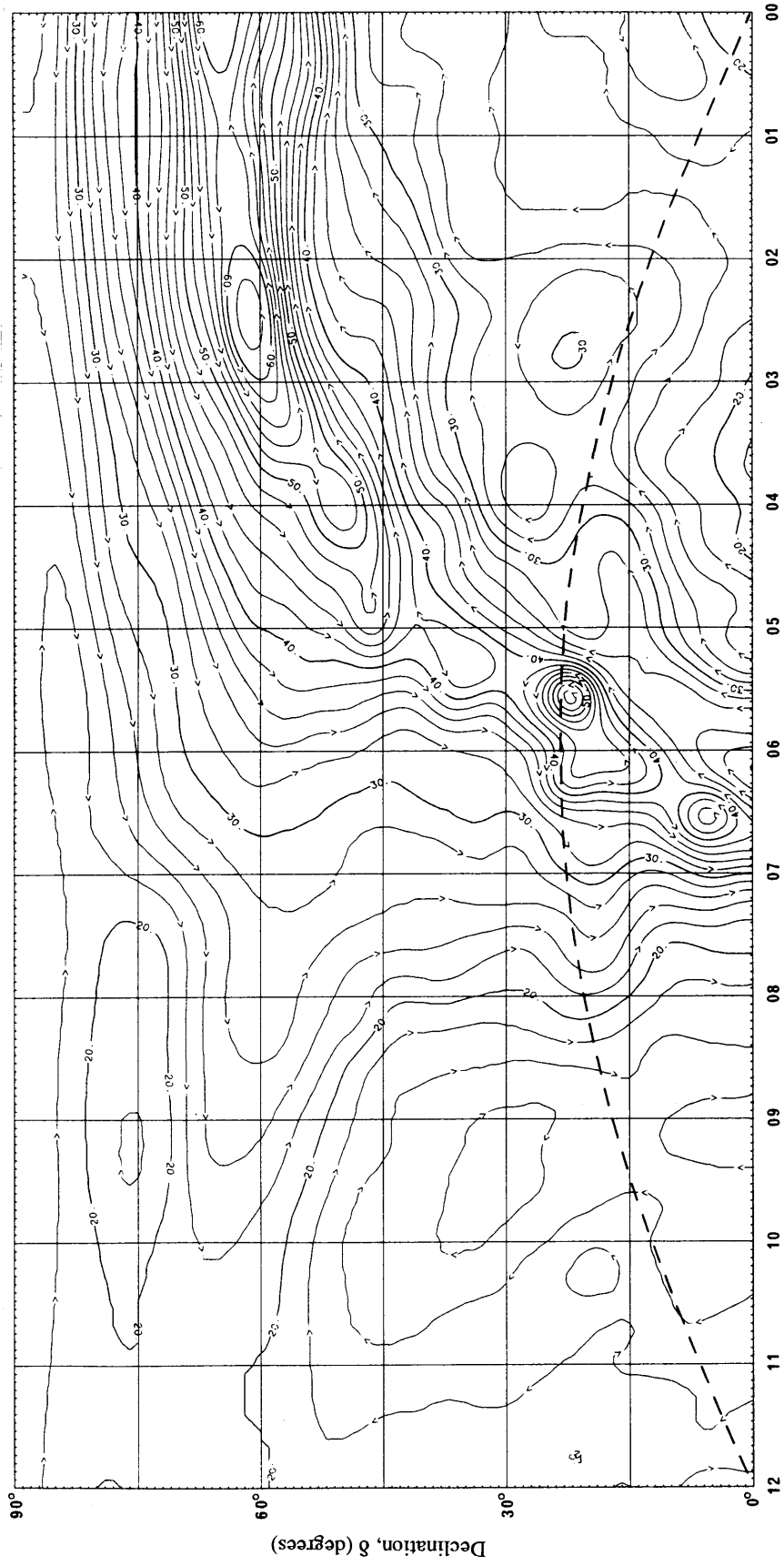

Right ascension 0000 h to 1200 h, declination 0° to +90°, dashed curve; ecliptic

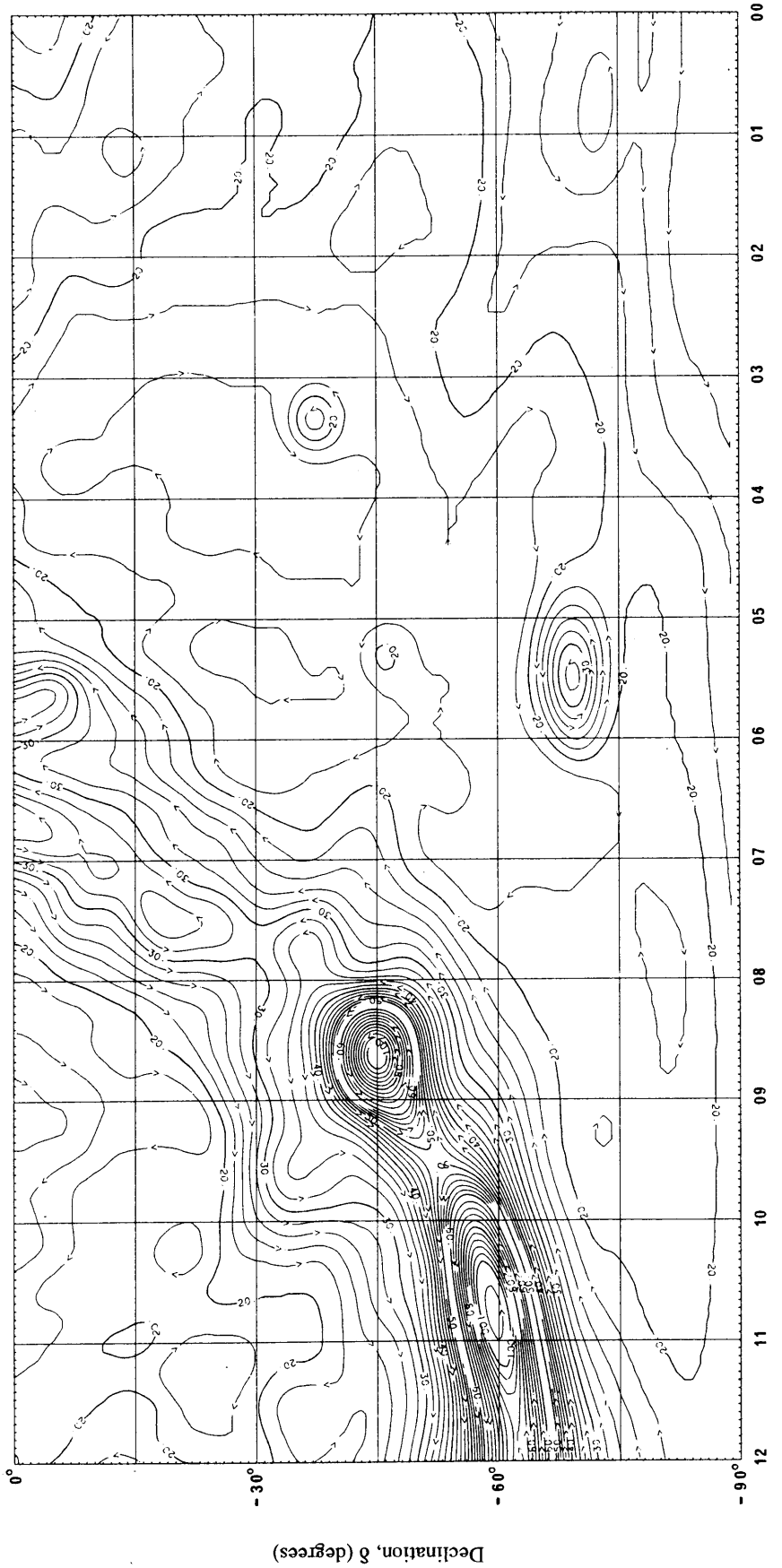

FIGURE 13b

Radio sky temperature at 408 MHz

Right ascension 0000 h to 1200 h, declination 0° to –90°

FIGURE 13c

Radio sky temperature at 408 MHz

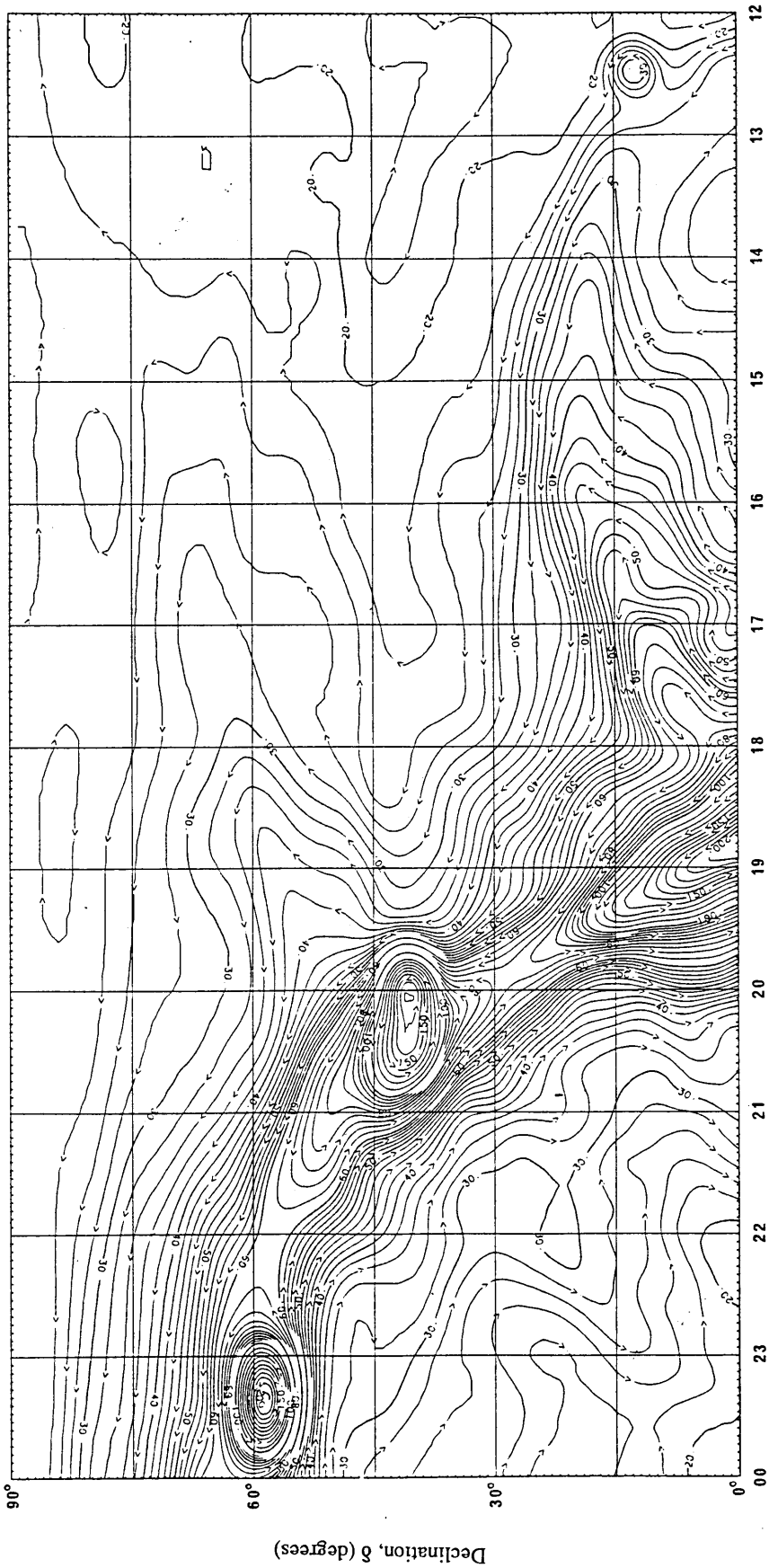

Right ascension 1200 h to 2400 h, declination 0° to +90°

FIGURE 13d

Radio sky temperature at 408 MHz

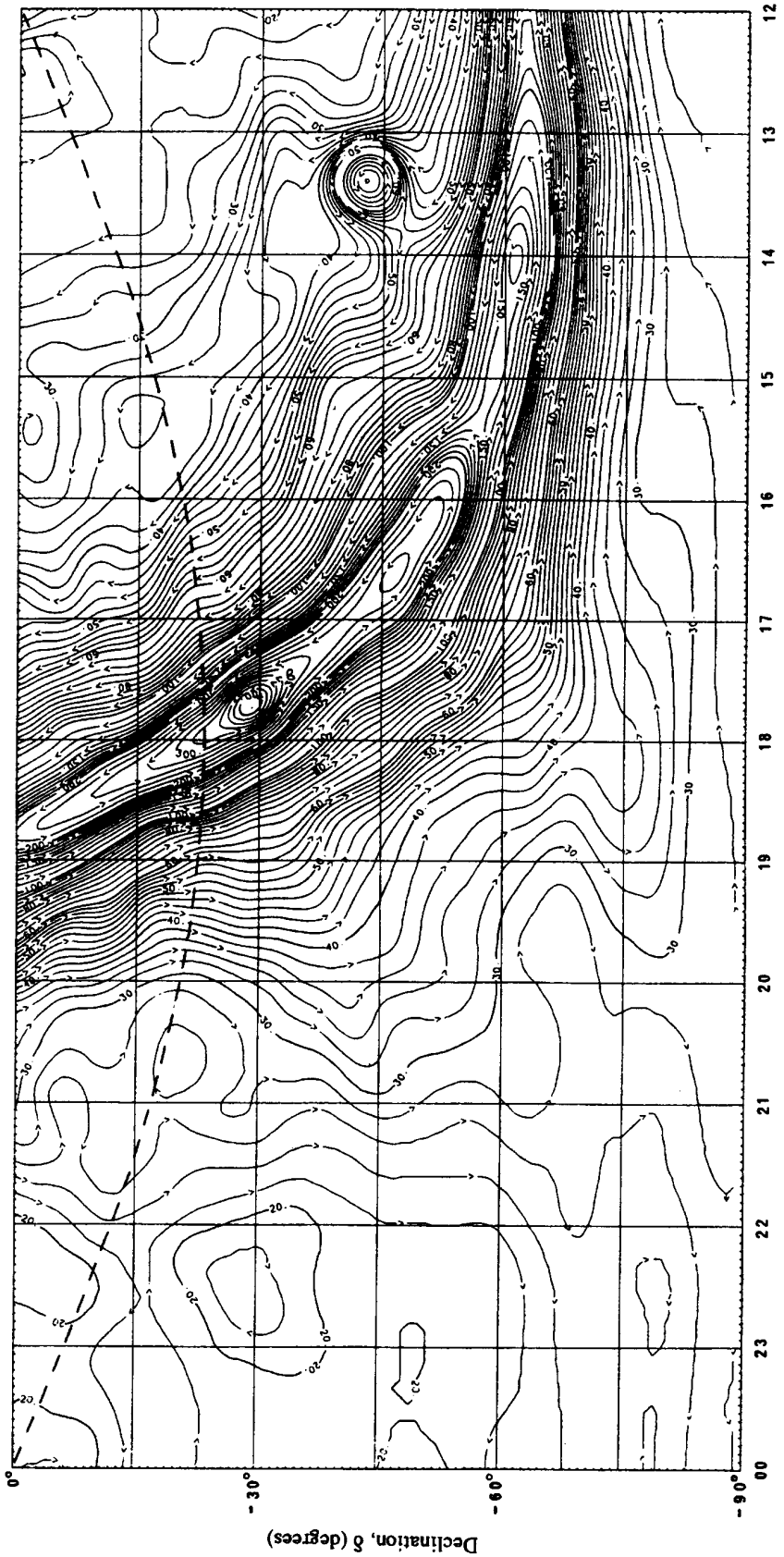

Right ascension 1200 h to 2400 h, declination 0° to –90°, dashed curve: ecliptic

FIGURE 14

Part of the sky which is relevant for telecommunication with satellites in geostationary orbit

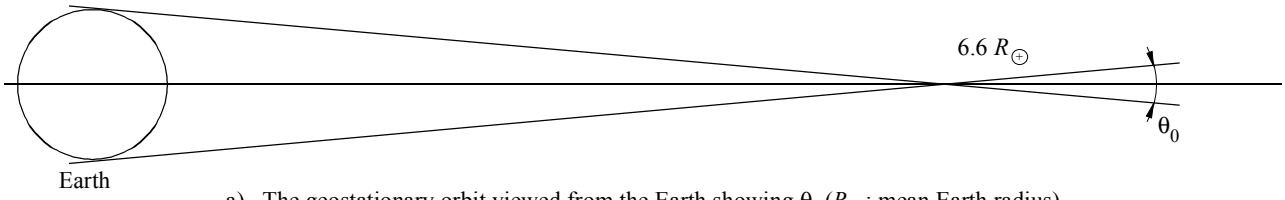

a) The geostationary orbit viewed from the Earth showing θ_0 ($R_\oplus$: mean Earth radius)

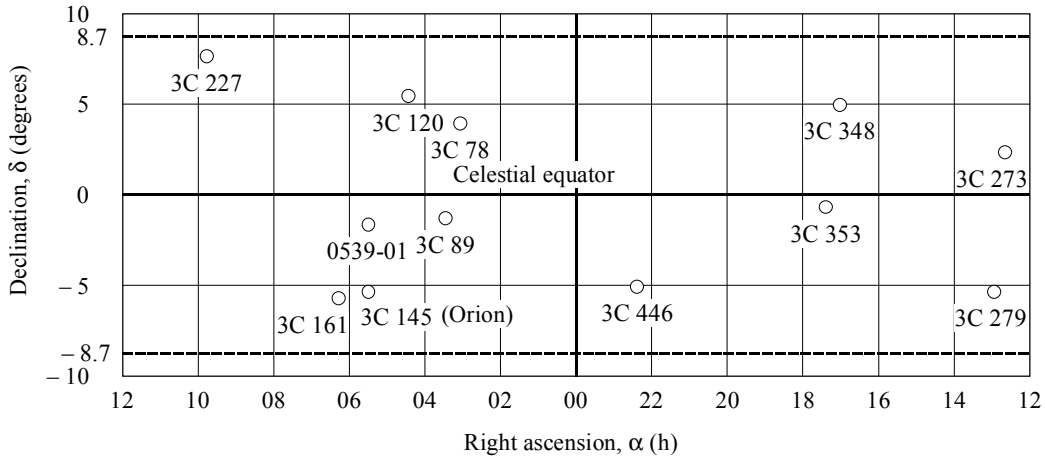

b) Locations of strongest radio sources (○) for a band of ± 8.7° about the celestial equator. The numbers refer to catalogue designations, e.g., 3C indicates third Cambridge

0372-14

The Sun is a strong variable noise source with a noise temperature of about 10^6 K at 50 to 200 MHz and at least 10^4 K at 10 GHz under quiet Sun conditions. Large increases occur when the Sun is disturbed. The brightness temperature of the Moon is almost independent of frequency above 1 GHz; it varies from about 140 K at new Moon up to 280 K at full Moon. The Sun's path is in the plane of ecliptic (dashed line in Figs. 13). The Moon is observed within ±5° in declination of the plane of the ecliptic.

7 Atmospheric noise due to lightning

World charts, showing the expected median values of background atmospheric radio noise, F_{am} in dB above kT_0b, at 1 MHz for each season, 4-hour-time block, in local time, are shown in Figs. 15a to 38a. The only geographical variation given is for the 1 MHz F_{am}. The variation of F_{am} with frequency for each season-time block is given in Figs. 15b to 38b and the variation with frequency of the other noise parameters is given in Figs. 15c to 38c. The reference antenna for these atmospheric noise estimates is a short vertical monopole over a perfectly conducting ground plane. The incident field strength can be obtained, see § 2.

It will be observed that values of atmospheric noise are indicated that are below the expected levels of man-made noise and galactic noise. These values should be used with caution, as they represent only estimates of what atmospheric noise levels would be recorded if the other types of noise were not present. An examination of the data, however, shows that such low levels were, on rare occasions, actually measured.

APD curves corresponding to various values of V_d, are given in Fig. 39, in which the r.m.s. envelope voltage A_{rms}, is taken as the reference. The measured values of V_d vary about the predicted median value, V_{dm}, and their variation is given by σ_{Vd}. The APD curves can be used for a wide range of bandwidths. The estimates of V_d given (Figs. 15c-38c) are for a 200 Hz bandwidth and Fig. 40 gives a means to convert the 200 Hz V_d to the corresponding V_d in other bandwidths. Figure 40 is strictly valid only at MF and HF frequencies, so care should be exercised when applying these results to lower frequencies (i.e., LF, VLF, ELF).

The figures are used in the following way. The value of F_{am} for 1 MHz is found from the noise charts (Figs. 15a-38a) for the season under consideration. Using this value as the noise grade, the value of F_{am} for the required frequency is determined from the frequency curves (Figs. 15b-38b). The variability parameters σ_{Fam}, D_u, σ_{Du}, etc., are obtained for the required frequency from Figs. 15c to 38c. Values of D and σ_D for other percentages of time may be obtained assuming log-normal half distributions each side of the median values.

8 The combination of noises from several sources

There are occasions where more than one type of noise needs to be considered because two or more types are of comparable size. This can be true at any frequency, in general, but occurs most often at HF where atmospheric, man-made, and galactic noise can be of comparable size (Fig. 2, 10 MHz, for example). The values given are median F_a values, F_{am}. The f_a values have distributions about the median f_a. As noted earlier, these distributions are log-normal distributions each side of the median. An appropriate method for obtaining the median value and distribution for the sum of two or more noise processes has been developed in which the resultant noise is also assumed to be log-normally distributed. In this method the resultant median noise power is given by the sum of the median noise powers of the individual noise processes. The standard deviation of the resultant noise is obtained by summing noise powers determined one standard deviation above the median power for each of the noise processes involved, and then subtracting the resultant median noise power from that result.

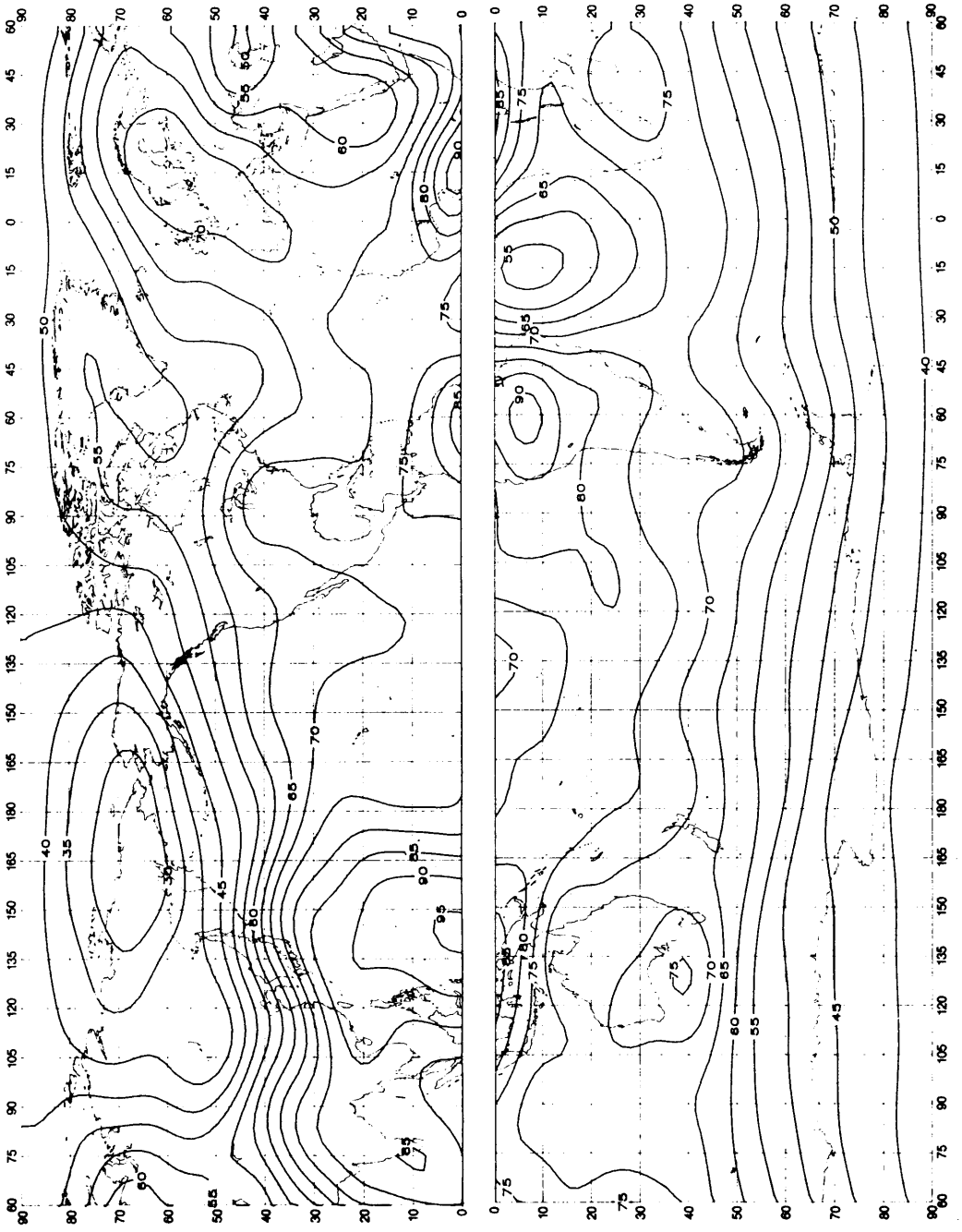

0372-15a

FIGURE 15a – *Expected values of atmospheric radio noise, F_{am} (dB above kT_0b at 1 MHz) (Winter; 0000-0400 LT)*

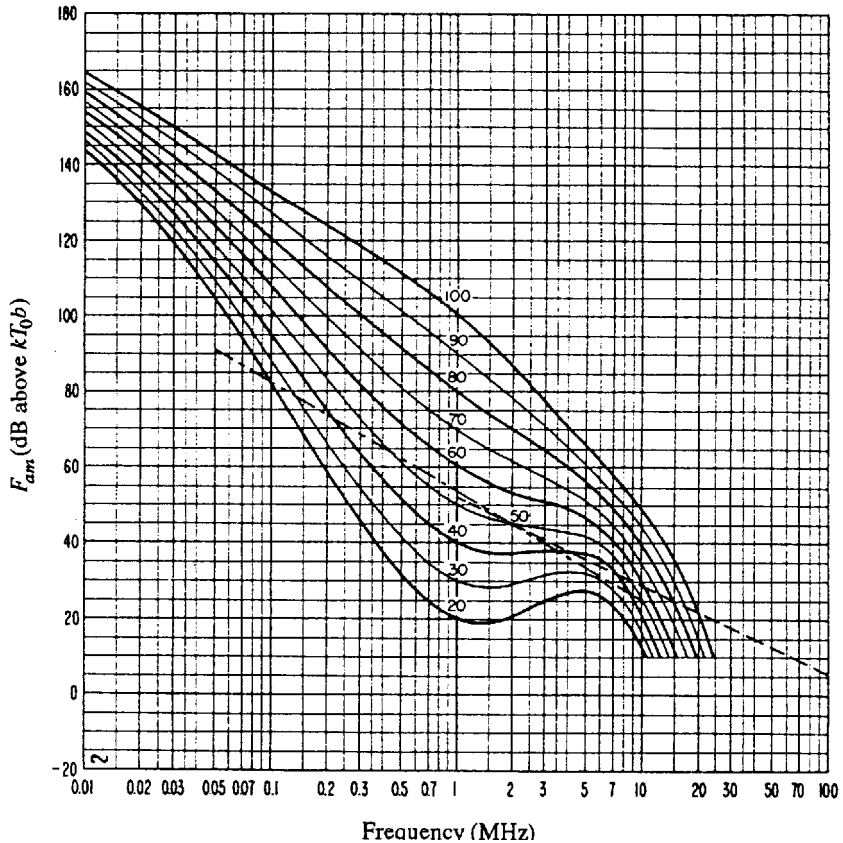

FIGURE 15b – *Variation of radio noise with frequency (Winter; 0000-0400 LT)*

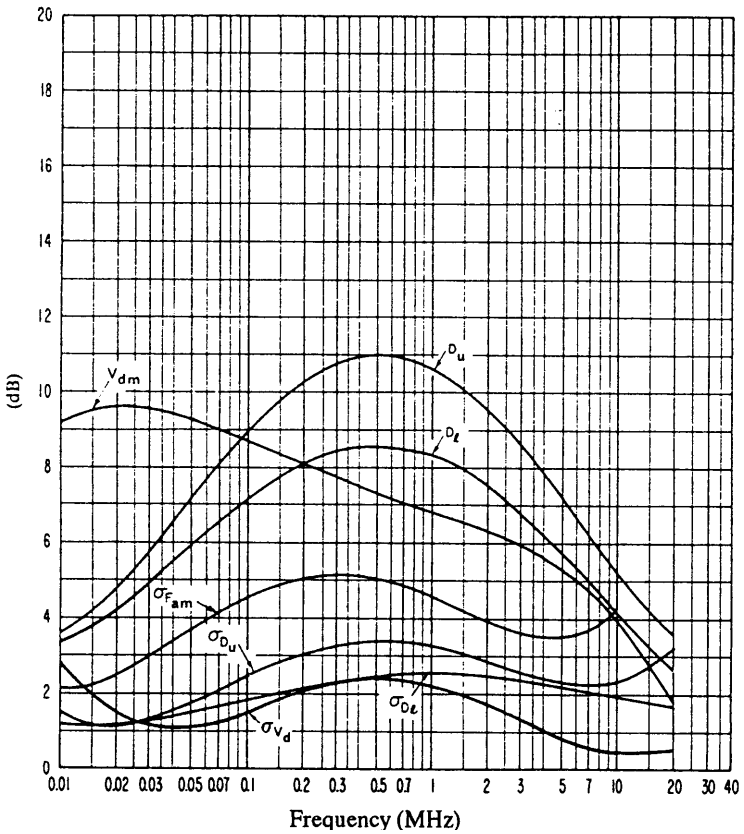

FIGURE 15c – *Data on noise variability and character (Winter; 0000-0400 LT)*

——— Expected values of atmospheric noise

—·—·— Expected values of man-made noise at a quiet receiving location

- - - - - Expected values of galactic noise

$\sigma_{F_{am}}$: Standard deviation of values of F_{am}

D_u : Ratio of upper decile to median value, F_{am}

σ_{D_u} : Standard deviation of values of D_u

D_l : Ratio of median value, F_{am}, to lower decile

σ_{D_l} : Standard deviation of values of D_l

V_{dm} : Expected value of median deviation of average voltage. The values shown are for a bandwidth of 200 Hz

σ_{V_d} : Standard deviation of V_d

0372-15b

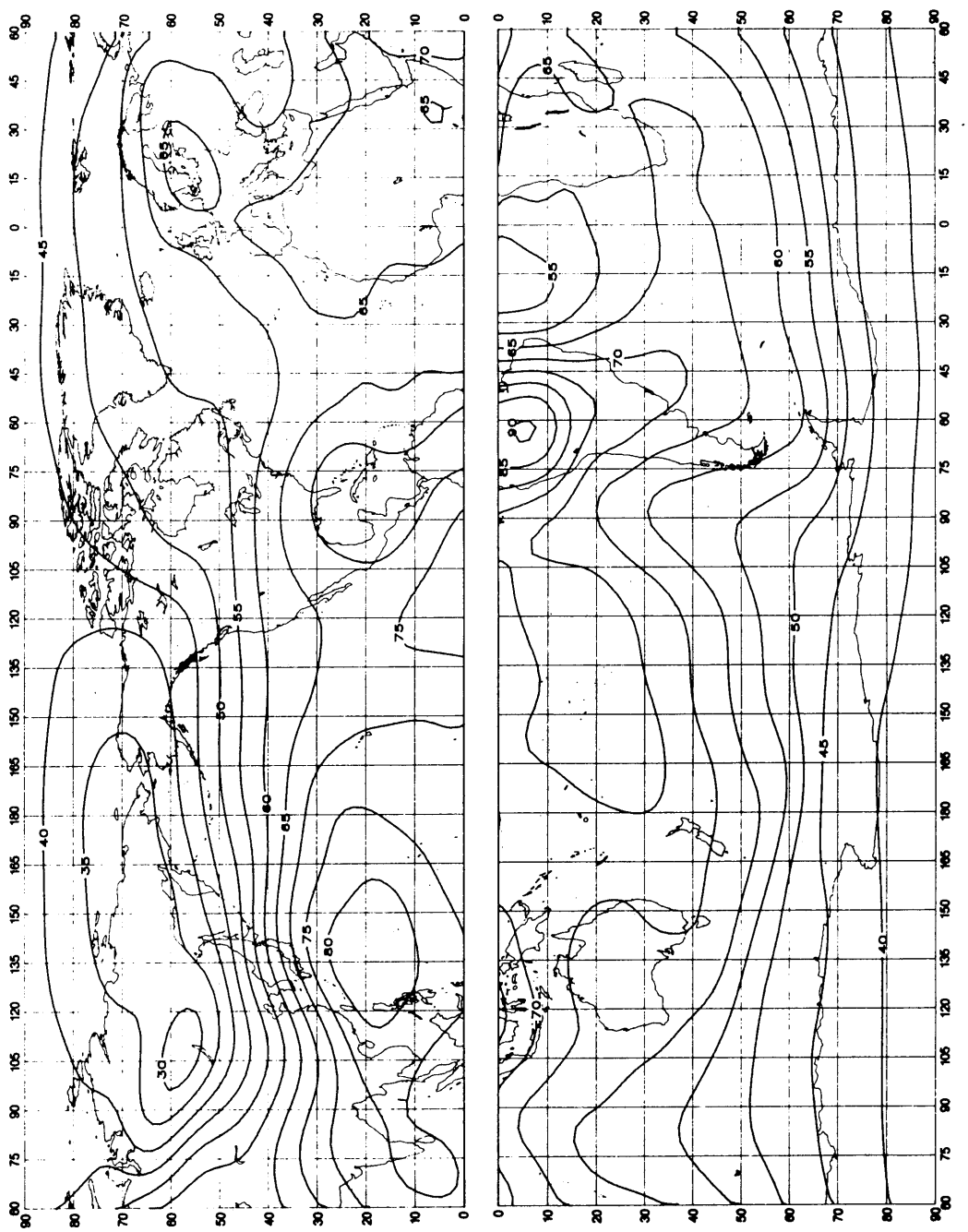

0372-16a

FIGURE 16a – *Expected values of atmospheric radio noise, F_{am} (dB above kT_0b at 1 MHz) (Winter; 0400-0800 LT)*

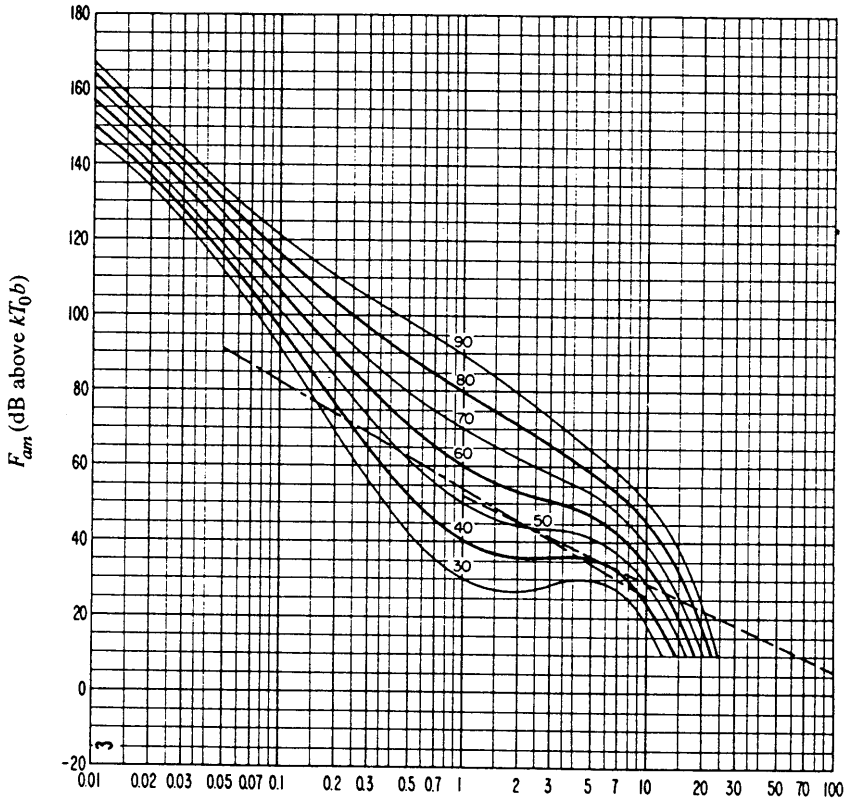

FIGURE 16b – *Variation of radio noise with frequency (Winter; 0400-0800 LT)*

See legend of Fig. 15b

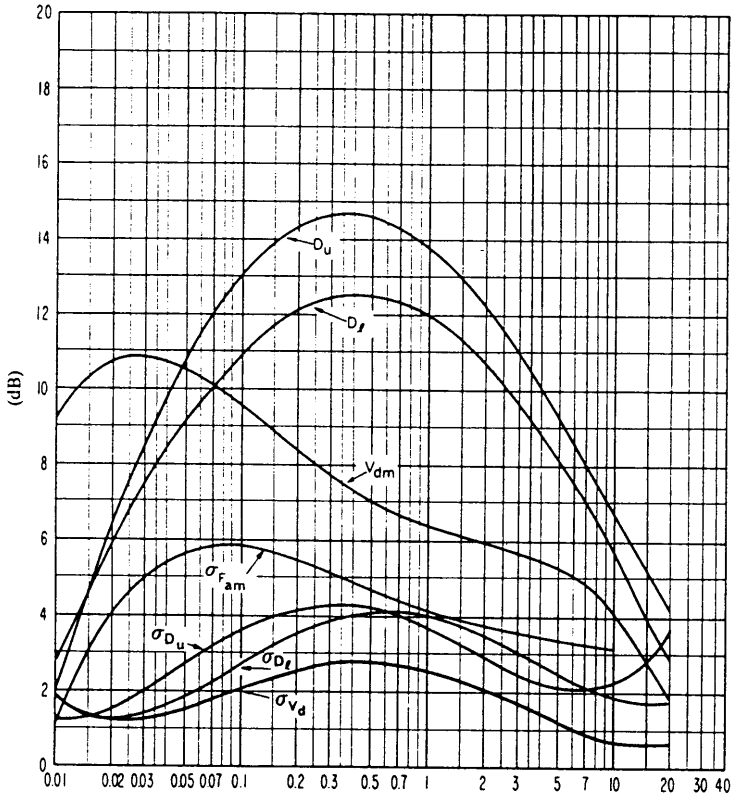

FIGURE 16c – *Data on noise variability and character (Winter; 0400-0800 LT)*

0372-16b

See legend of Fig. 15c

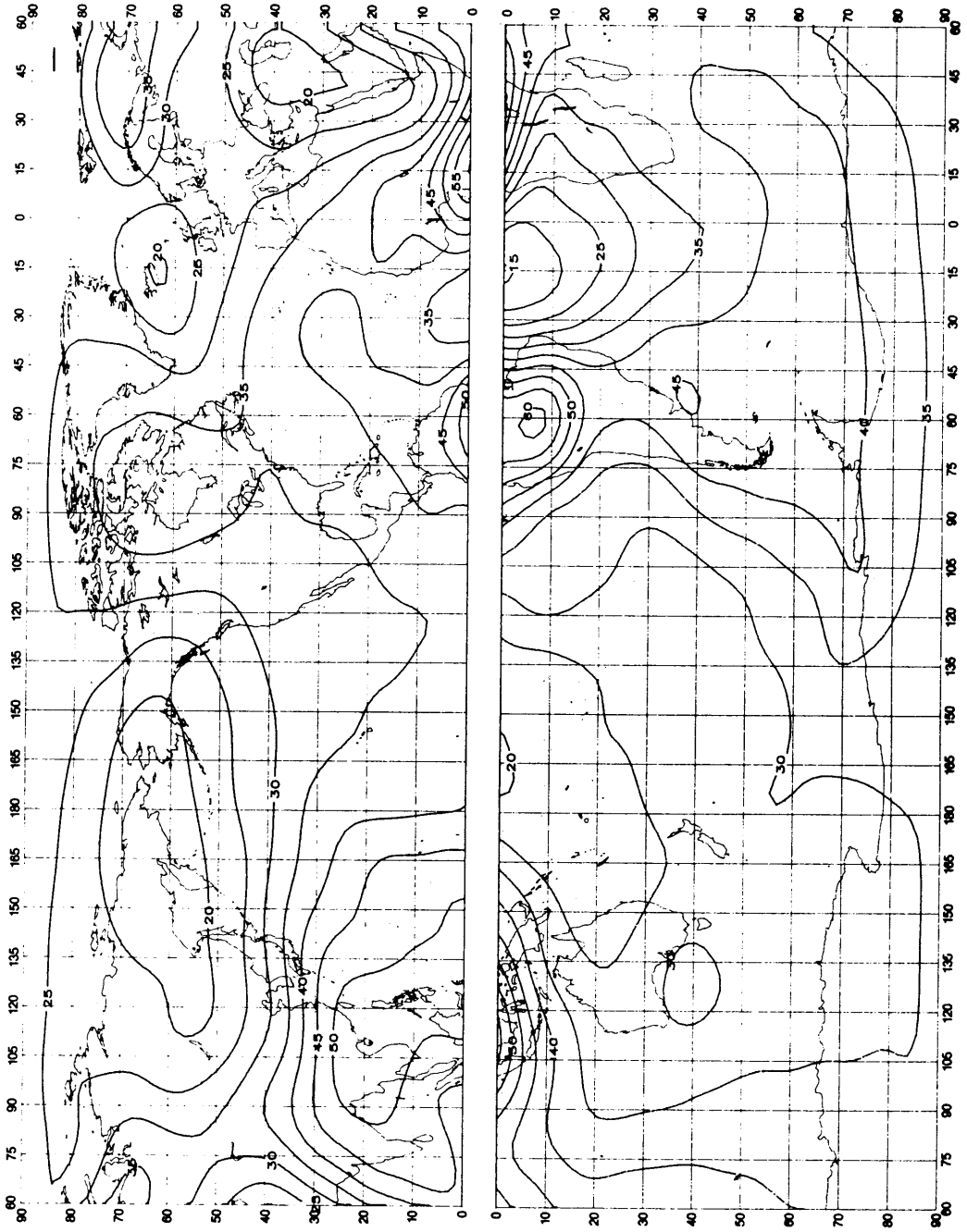

0372-17a

FIGURE 17a – *Expected values of atmospheric radio noise, F_{am} (dB above kT_0b at 1 MHz) (Winter; 0800-1200 LT)*

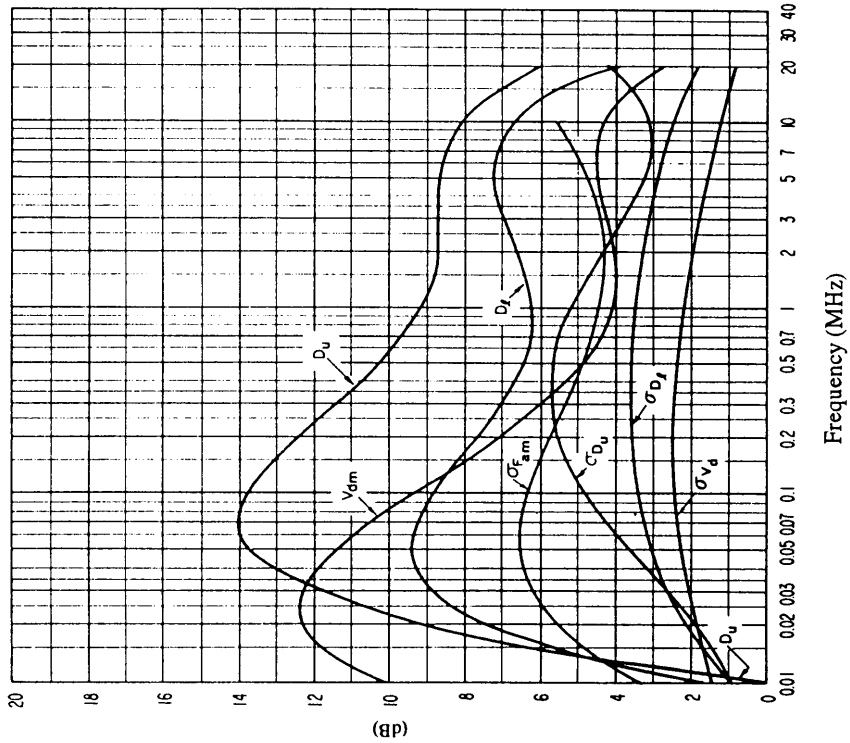

FIGURE 17c – *Data on noise variability and character (Winter; 0800-1200 LT)*

See legend of Fig. 15c

0372-17b

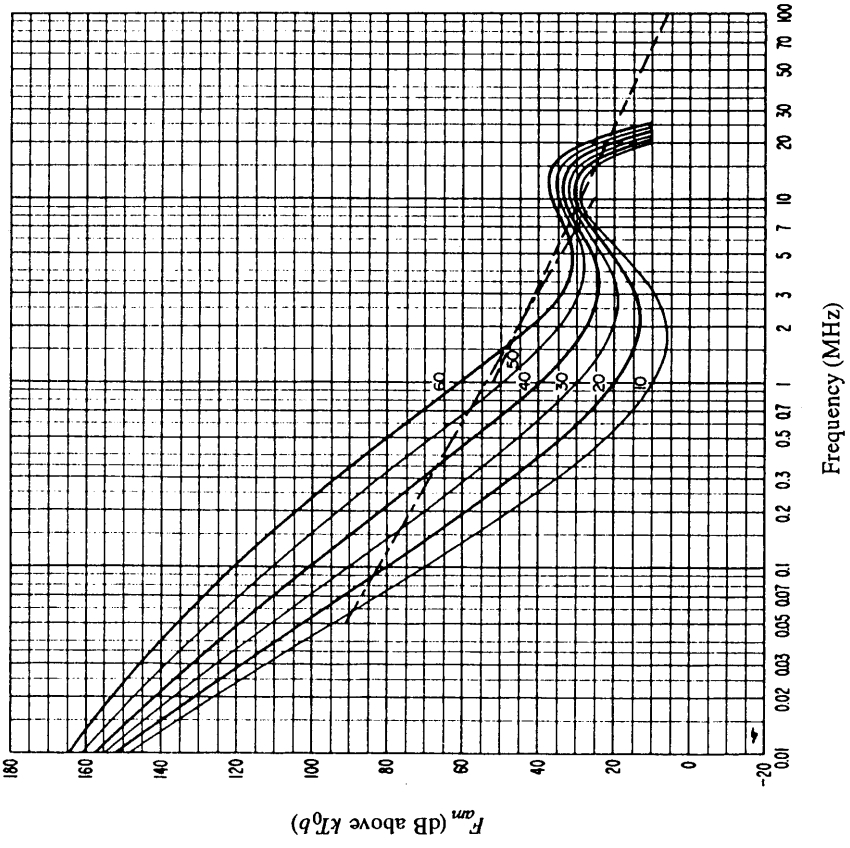

FIGURE 17b – *Variation of radio noise with frequency (Winter; 0800-1200 LT)*

See legend of Fig. 15b

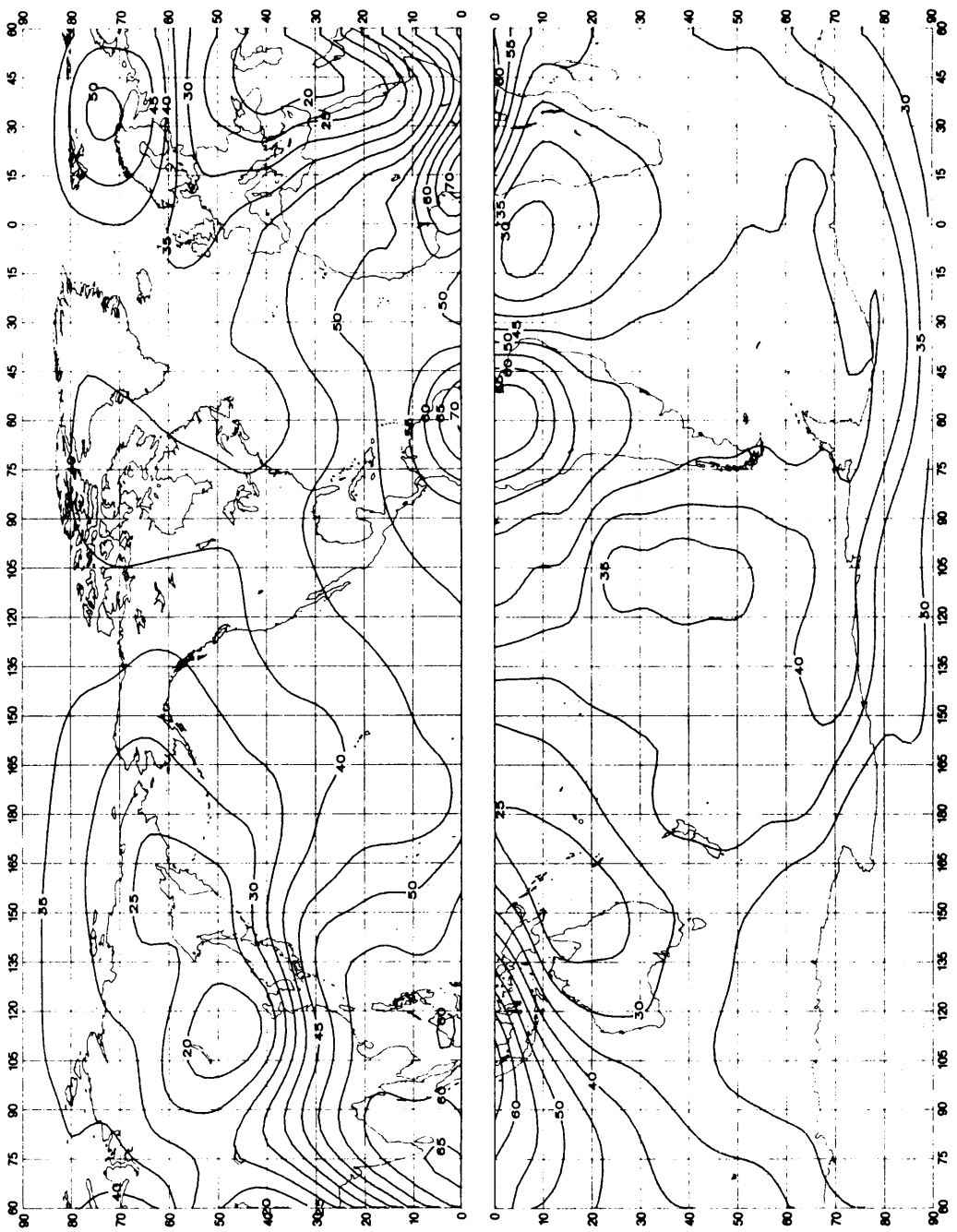

0372-18a

FIGURE 18a – *Expected values of atmospheric radio noise, F_{am} (dB above kT_0b at 1 MHz) (Winter; 1200-1600 LT)*

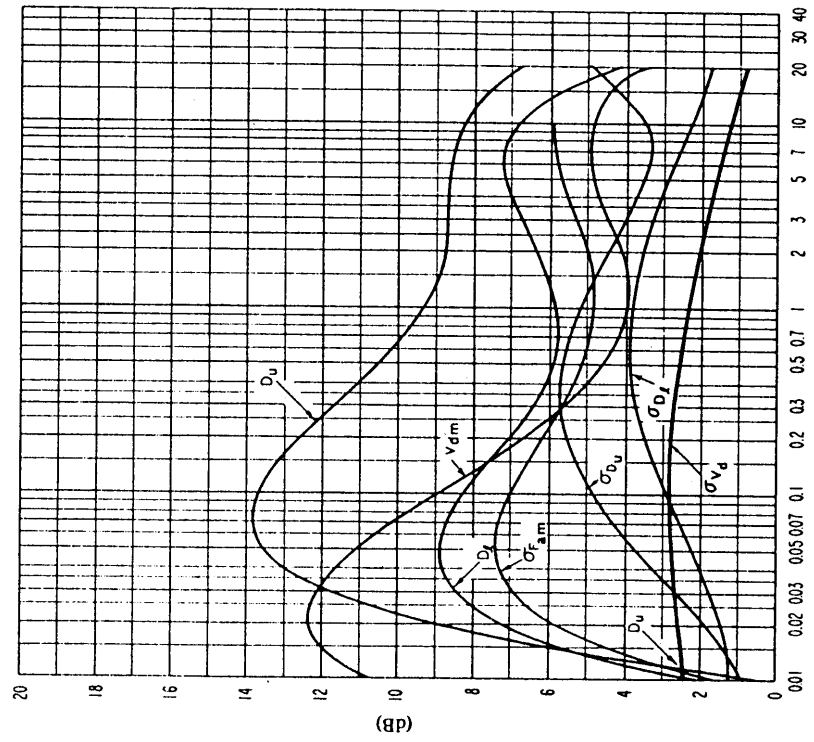

FIGURE 18c – *Data on noise variability and character (Winter; 1200-1600 LT)*

See legend of Fig. 15c

0372-18b

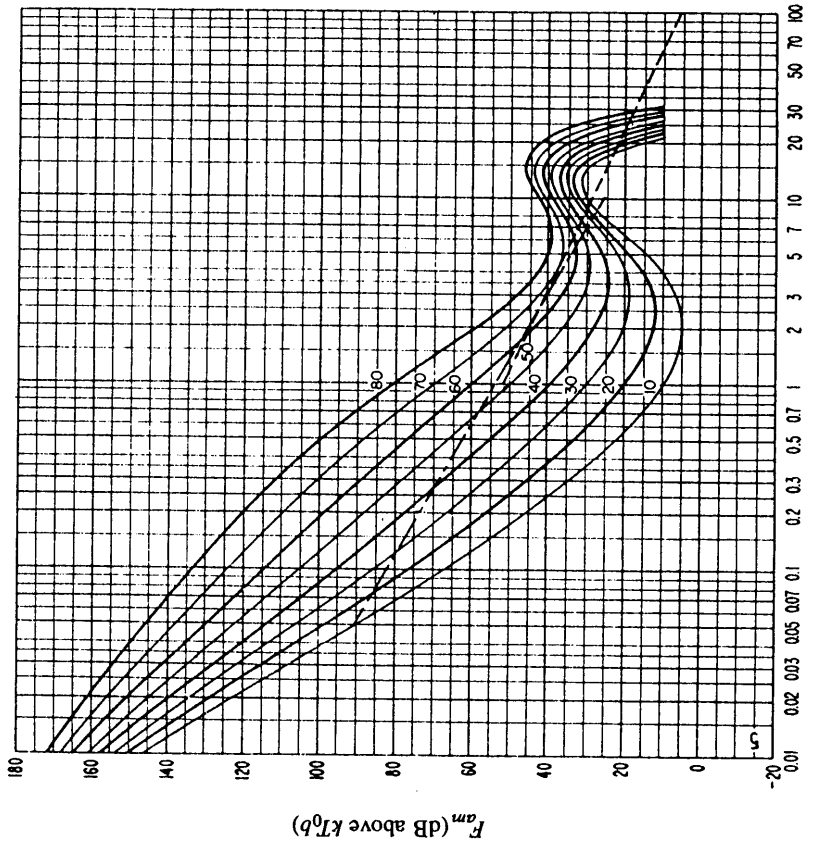

FIGURE 18b – *Variation of radio noise with frequency (Winter; 1200-1600 LT)*

See legend of Fig. 15b

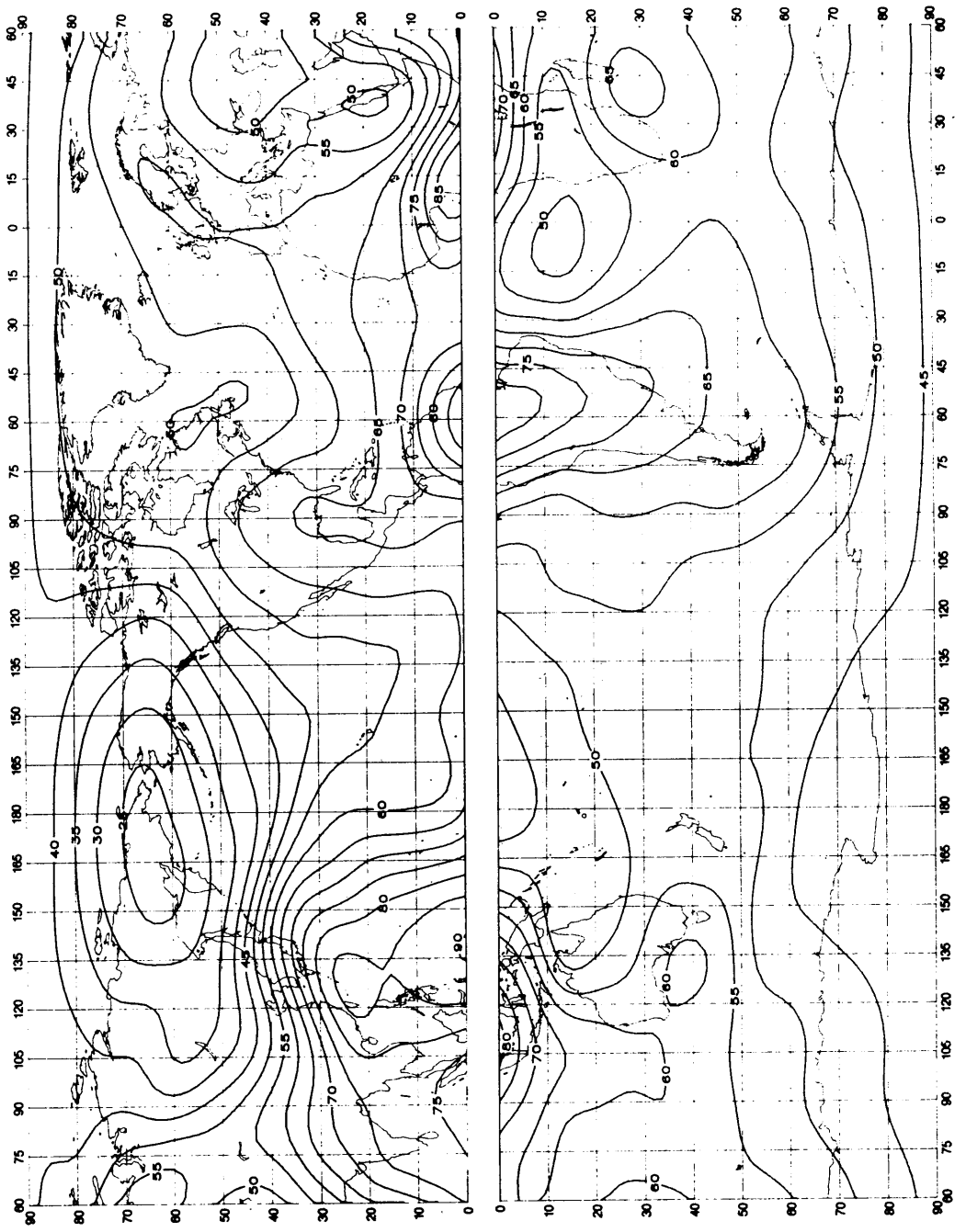

0372-19a

FIGURE 19a – *Expected values of atmospheric radio noise, F_{am} (dB above kT_0b at 1 MHz) (Winter; 1600-2000 LT)*

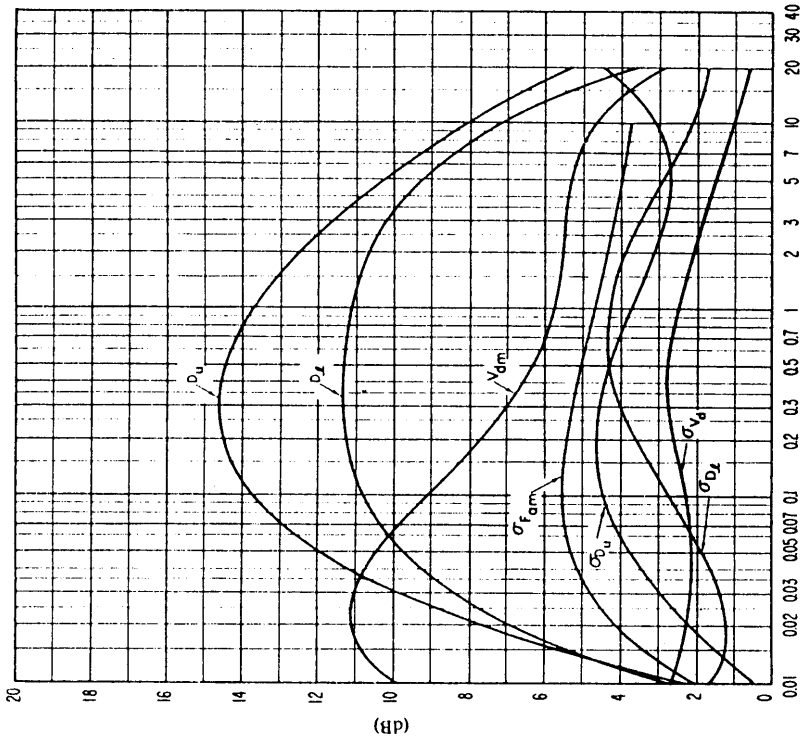

FIGURE 19c – *Data on noise variability and character (Winter; 1600-2000 LT)*

See legend of Fig. 15c

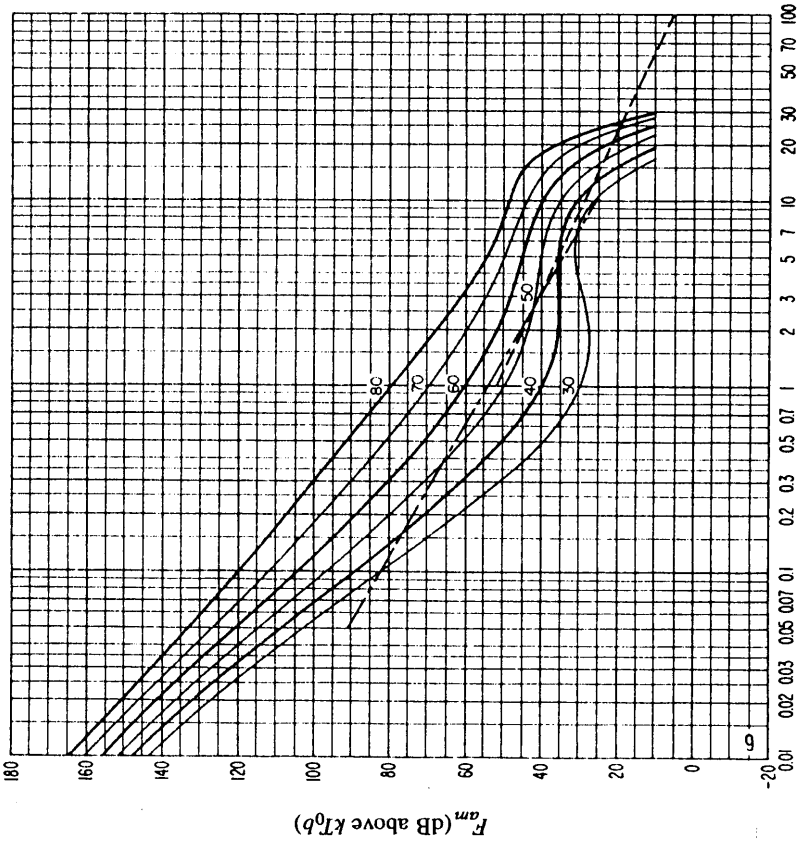

FIGURE 19b – *Variation of radio noise with frequency (Winter; 1600-2000 LT)*

See legend of Fig. 15b

0372-19b

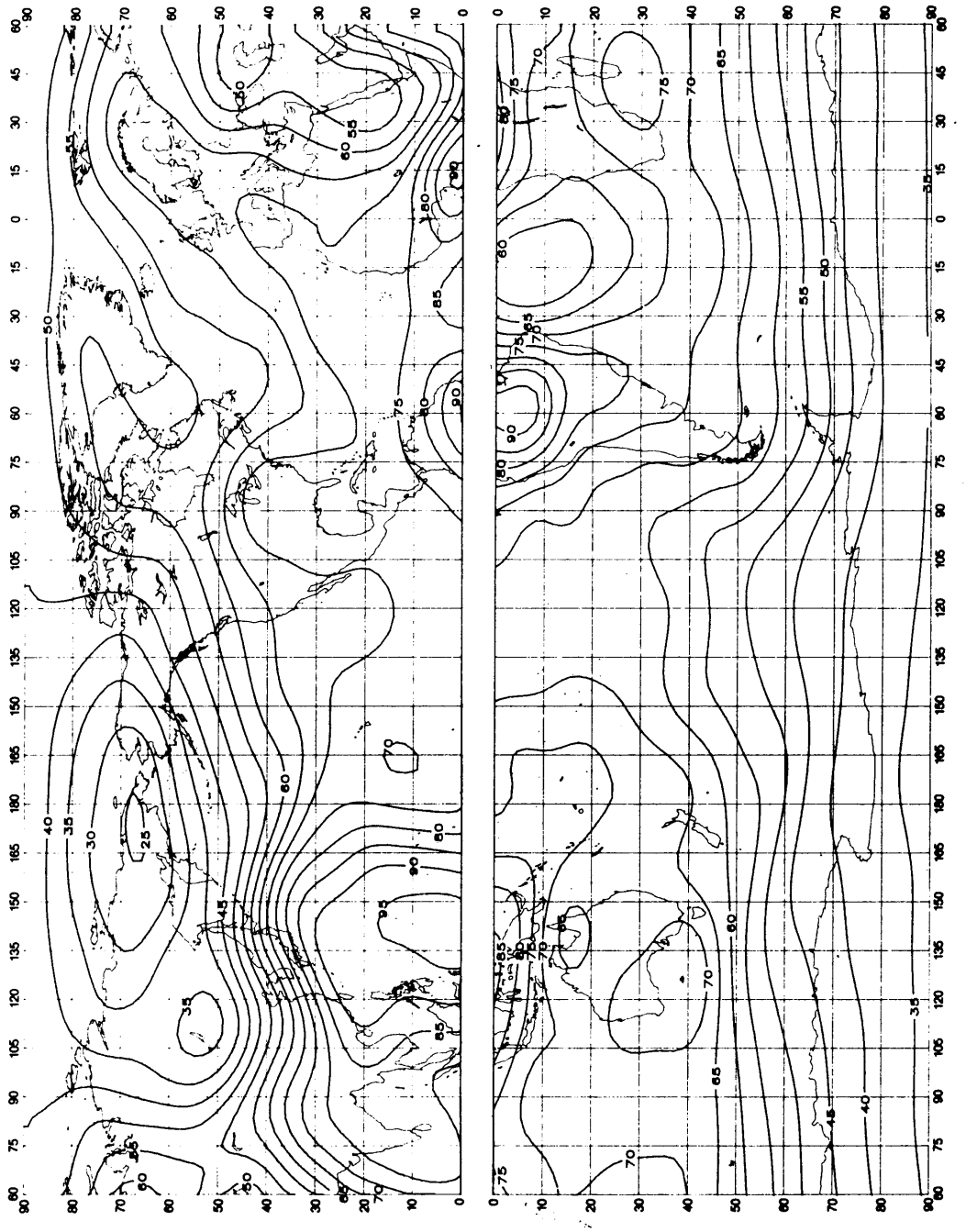

0372-20a

FIGURE 20a – *Expected values of atmospheric radio noise, F_{am} (dB above kT_0b at 1 MHz) (Winter; 2000-2400 LT)*

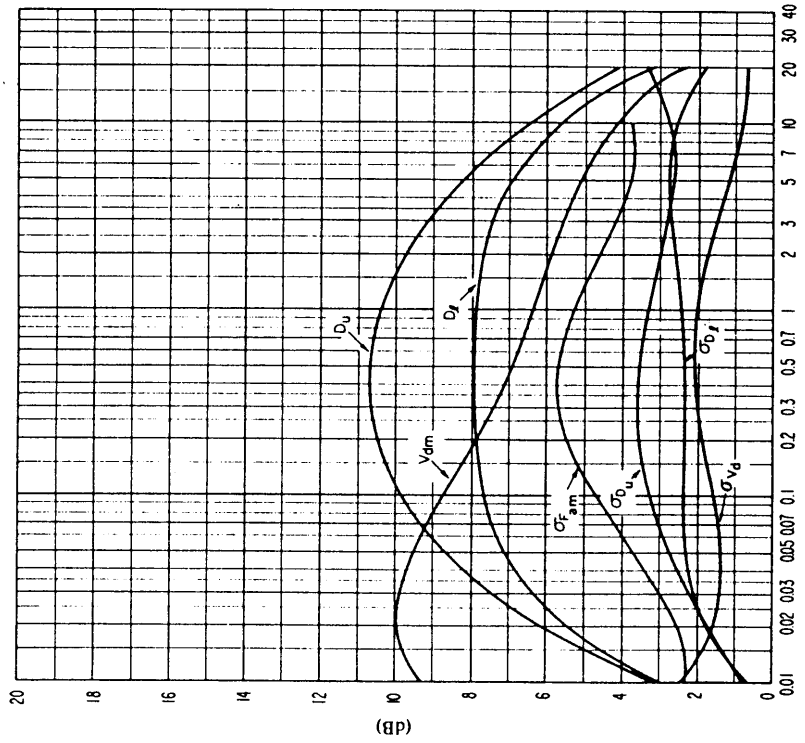

FIGURE 20c – *Data on noise variability and character (Winter; 2000-2400 LT)*

See legend of Fig. 15c

0372-20b

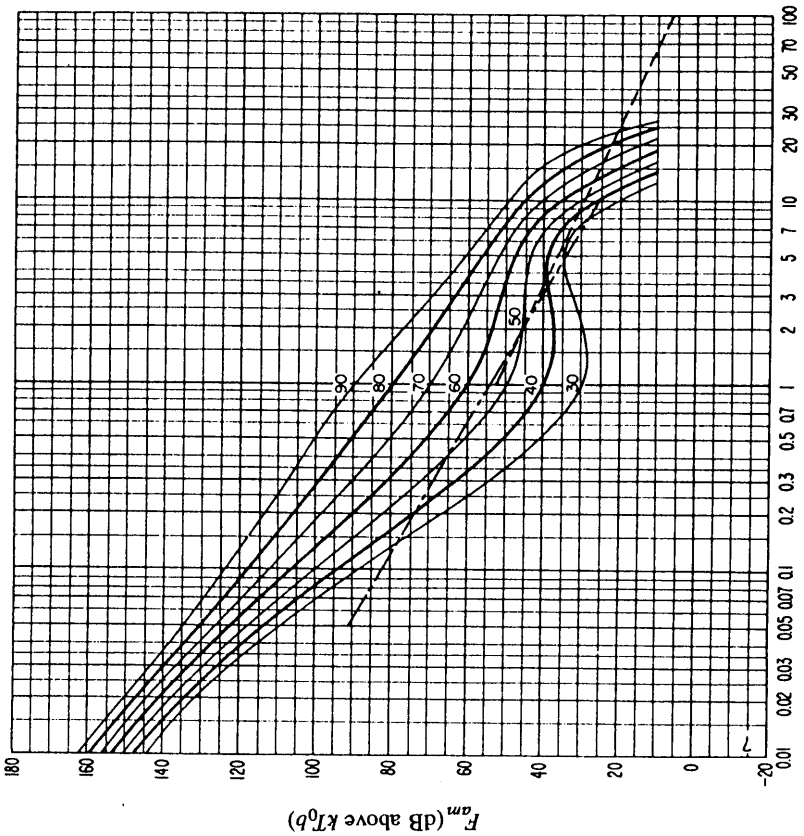

FIGURE 20b – *Variation of radio noise with frequency (Winter; 2000-2400 LT)*

See legend of Fig. 15b

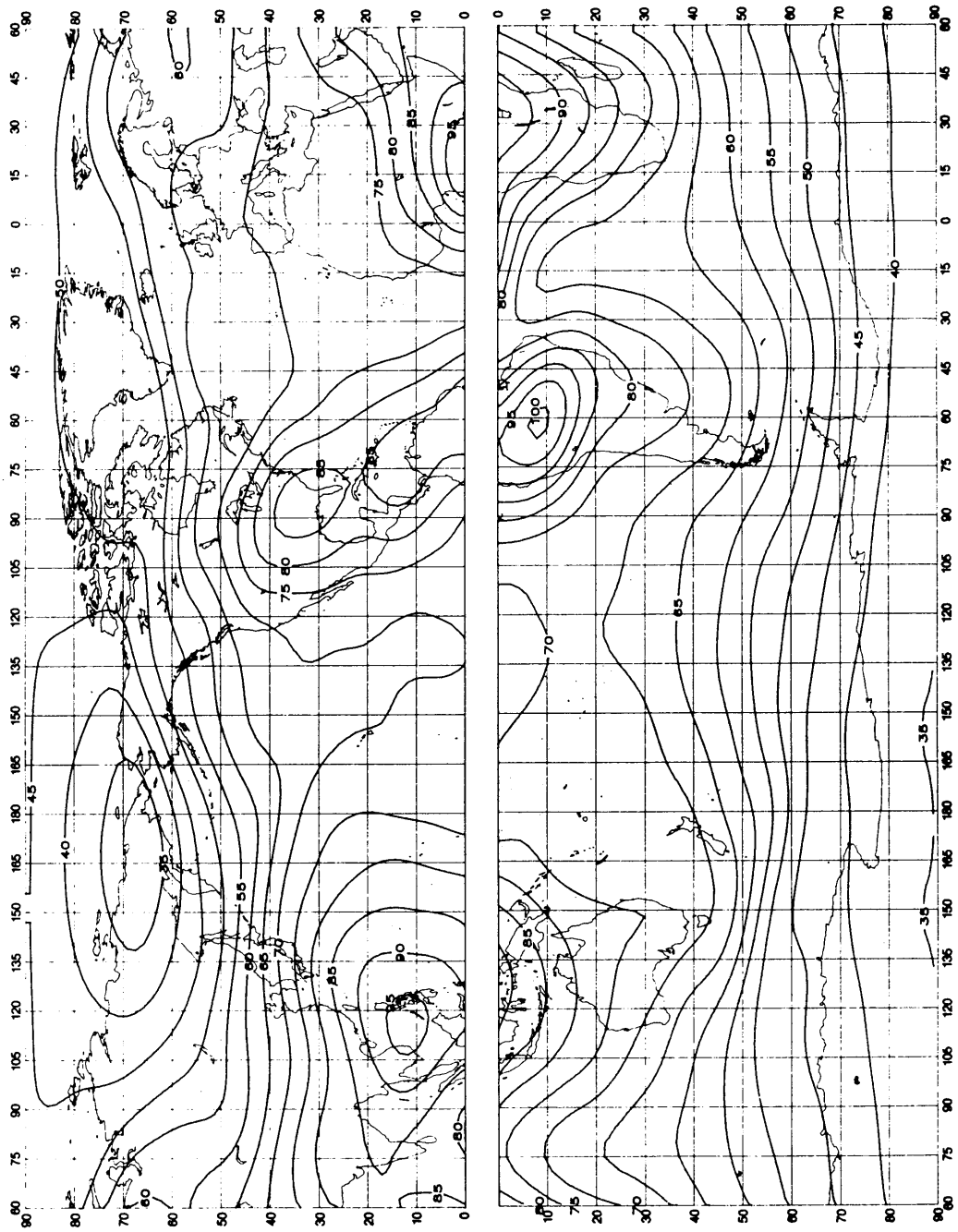

0372-21a

FIGURE 21a – *Expected values of atmospheric radio noise, F_{am} (dB above kT_0b at 1 MHz) (Spring; 0000-0400 LT)*

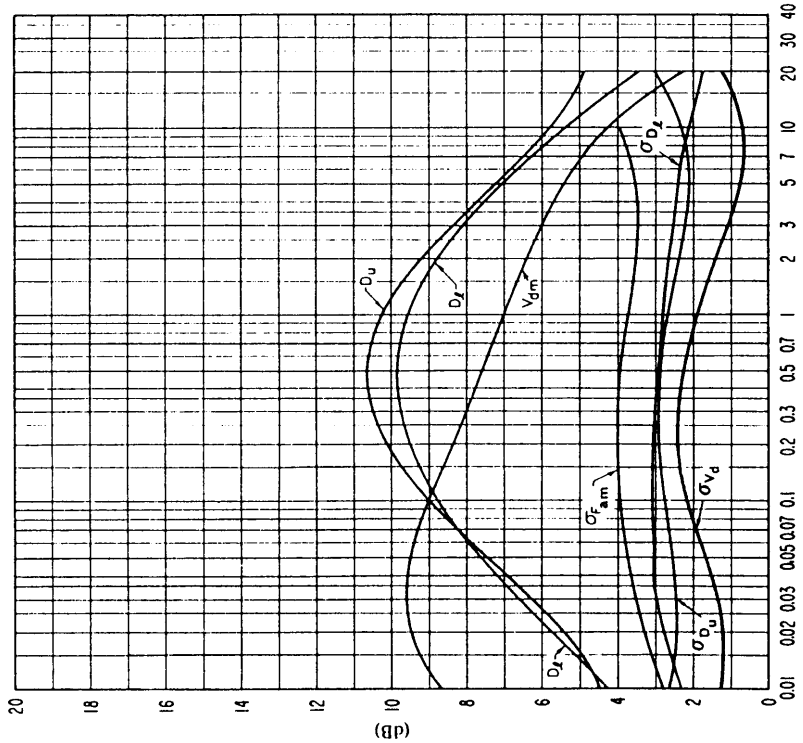

FIGURE 21c – *Data on noise variability and character*
(Spring; 0000-0400 LT)

See legend of Fig. 15c

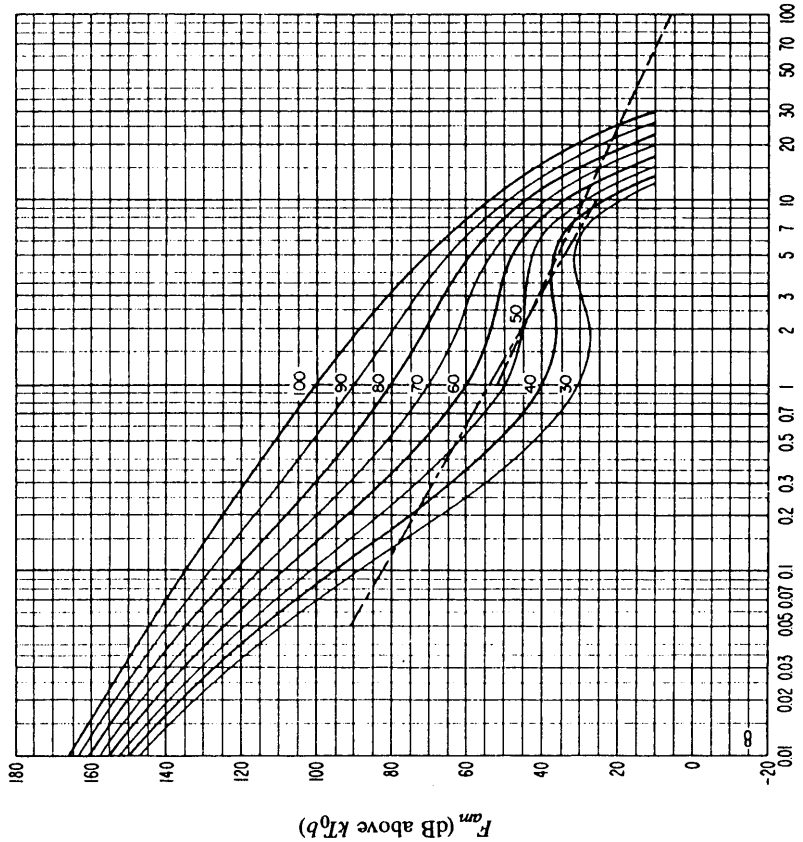

FIGURE 21b – *Variation of radio noise with frequency*
(Spring; 0000-0400 LT)

See legend of Fig. 15b

0372-21b

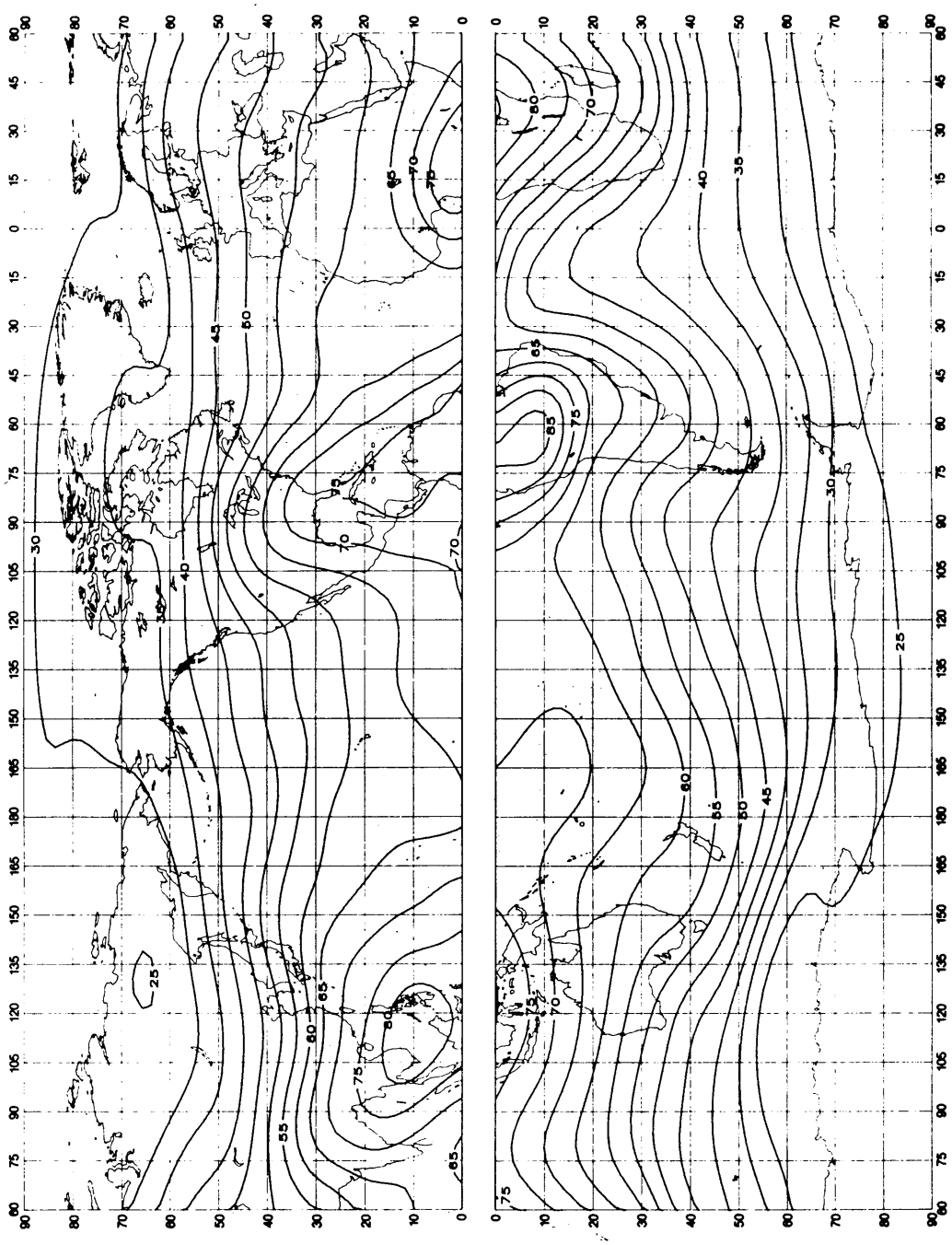

0372-22a

FIGURE 22a – *Expected values of atmospheric radio noise, F_{am} (dB above kT_0b at 1 MHz) (Spring; 0400-0800 LT)*

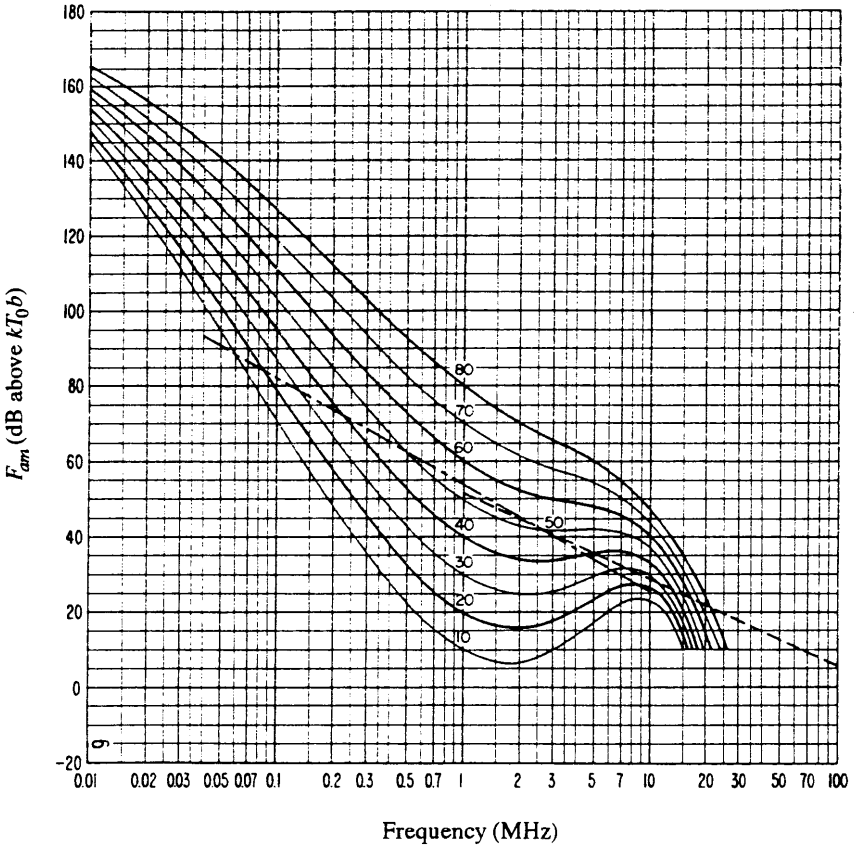

FIGURE 22b – *Variation of radio noise with frequency*
(Spring; 0400-0800 LT)

See legend of Fig. 15b

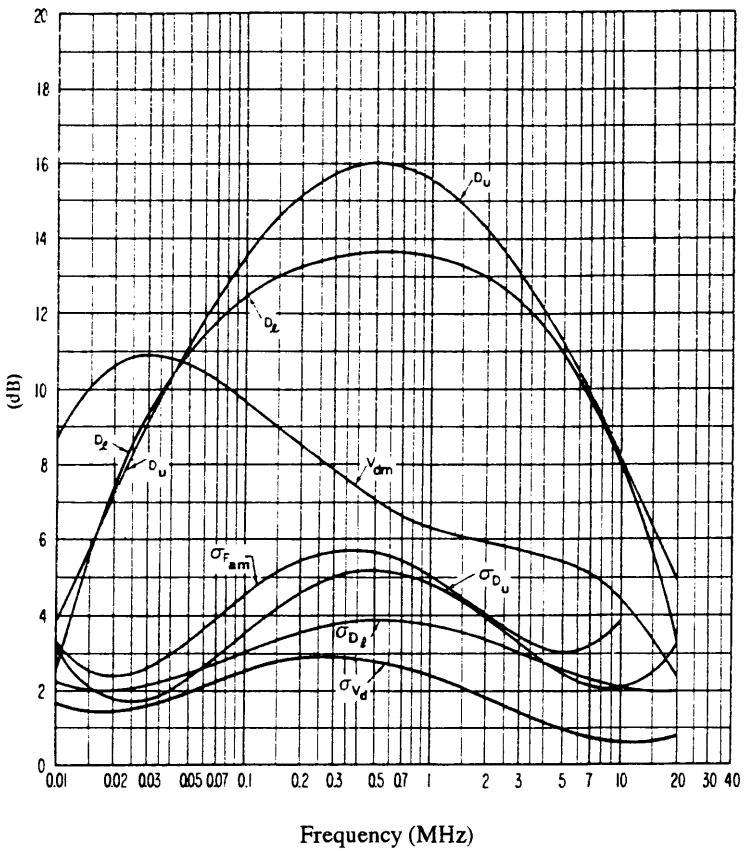

FIGURE 22c – *Data on noise variability and character*
(Spring; 0400-0800 LT)

See legend of Fig. 15c

0372-22b

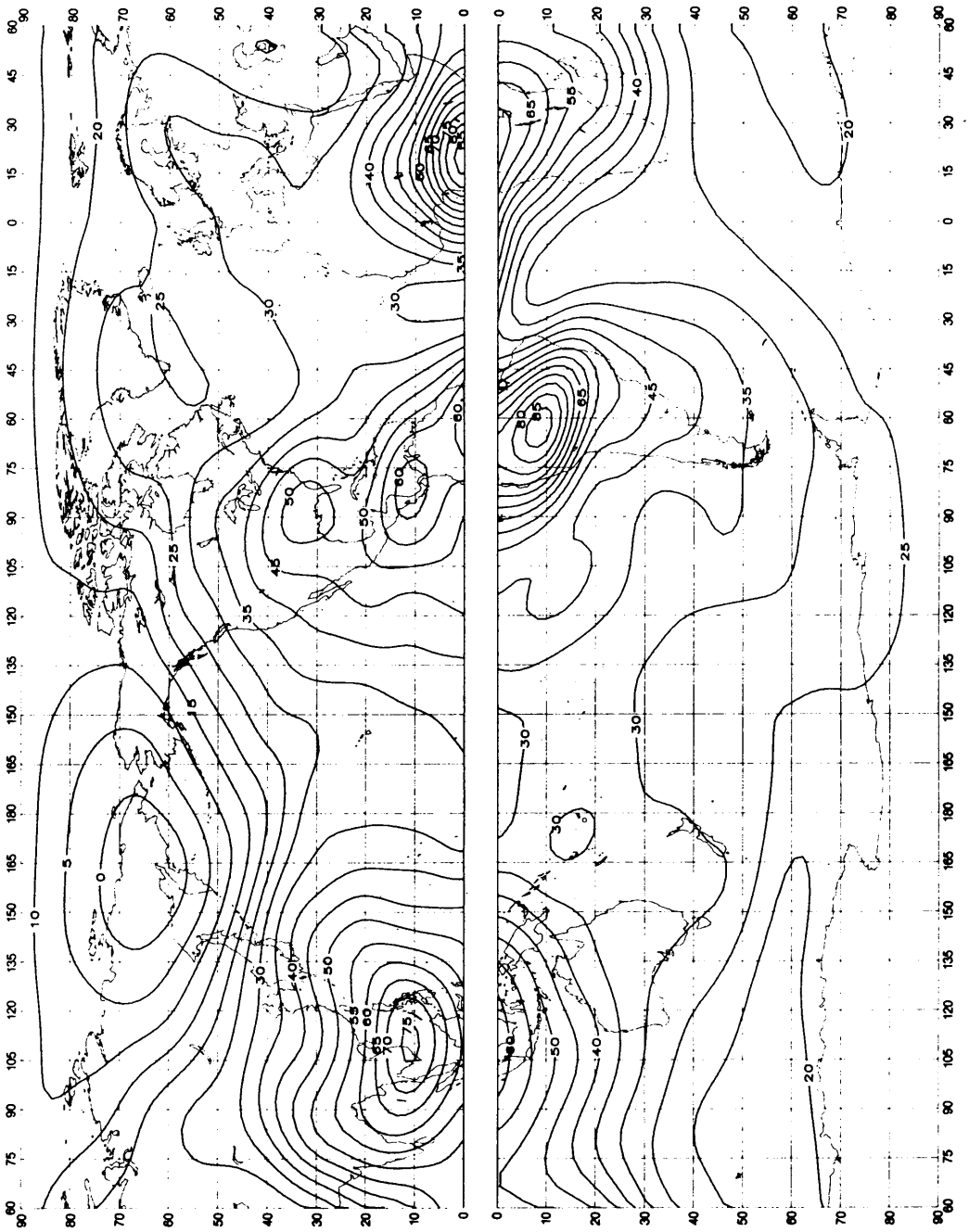

0372-23a

FIGURE 23a – *Expected values of atmospheric radio noise, F_{am} (dB above kT_0b at 1 MHz) (Spring; 0800-1200 LT)*

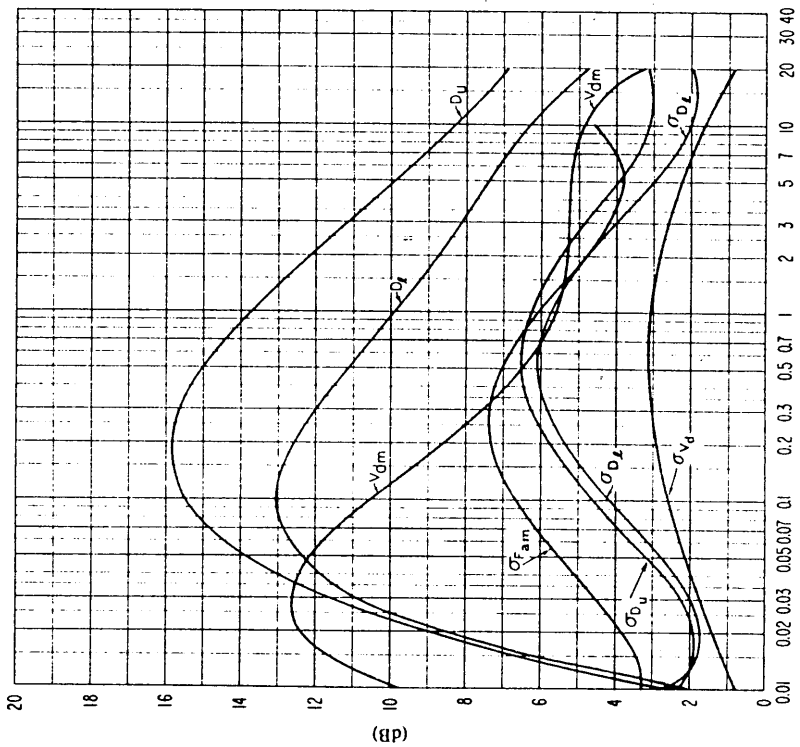

FIGURE 23c – *Data on noise variability and character (Spring; 0800-1200 LT)*

See legend of Fig. 15c

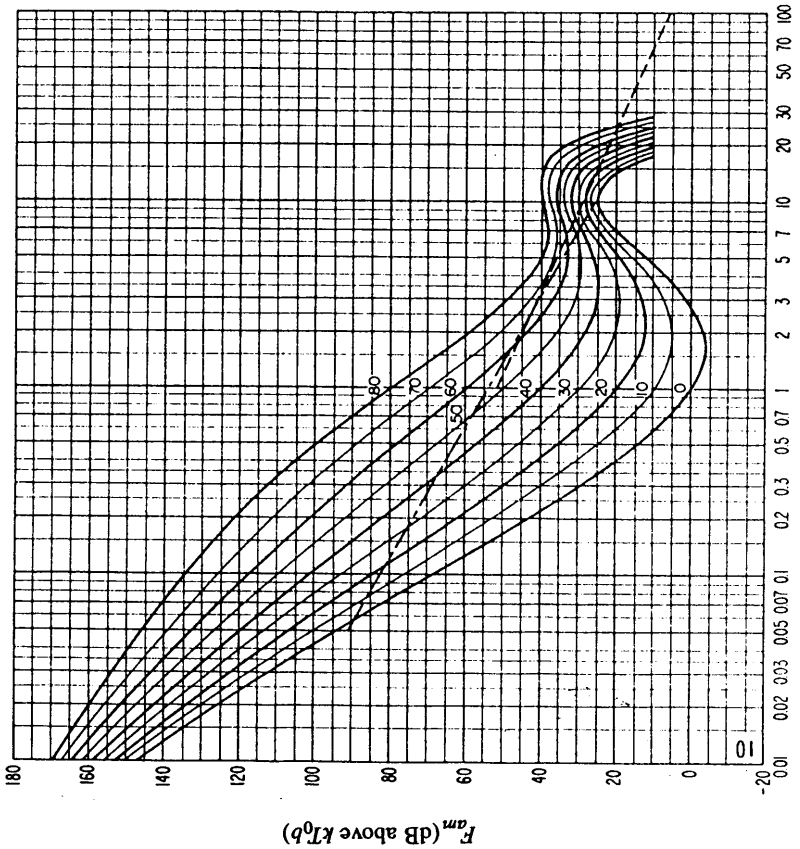

FIGURE 23b – *Variation of radio noise with frequency (Spring; 0800-1200 LT)*

See legend of Fig. 15b

0372-23b

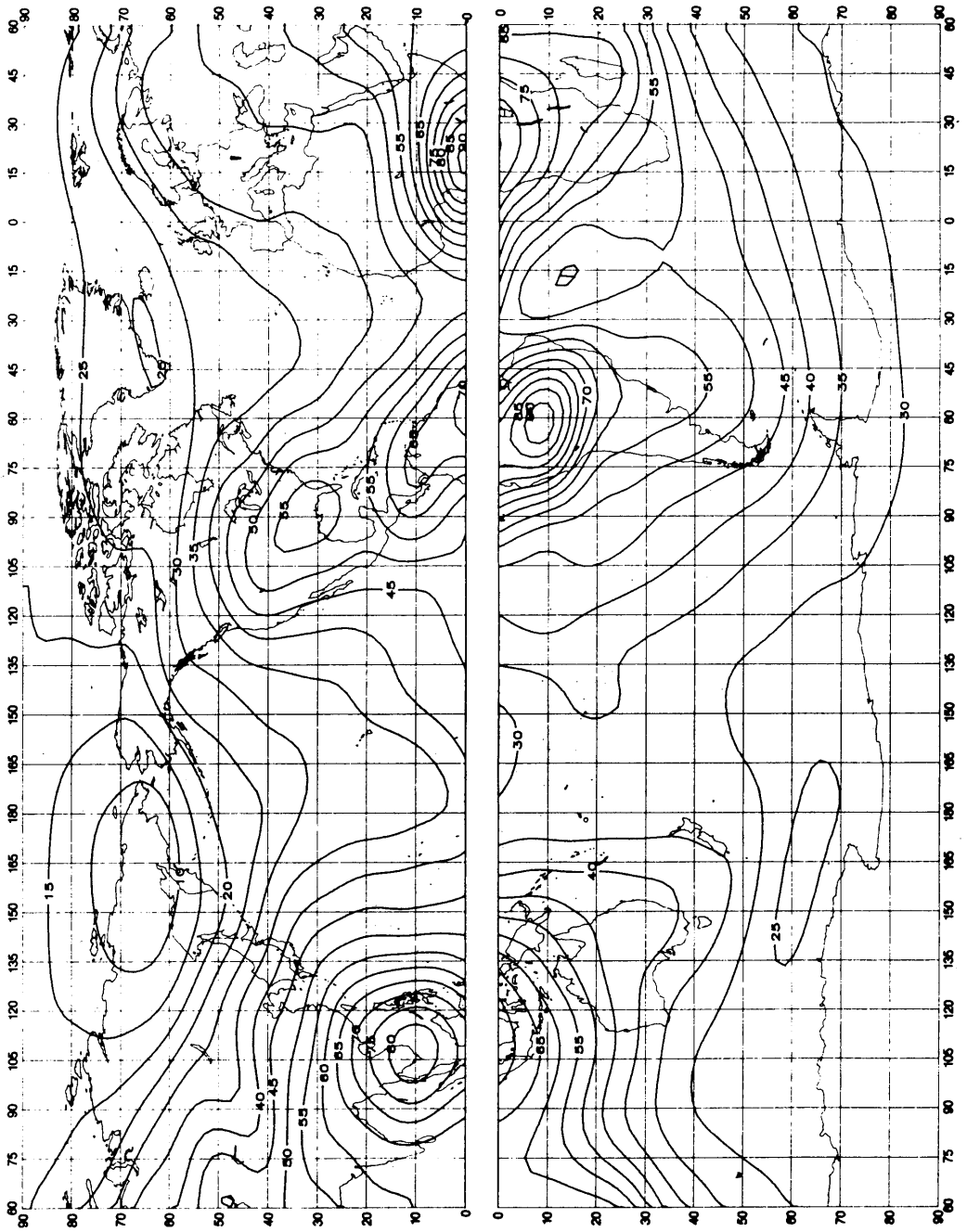

0372-24a

FIGURE 24a – *Expected values of atmospheric radio noise, F_{am} (dB above kT_0b at 1 MHz) (Spring; 1200-1600 LT)*

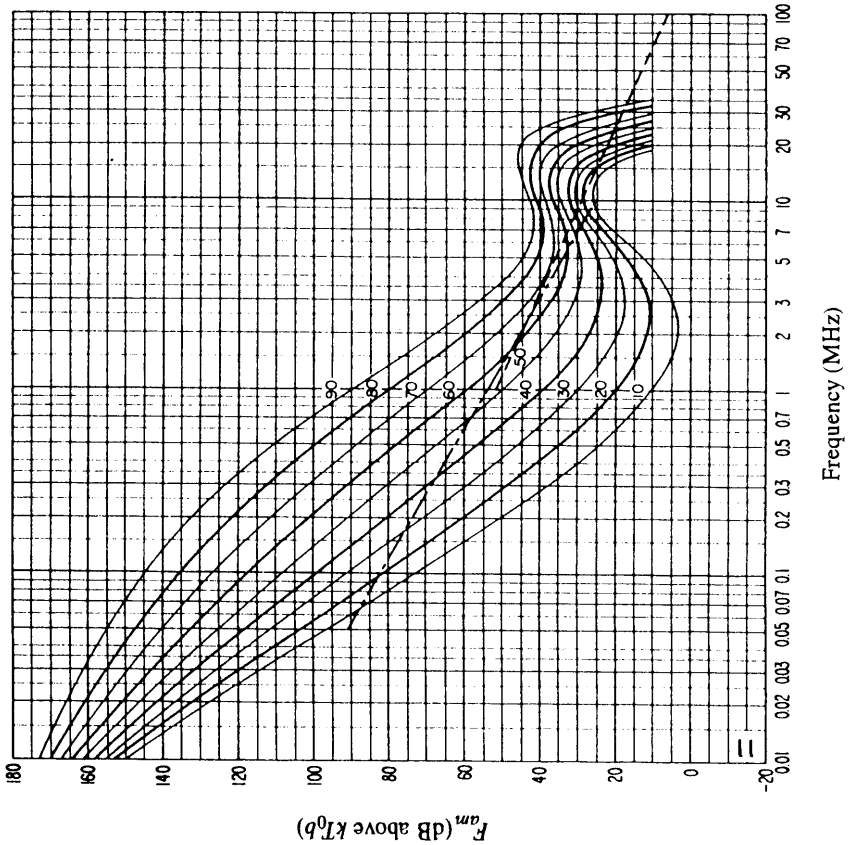

FIGURE 24b – *Variation of radio noise with frequency*
(Spring; 1200-1600 LT)

See legend of Fig. 15b

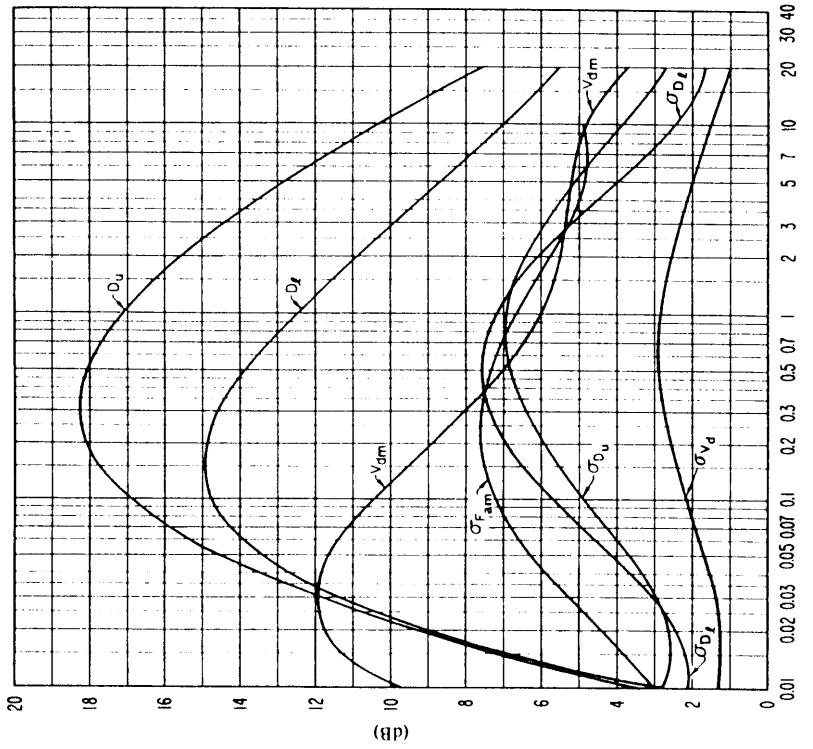

FIGURE 24c – *Data on noise variability and character*
(Spring; 1200-1600 LT)

See legend of Fig. 15c

0372-24b

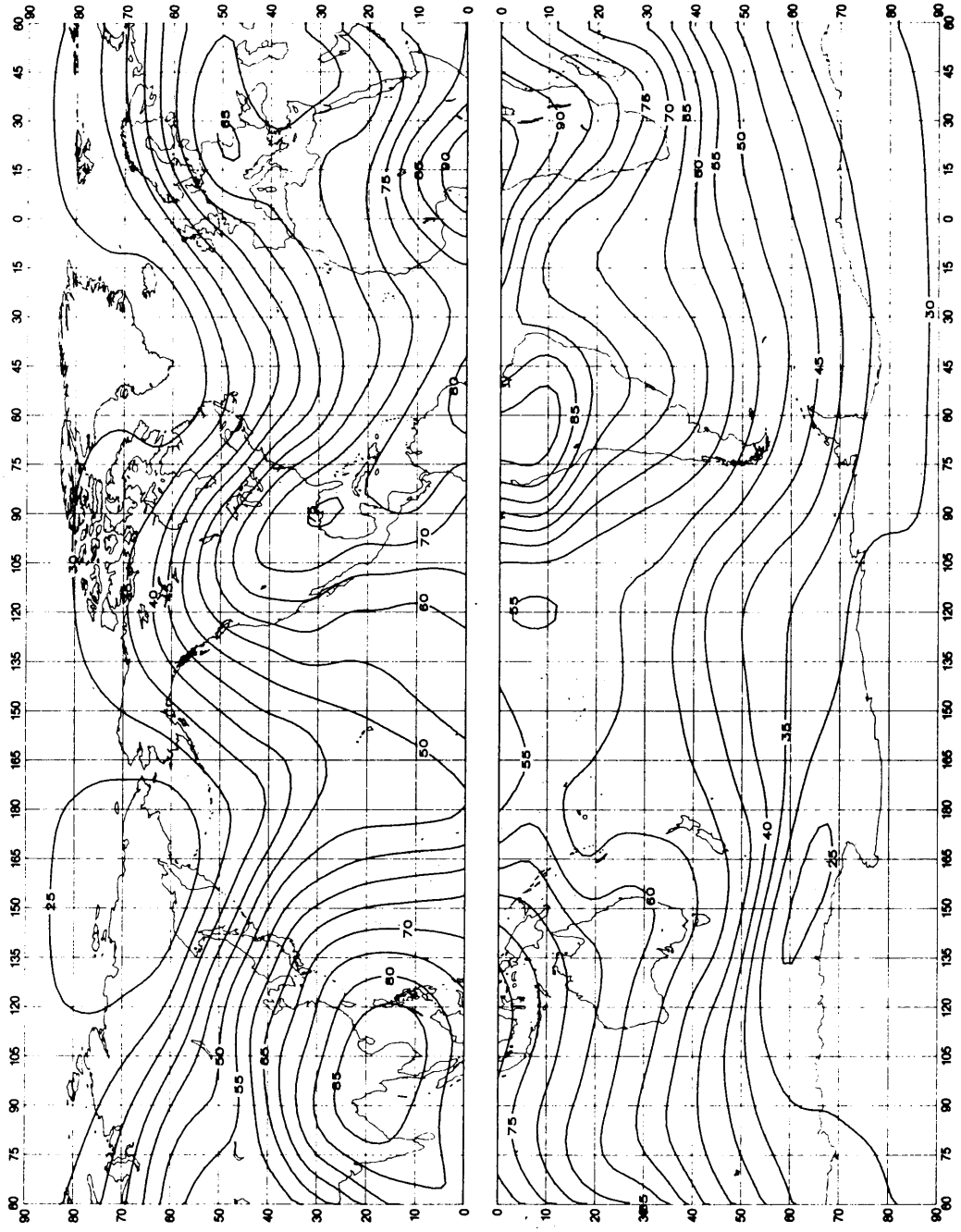

0372-25a

FIGURE 25a – *Expected values of atmospheric radio noise, F_{am} (dB above kT_0b at 1 MHz) (Spring; 1600-2000 LT)*

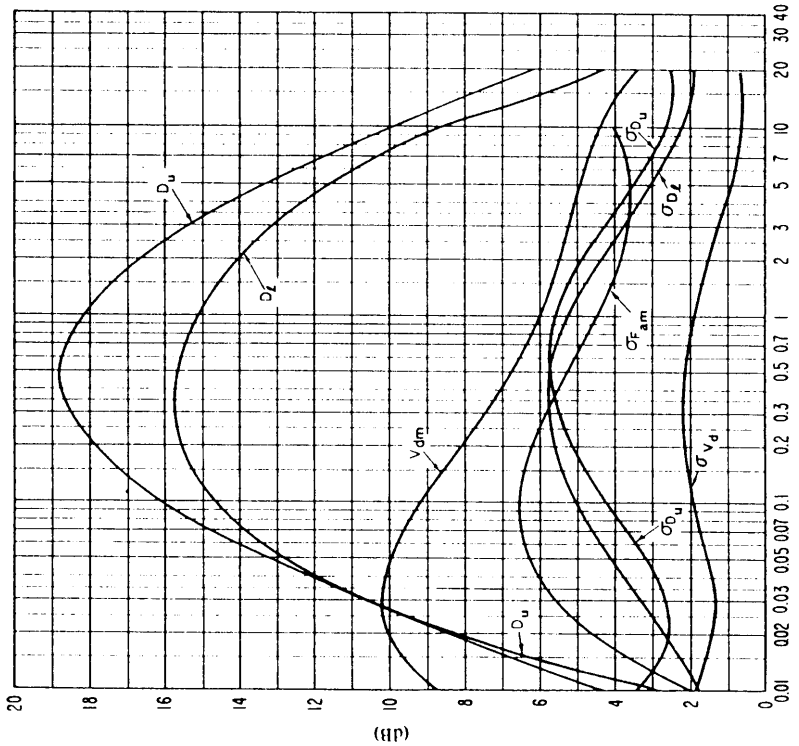

FIGURE 25c – *Data on noise variability and character (Spring; 1600-2000 LT)*

See legend of Fig. 15c

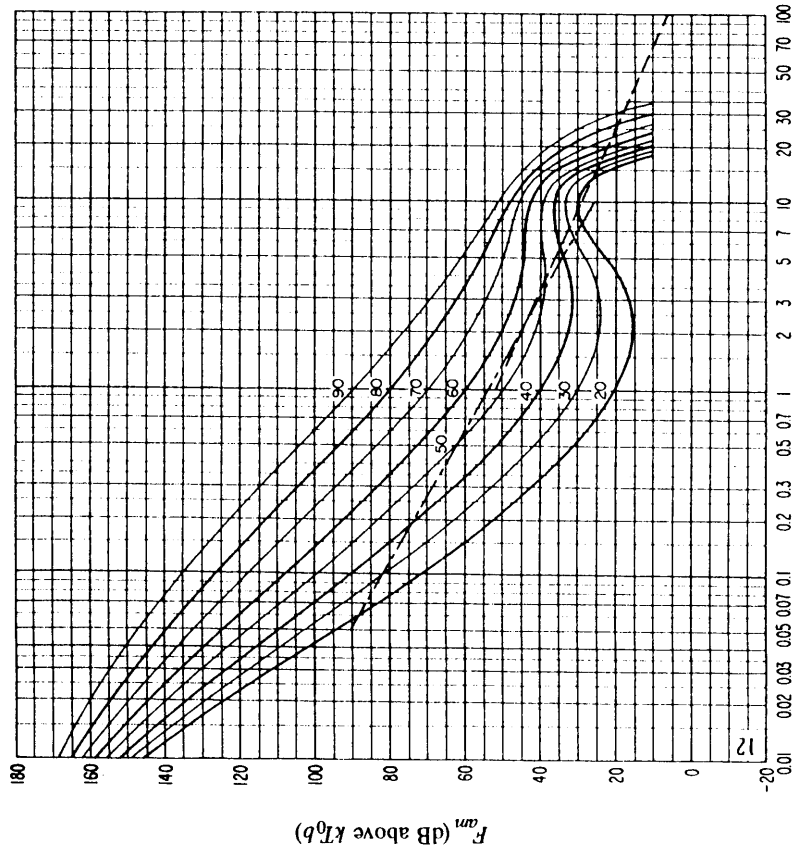

FIGURE 25b – *Variation of radio noise with frequency (Spring; 1600-2000 LT)*

See legend of Fig. 15b

0372-25b

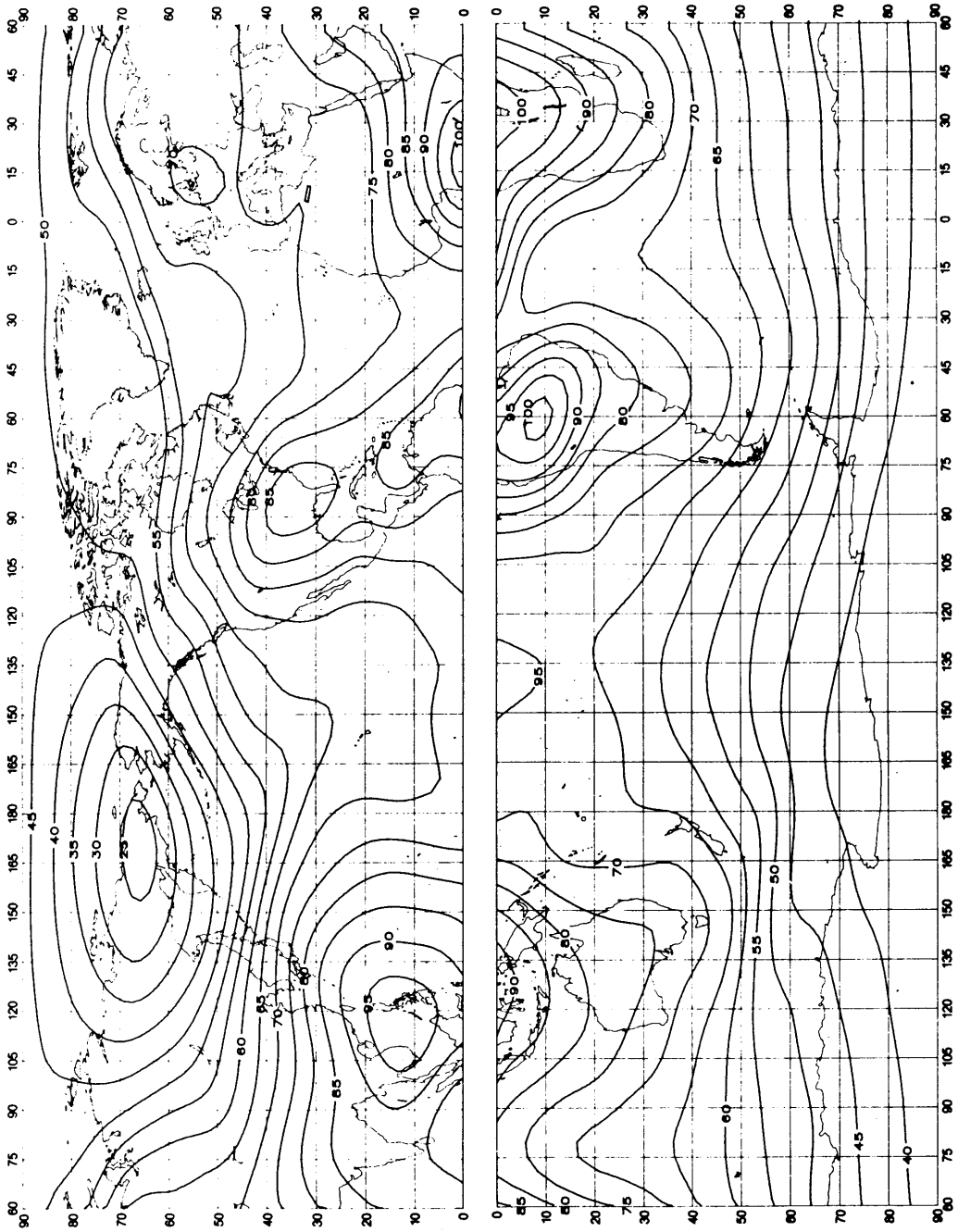

0372-26a

FIGURE 26a – *Expected values of atmospheric radio noise, F_{am} (dB above kT_0b at 1 MHz) (Spring; 2000-2400 LT)*

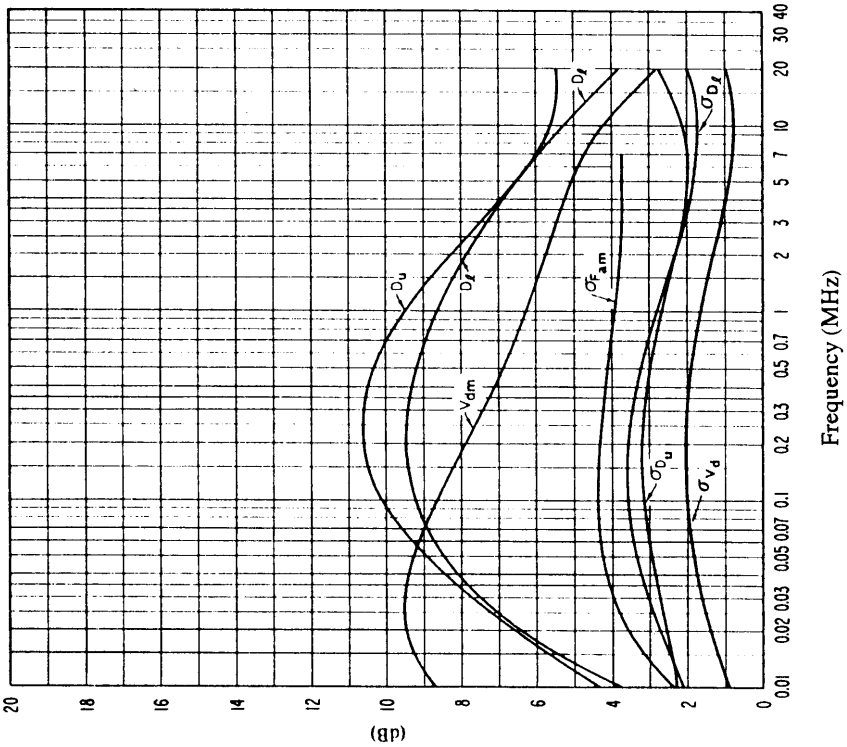

FIGURE 26c – *Data on noise variability and character (Spring; 2000-2400 LT)*

See legend of Fig. 15c

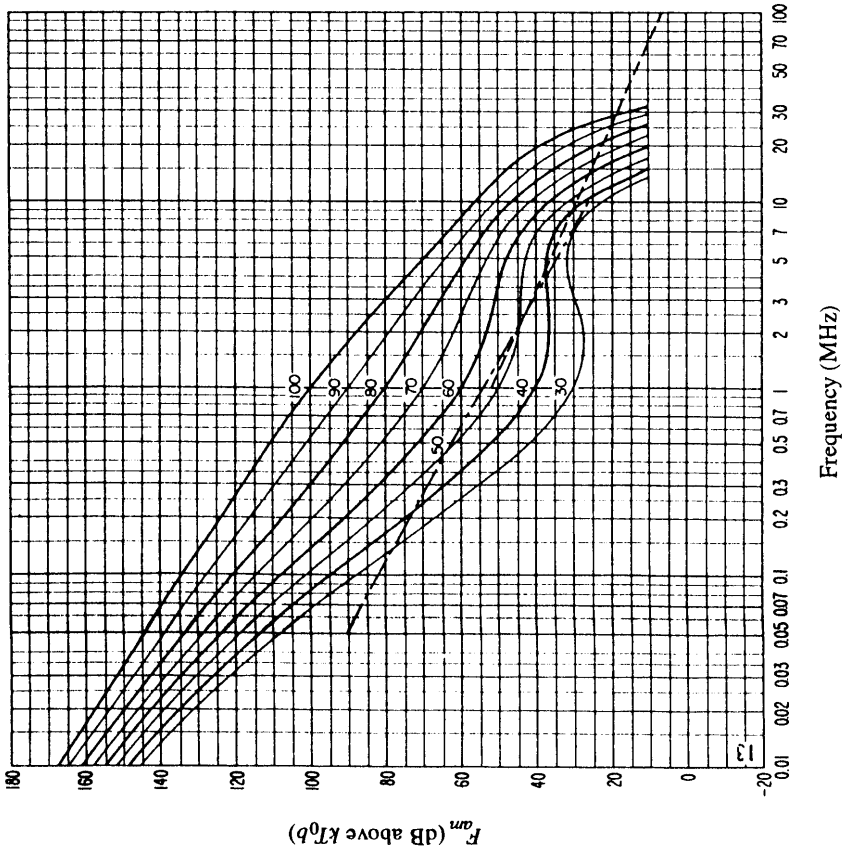

FIGURE 26b – *Variation of radio noise with frequency (Spring; 2000-2400 LT)*

See legend of Fig. 15b

0372-26b

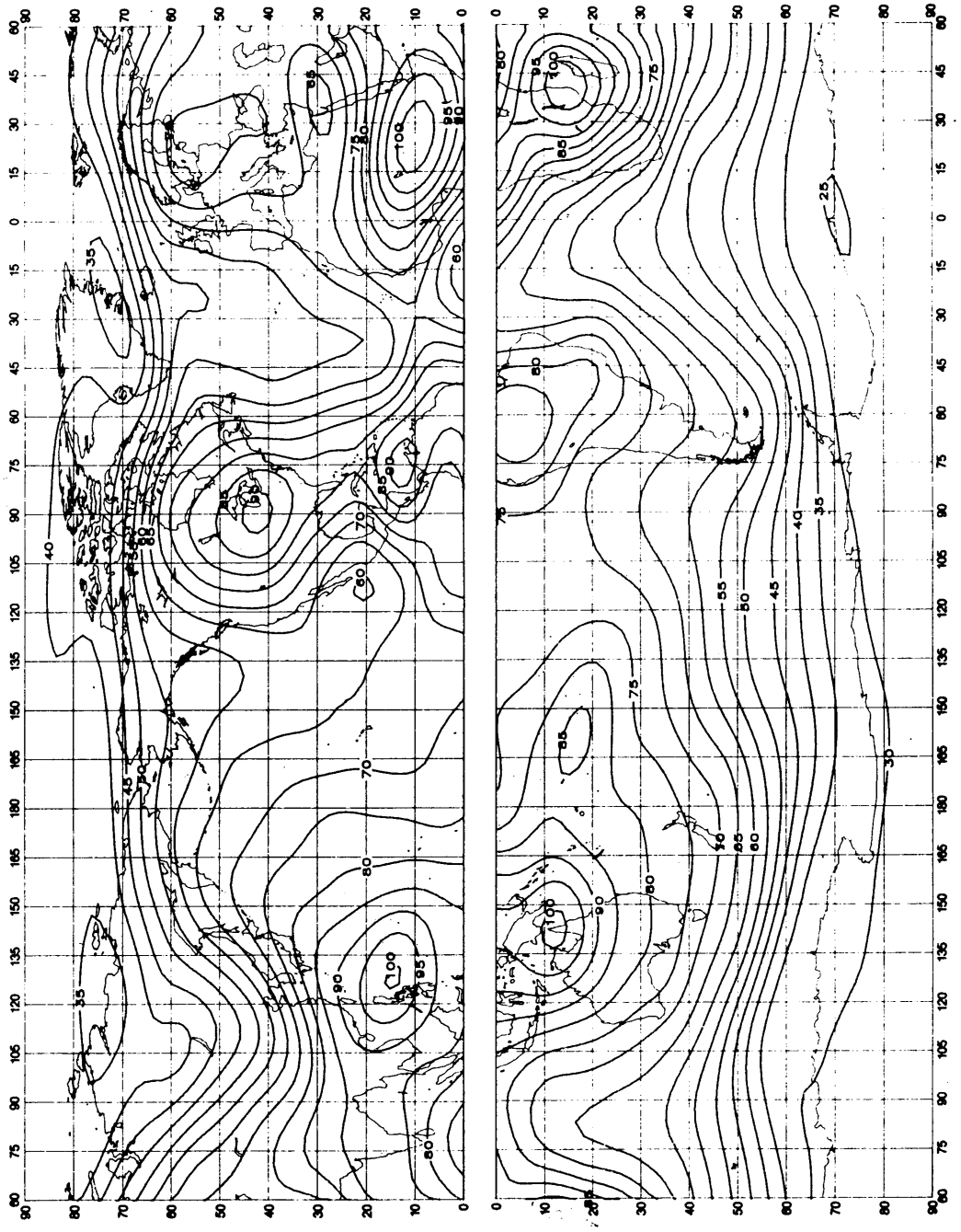

0372-27a

FIGURE 27a – *Expected values of atmospheric radio noise, F_{am} (dB above kT_0b at 1 MHz) (Summer; 0000-0400 LT)*

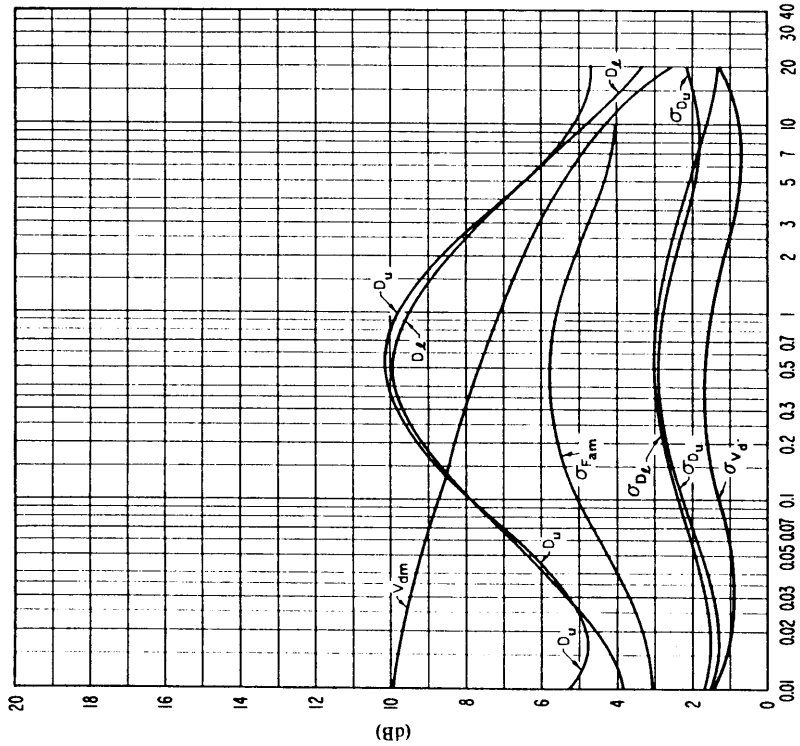

FIGURE 27c – *Data on noise variability and character*
(Summer; 0000-0400 LT)

See legend of Fig. 15c

0372-27b

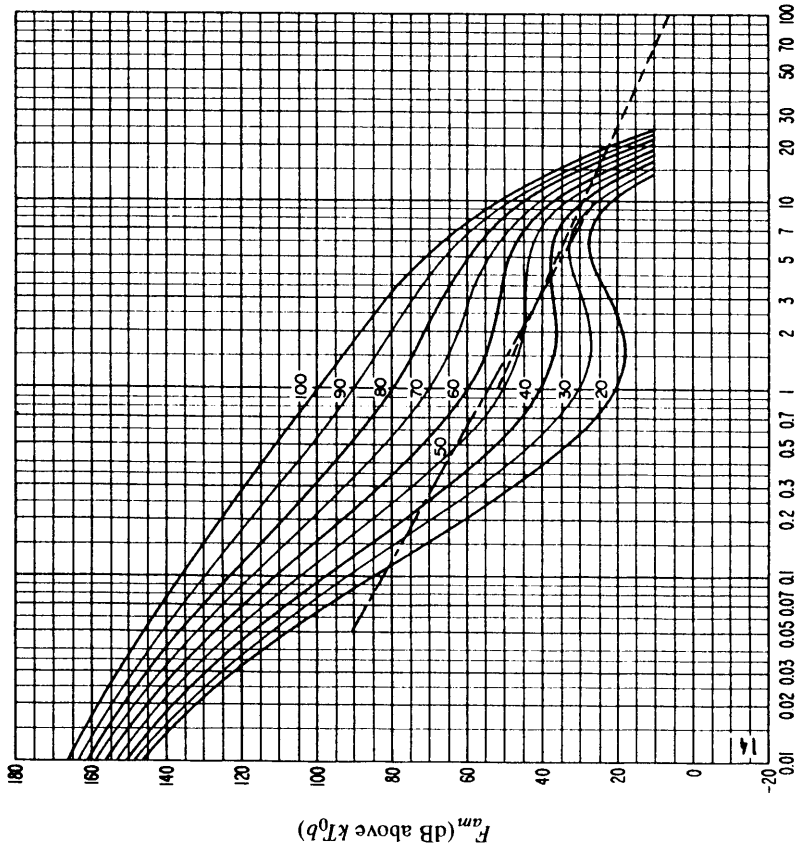

FIGURE 27b – *Variation of radio noise with frequency*
(Summer; 0000-0400 LT)

See legend of Fig. 15b

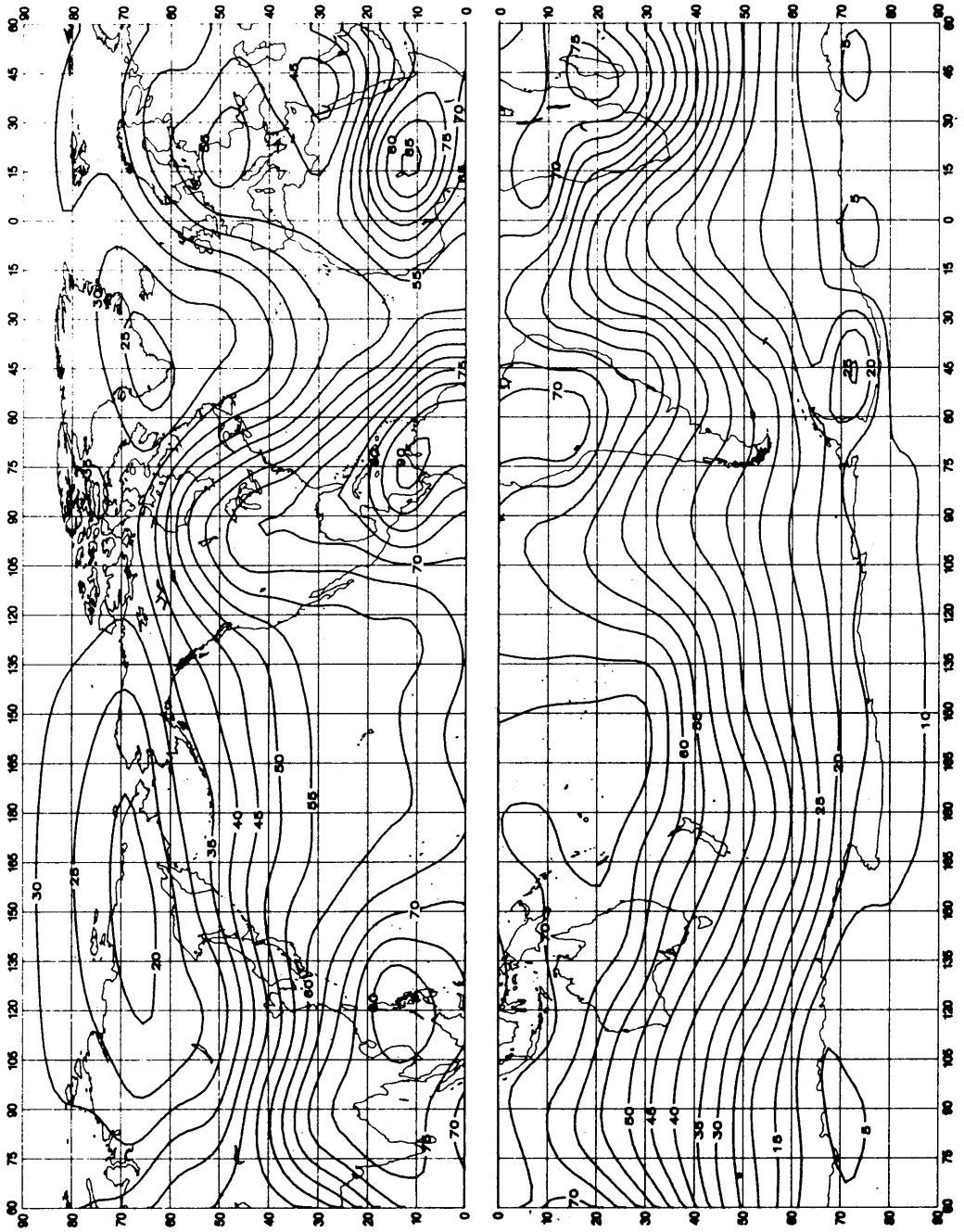

0372-28a

FIGURE 28a – *Expected values of atmospheric radio noise, F_{am} (dB above kT_0b at 1 MHz) (Summer; 0400-0800 LT)*

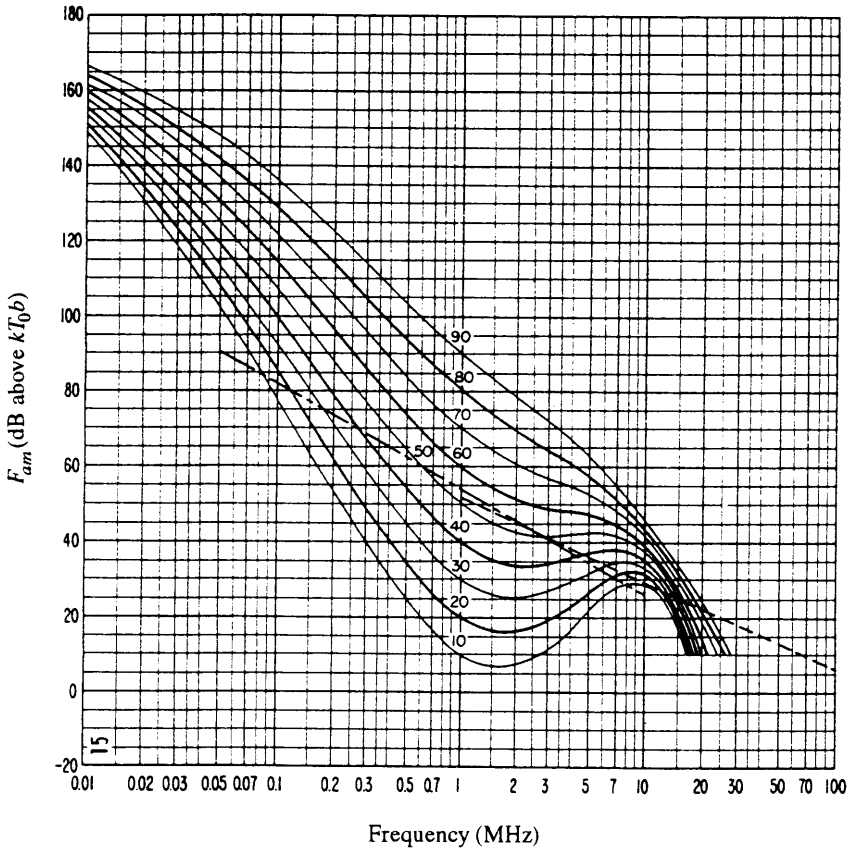

FIGURE 28b – *Variation of radio noise with frequency*
(Summer; 0400-0800 LT)

See legend of Fig. 15b

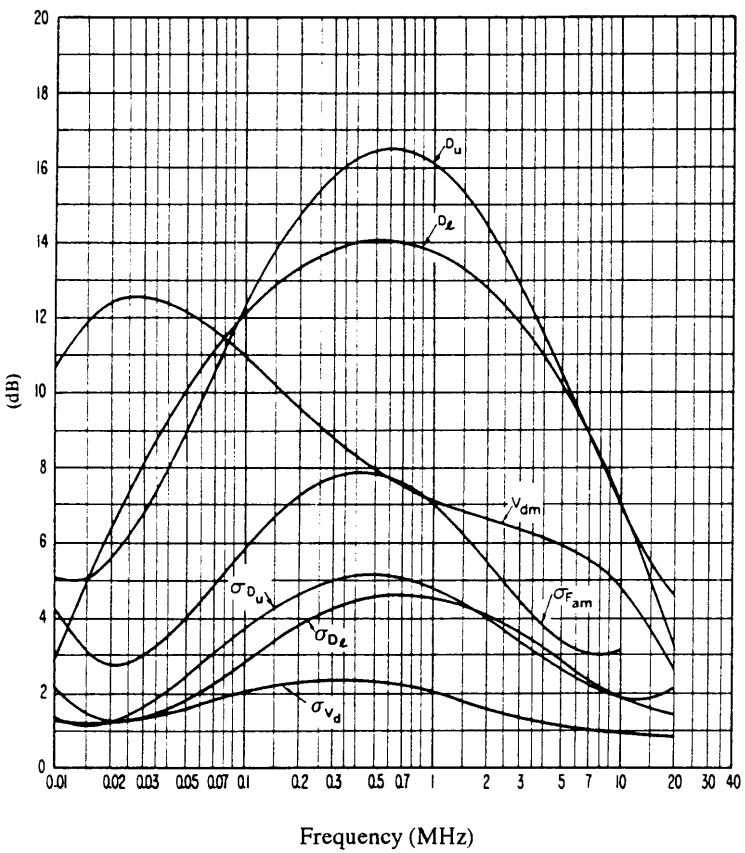

FIGURE 28c – *Data on noise variability and character*
(Summer; 0400-0800 LT)

0372-28b

See legend of Fig. 15c

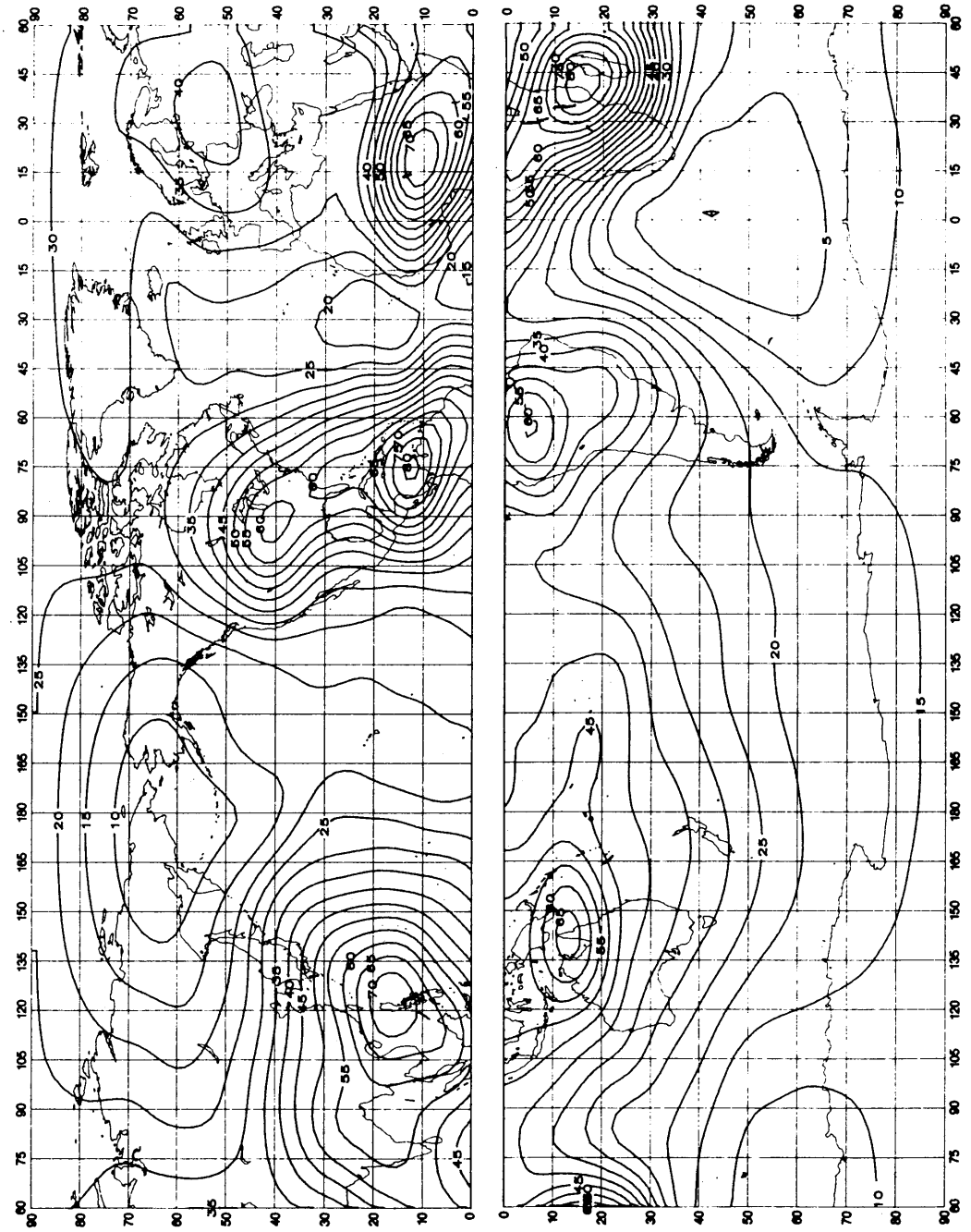

0372-29a

FIGURE 29a – *Expected values of atmospheric radio noise, F_{am} (dB above kT_0b at 1 MHz) (Summer; 0800-1200 LT)*

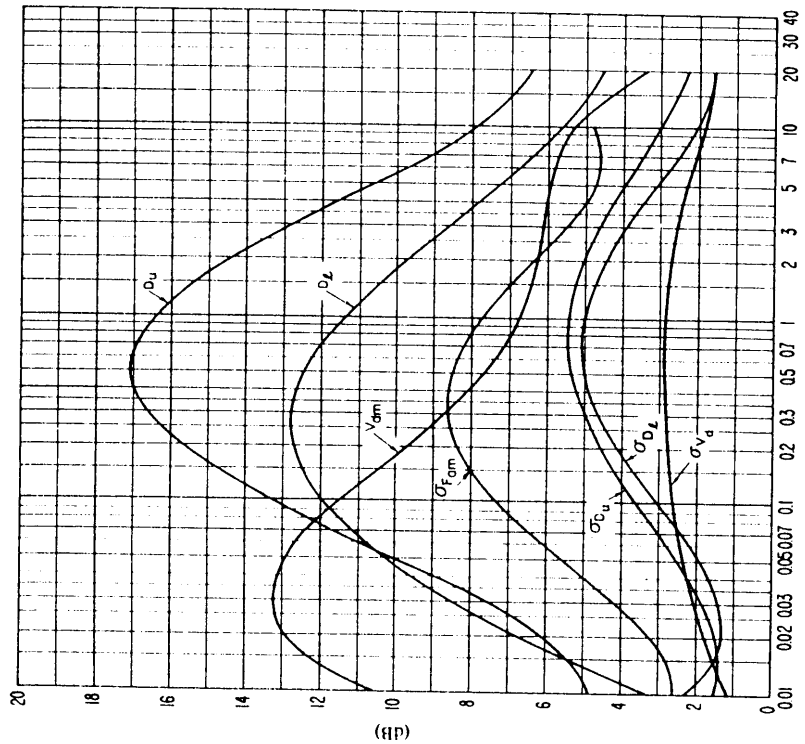

FIGURE 29c – *Data on noise variability and character (Summer; 0800-1200 LT)*

See legend of Fig. 15c

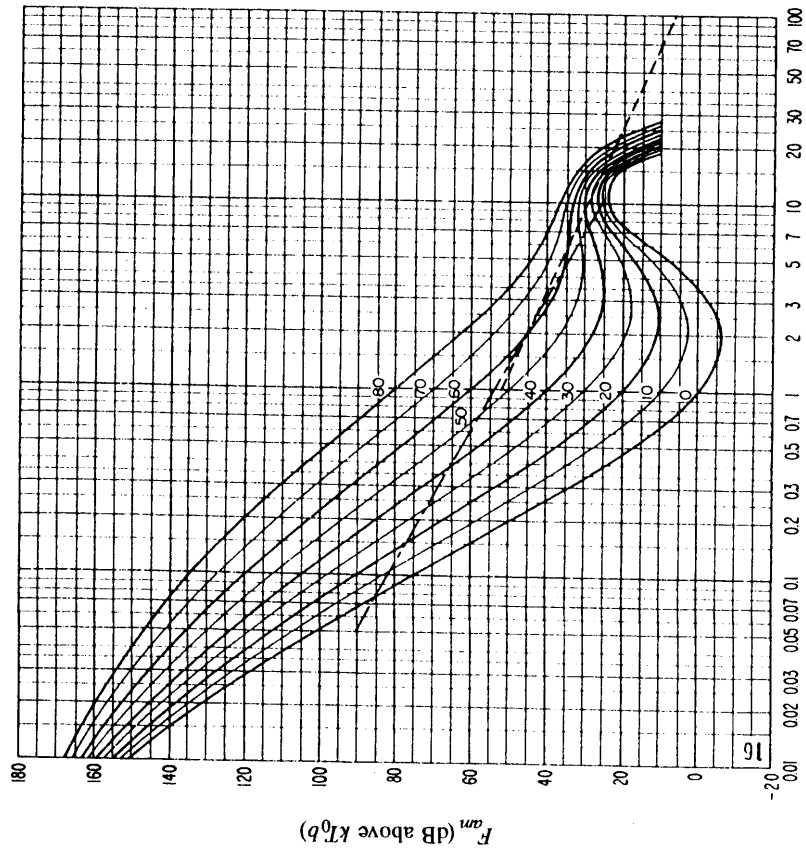

FIGURE 29b – *Variation of radio noise with frequency (Summer; 0800-1200 LT)*

See legend of Fig. 15b

0372-29b

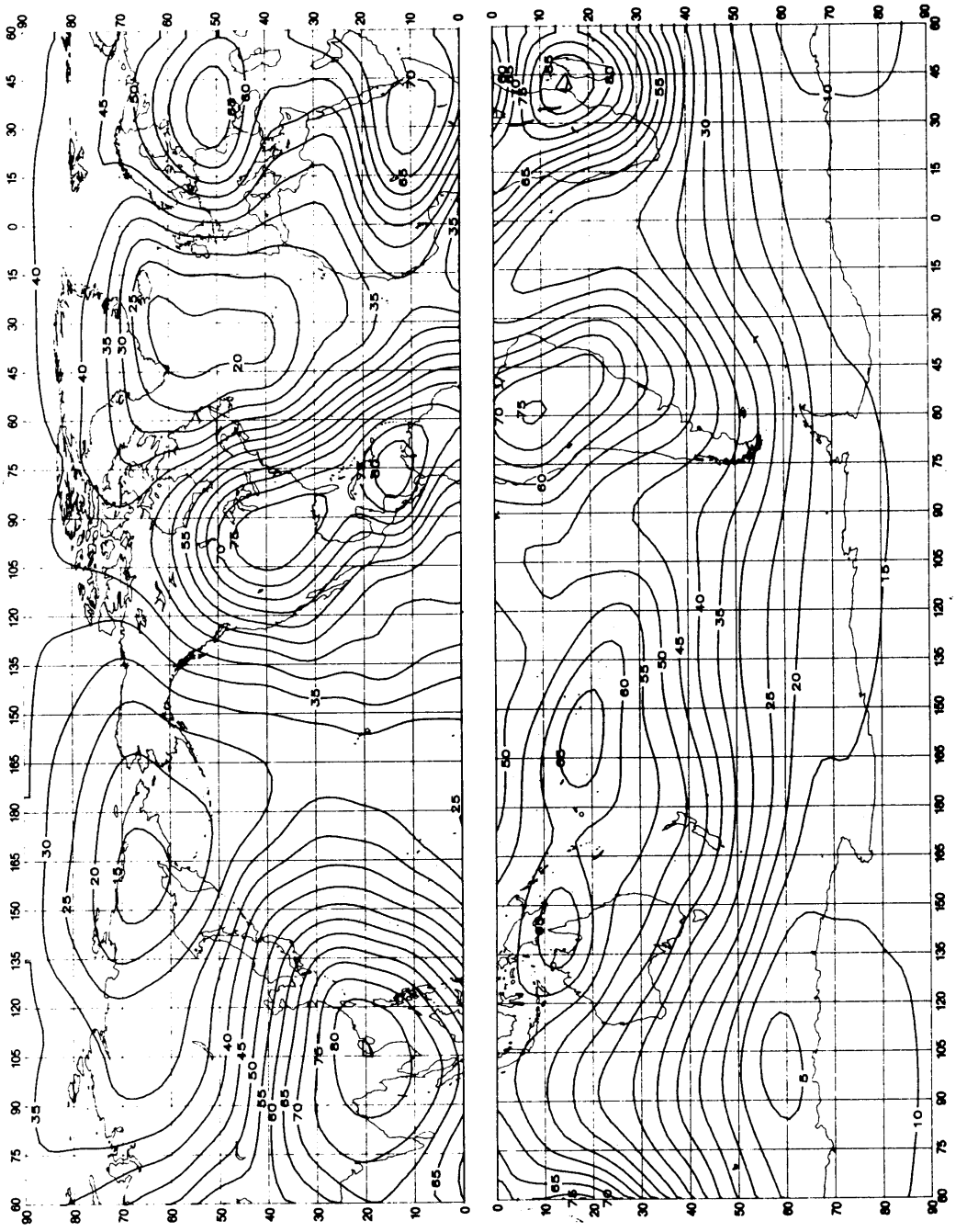

0372-30a

FIGURE 30a – *Expected values of atmospheric radio noise, F_{am} (dB above kT_0b at 1 MHz) (Summer; 1200-1600 LT)*

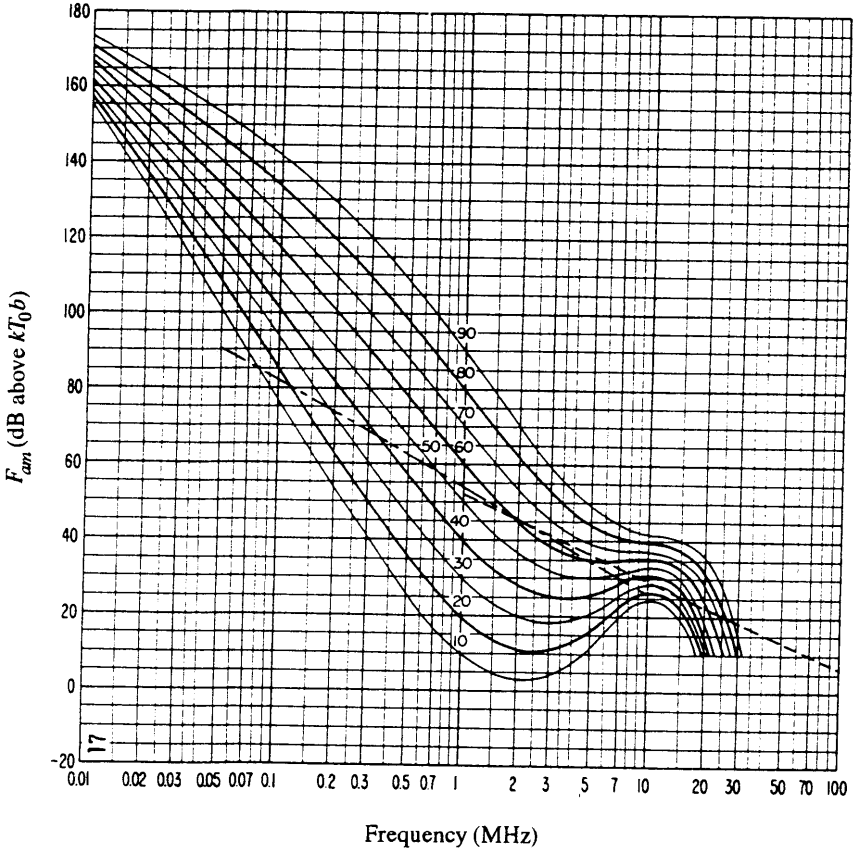

FIGURE 30b – *Variation of radio noise with frequency*
(Summer; 1200-1600 LT)

See legend of Fig. 15b

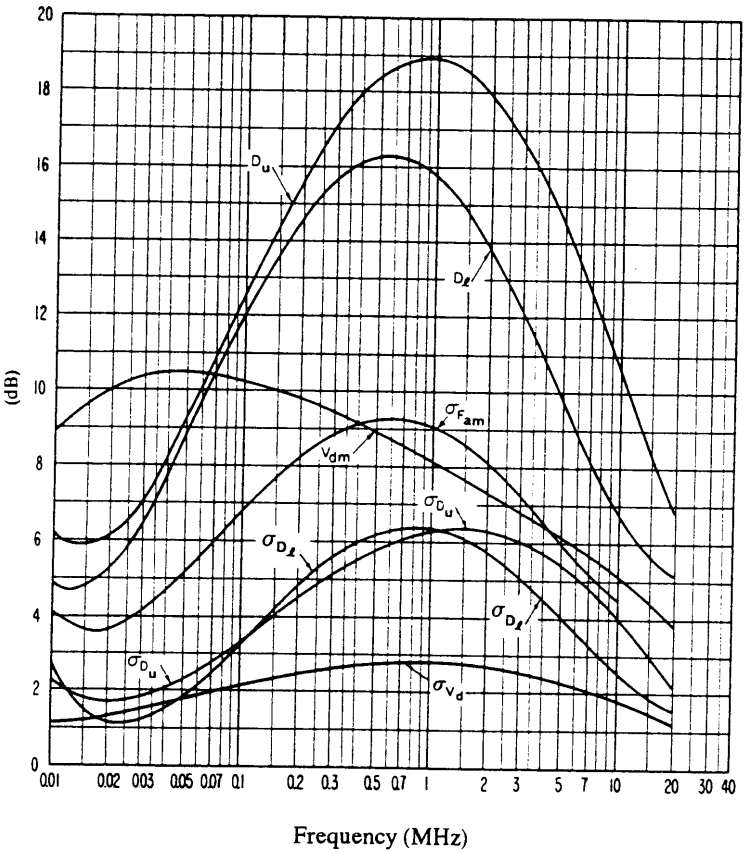

FIGURE 30c – *Data on noise variability and character*
(Summer; 1200-1600 LT)

See legend of Fig. 15c

0372-30b

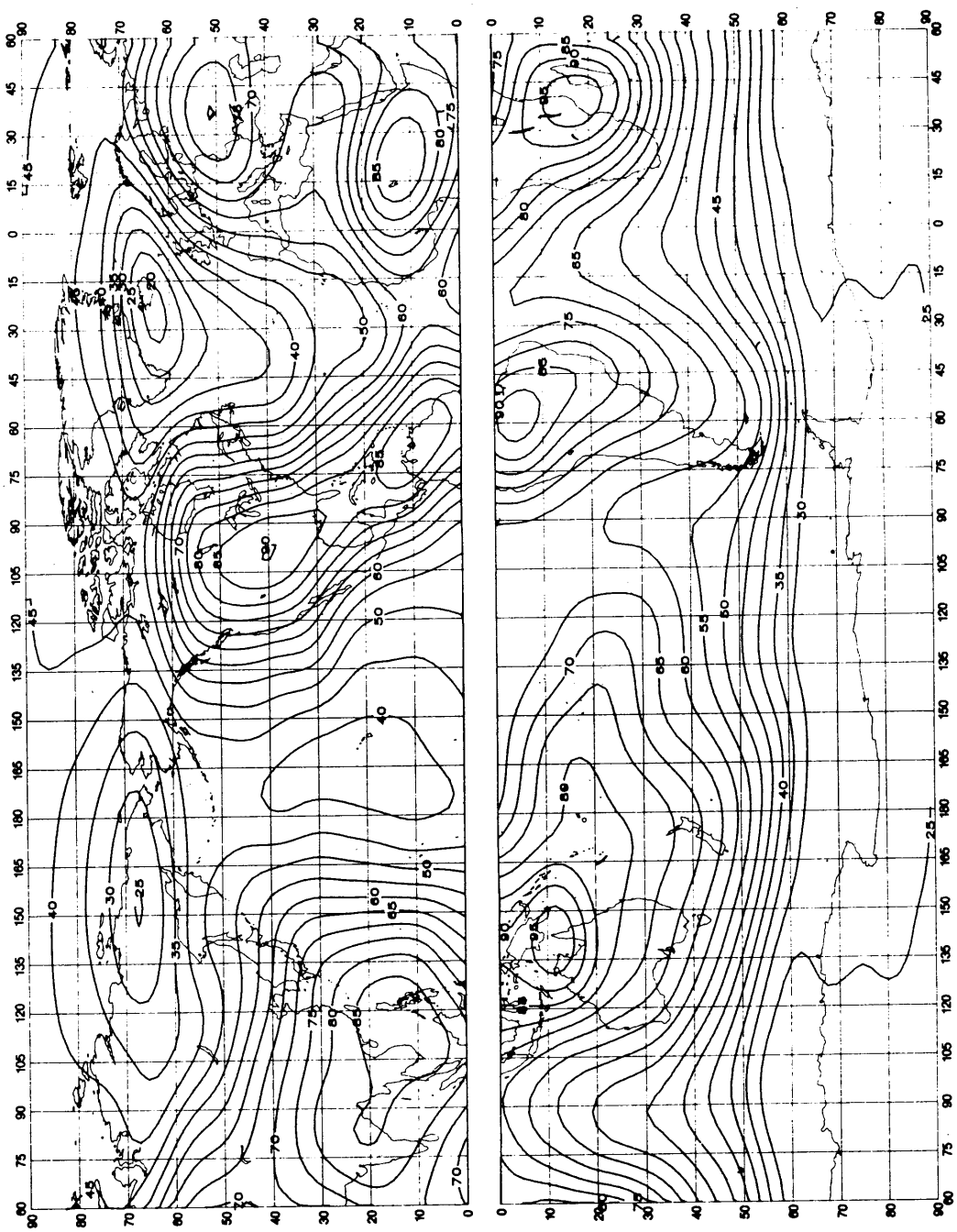

0372-31a

FIGURE 31a – *Expected values of atmospheric radio noise, F_{am} (dB above kT_0b at 1 MHz) (Summer; 1600-2000 LT)*

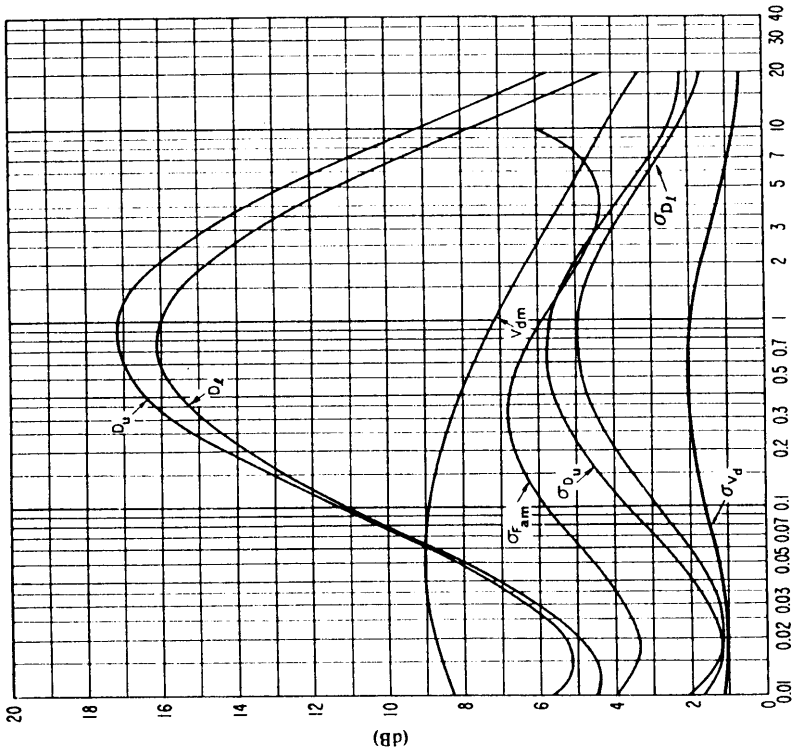

FIGURE 31c – *Data on noise variability and character*
(Summer; 1600-2000 LT)

See legend of Fig. 15c

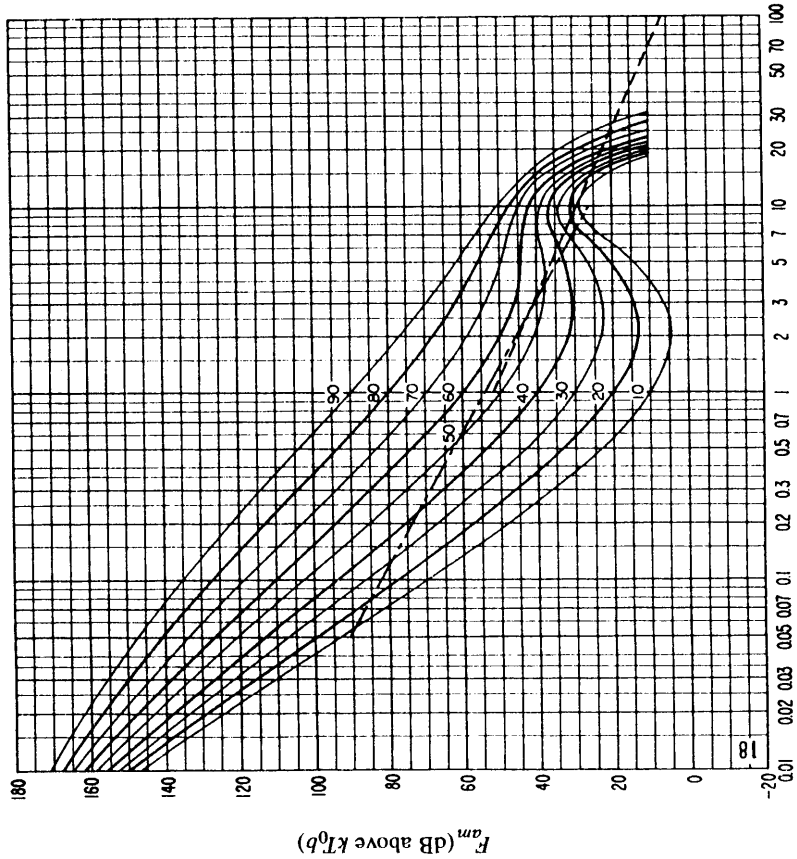

FIGURE 31b – *Variation of radio noise with frequency*
(Summer; 1600-2000 LT)

See legend of Fig. 15b

0372-31b

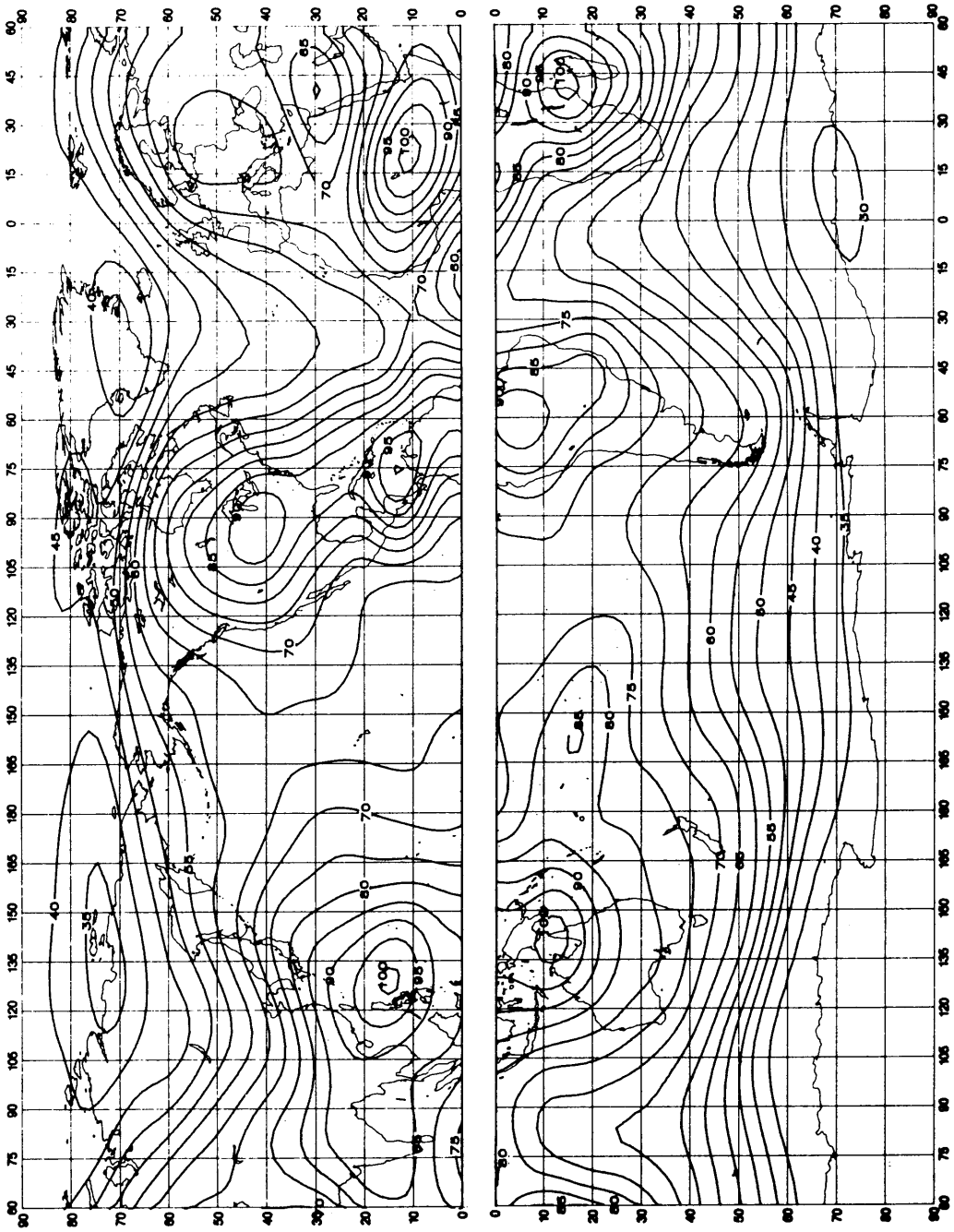

0372-32a

FIGURE 32a – *Expected values of atmospheric radio noise, F_{am} (dB above kT_0b at 1 MHz) (Summer; 2000-2400 LT)*

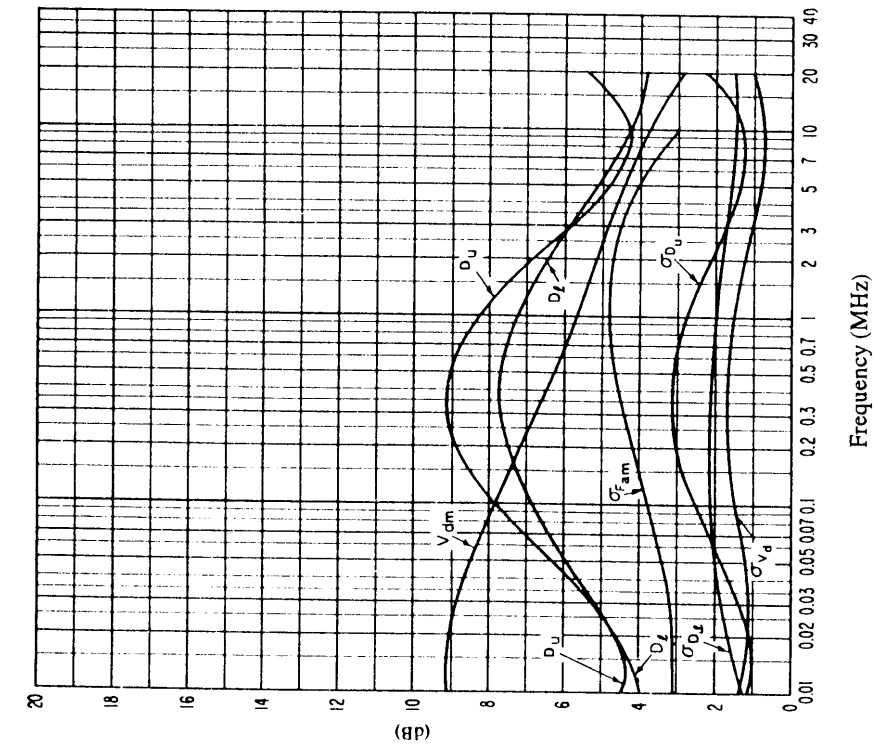

FIGURE 32c – *Data on noise variability and character (Summer; 2000-2400 LT)*

See legend of Fig. 15c

0372-32b

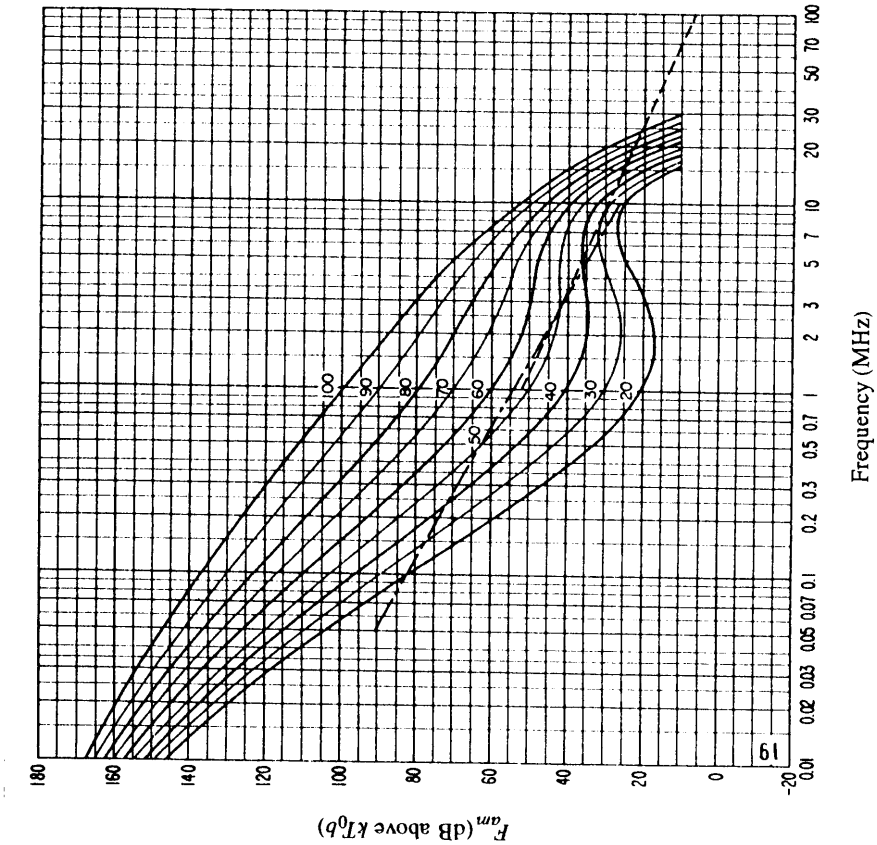

FIGURE 32b – *Variation of radio noise with frequency (Summer; 2000-2400 LT)*

See legend of Fig. 15b

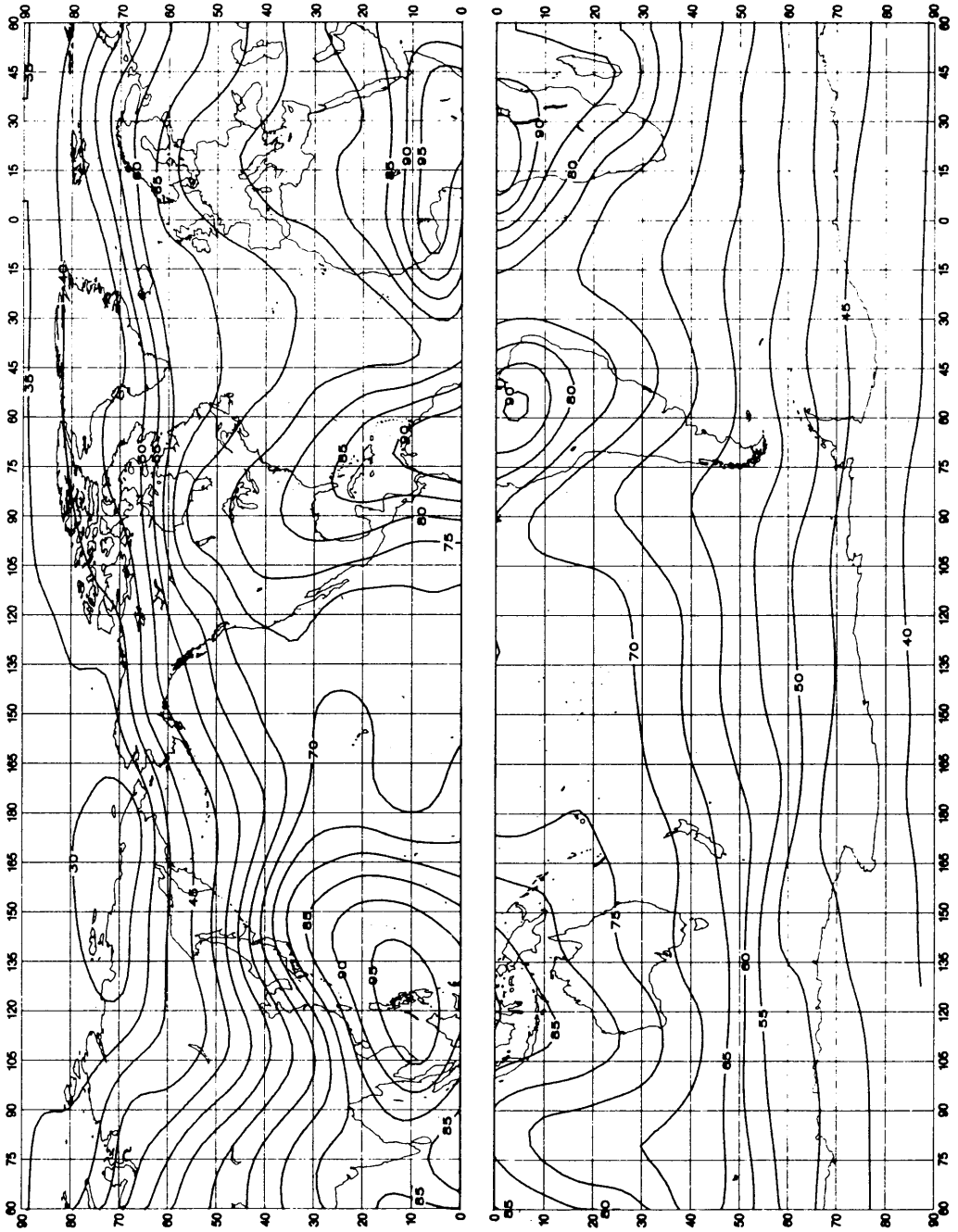

0372-33a

FIGURE 33a – *Expected values of atmospheric radio noise, F_{am} (dB above kT_0b at 1 MHz) (Autumn; 0000-0400 LT)*

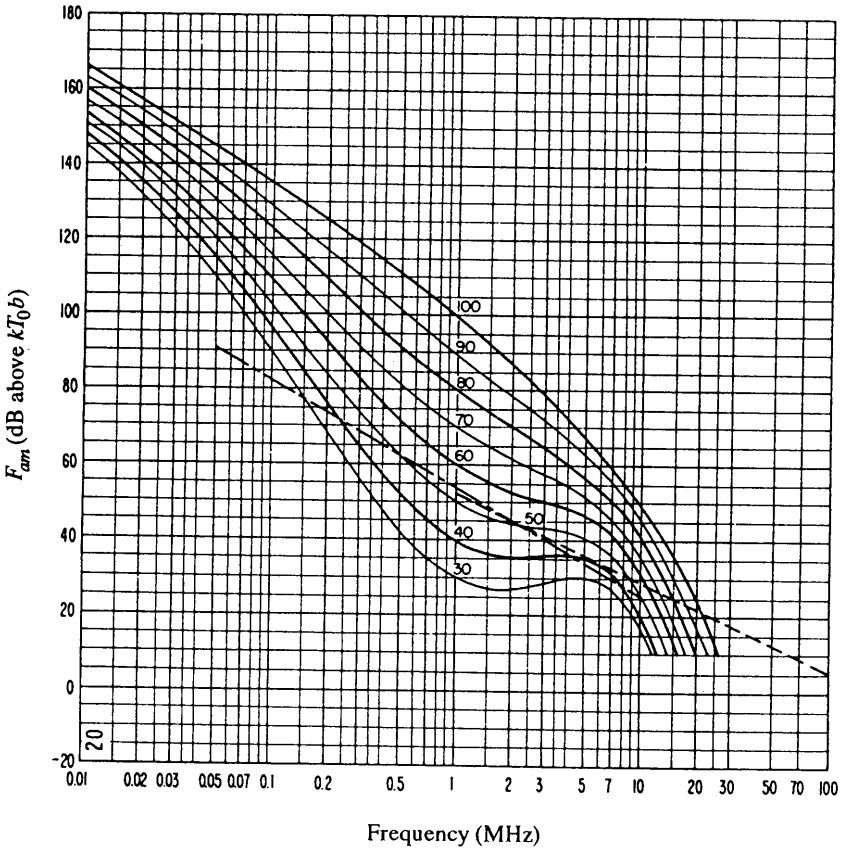

FIGURE 33b – *Variation of radio noise with frequency*
(Autumn; 0000-0400 LT)

See legend of Fig. 15b

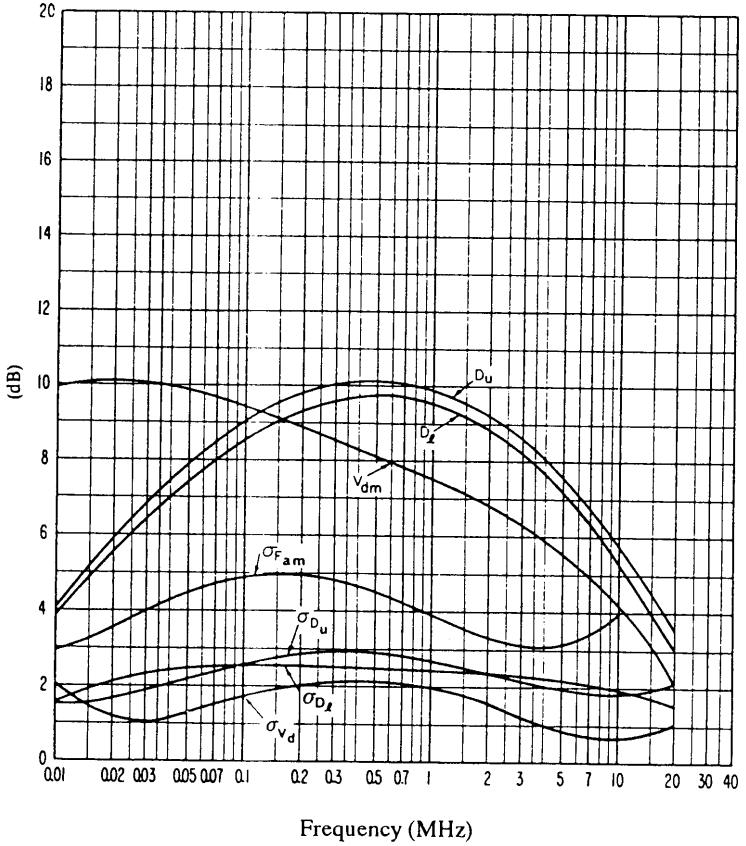

FIGURE 33c – *Data on noise variability and character*
(Autumn; 0000-0400 LT)

See legend of Fig. 15c

0372-33b

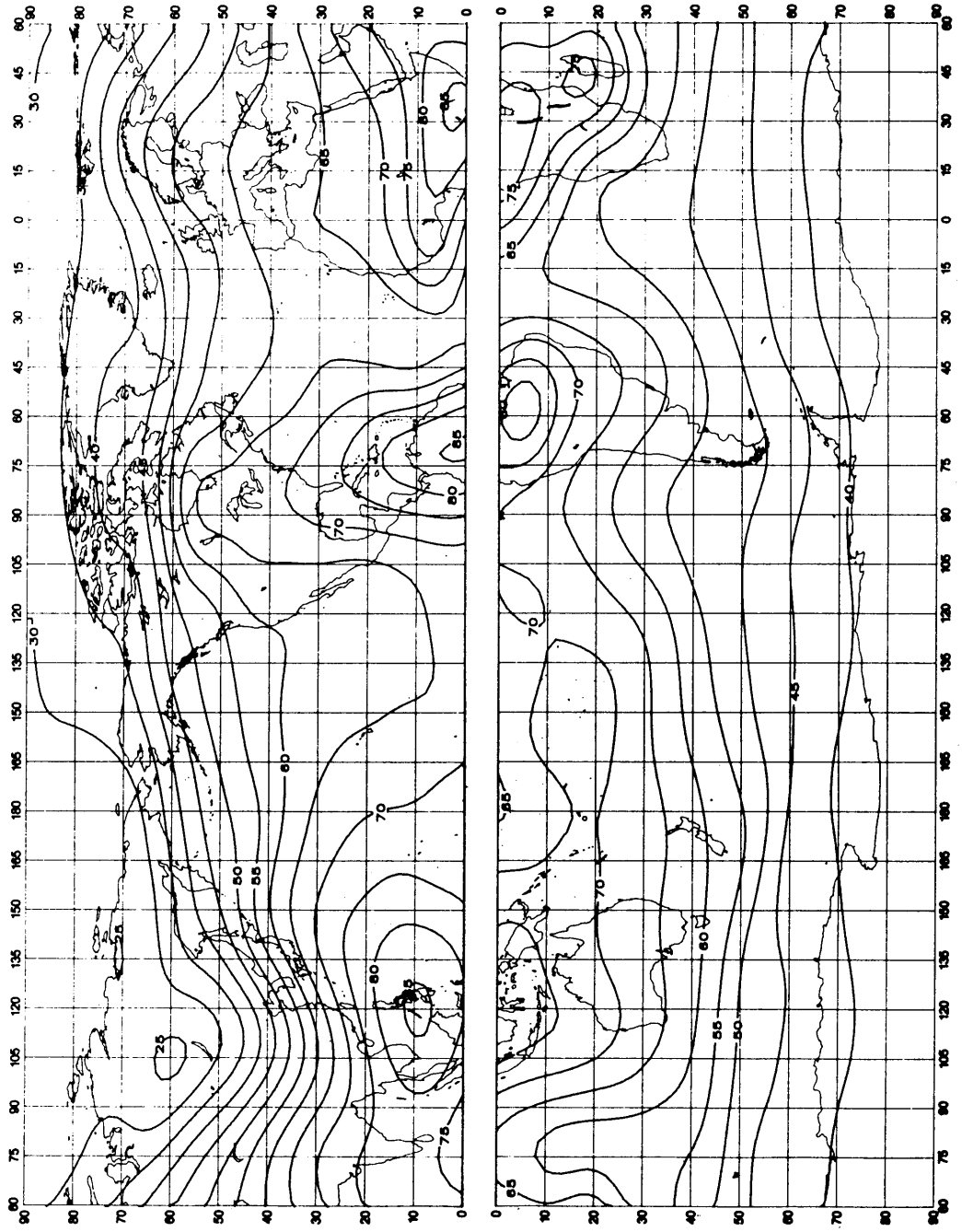

0372-34a

FIGURE 34a – *Expected values of atmospheric radio noise, F_{am} (dB above kT_0b at 1 MHz) (Autumn; 0400-0800 LT)*

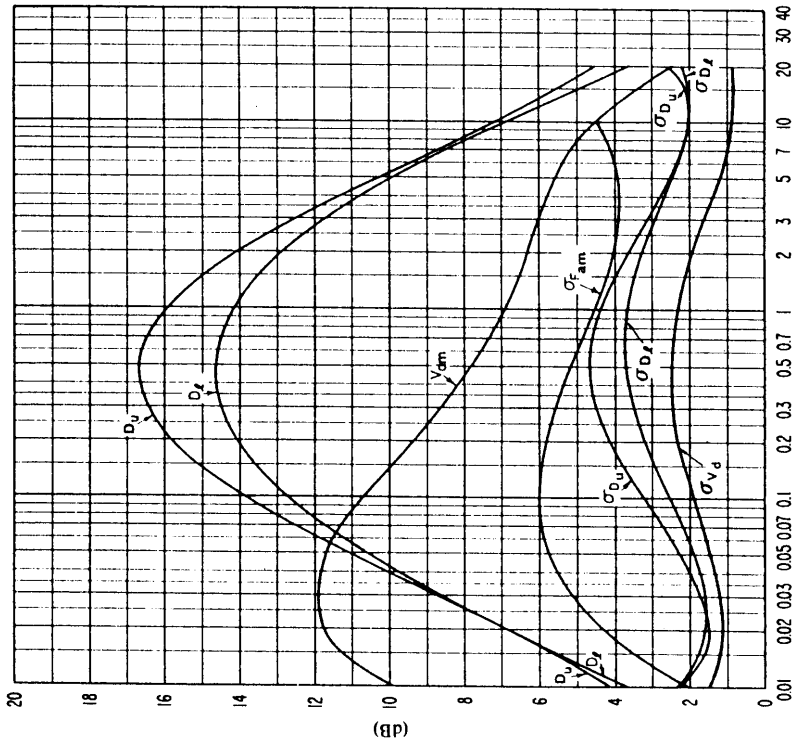

FIGURE 34c – *Data on noise variability and character*
(Autumn; 0400-0800 LT)

See legend of Fig. 15c

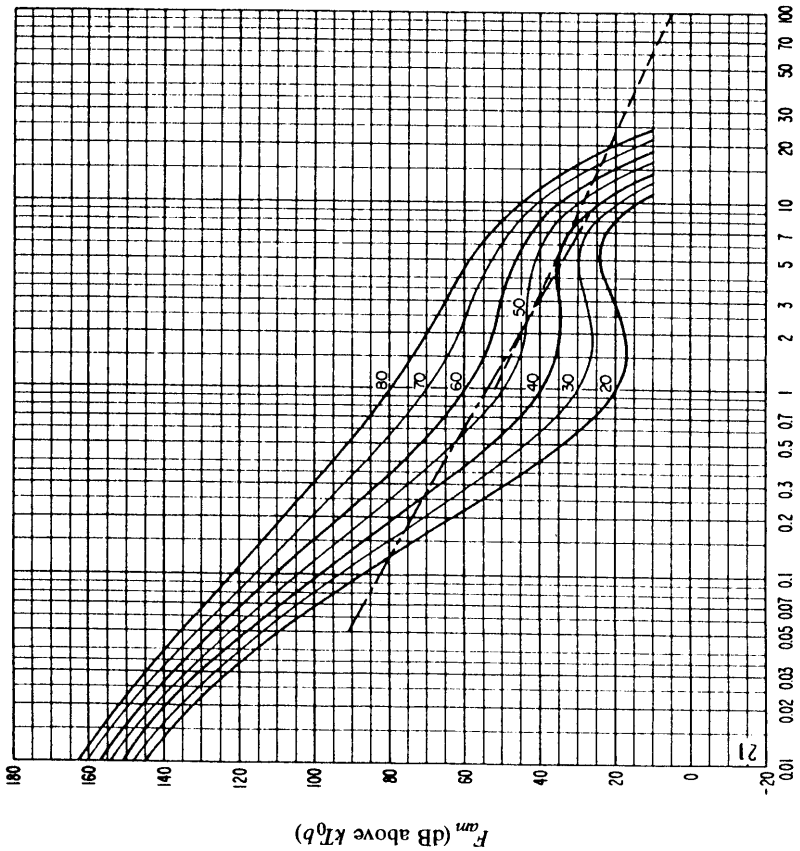

FIGURE 34b – *Variation of radio noise with frequency*
(Autumn; 0400-0800 LT)

See legend of Fig. 15b

0372-34b

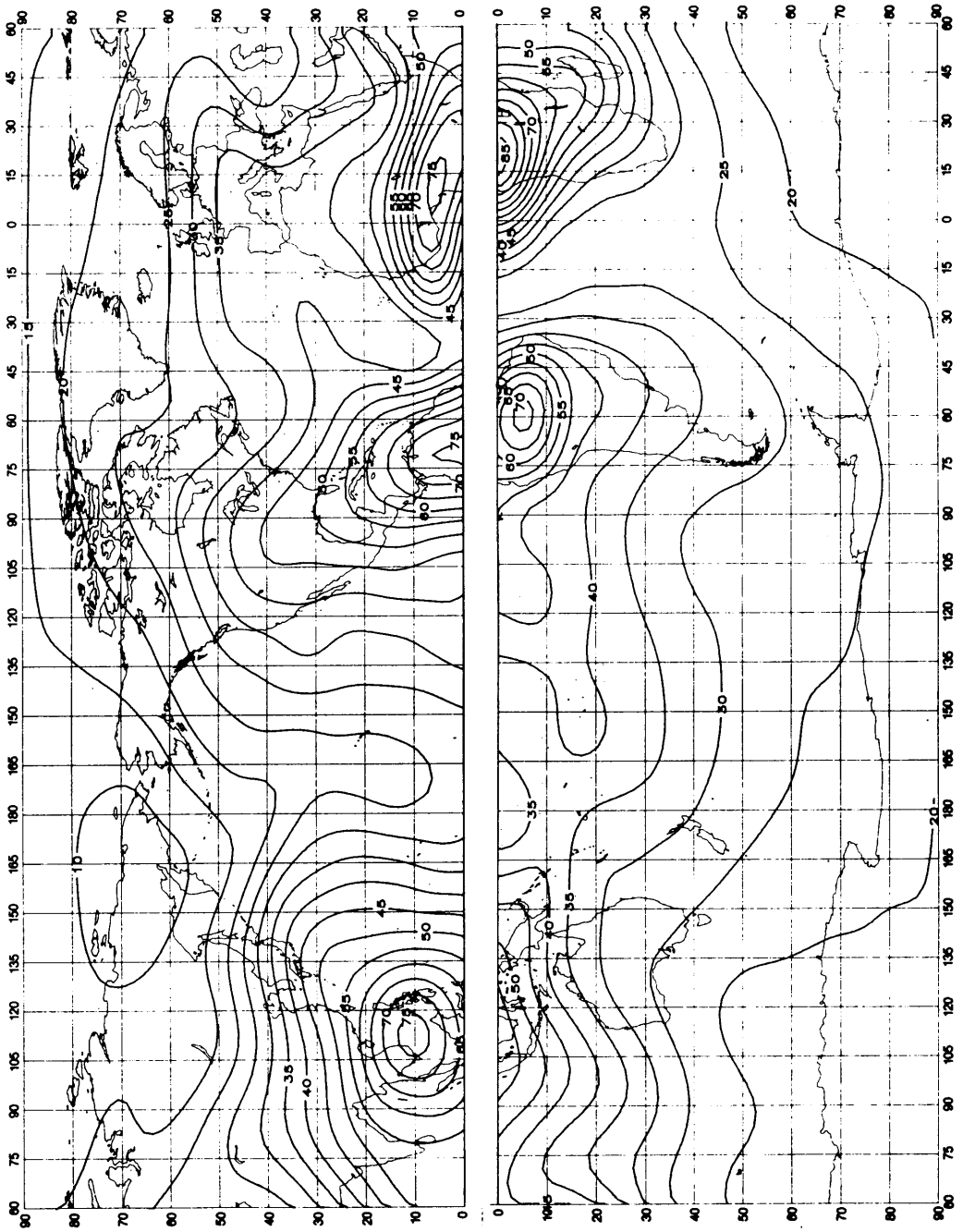

0372-35a

FIGURE 35a – *Expected values of atmospheric radio noise, F_{am} (dB above kT_0b at 1 MHz) (Autumn; 0800-1200 LT)*

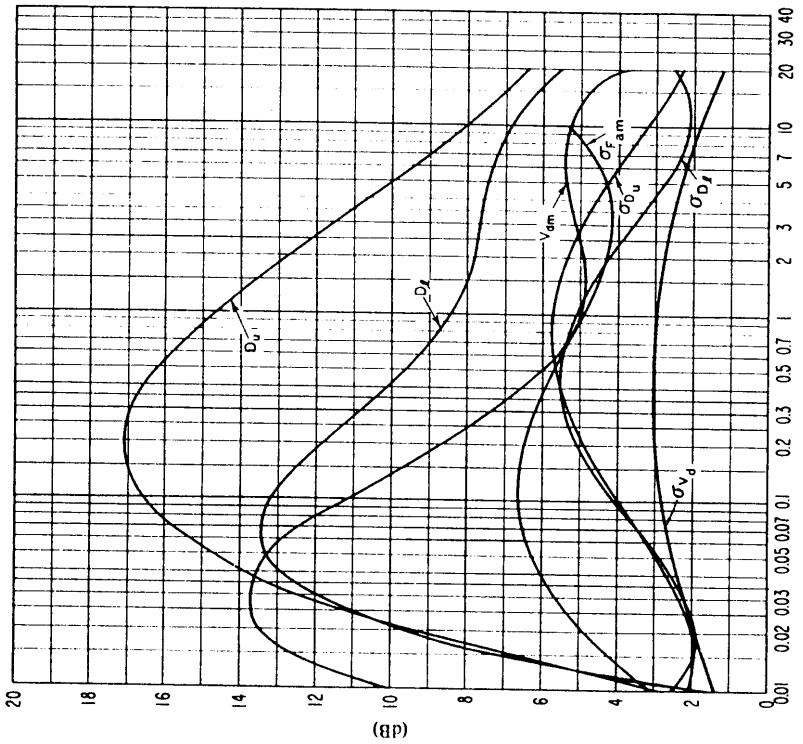

FIGURE 35c – *Data on noise variability and character (Autumn; 0800-1200 LT)*

See legend of Fig. 15c

0372-35b

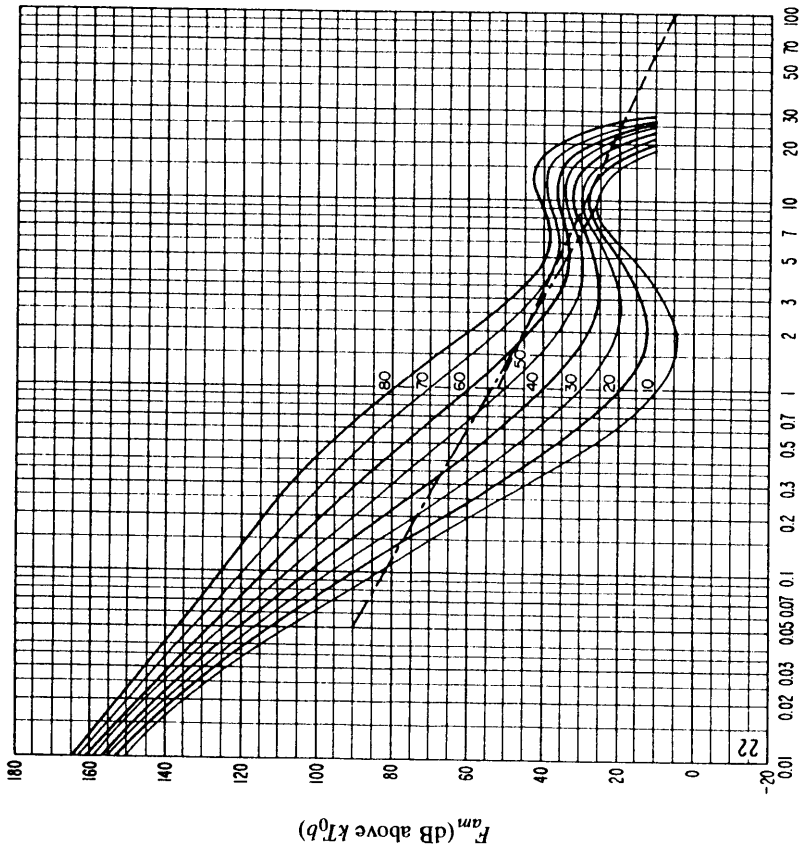

FIGURE 35b – *Variation of radio noise with frequency (Autumn; 0800-1200 LT)*

See legend of Fig. 15b

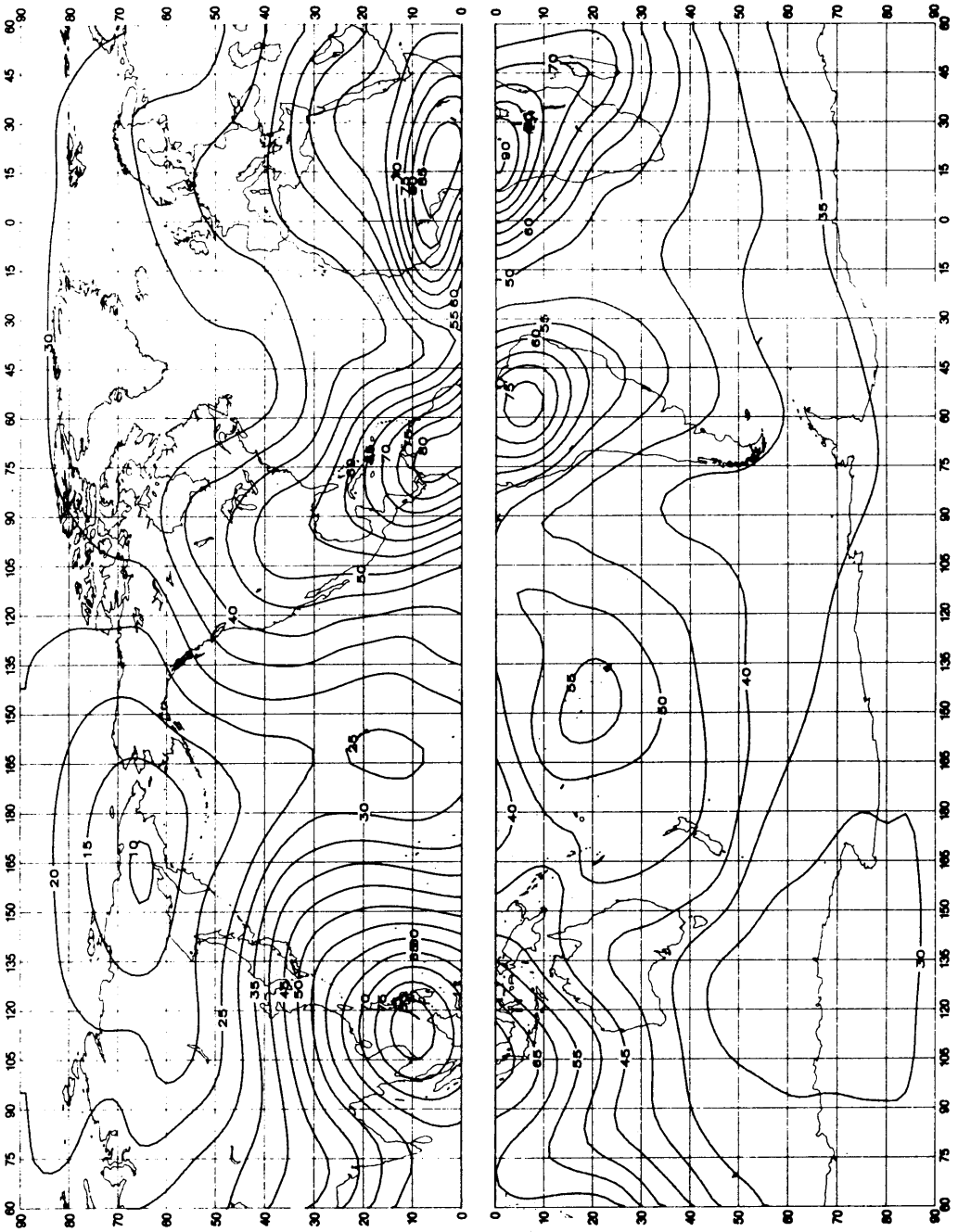

0372-36a

FIGURE 36a – *Expected values of atmospheric radio noise, F_{am} (dB above kT_0b at 1 MHz) (Autumn; 1200-1600 LT)*

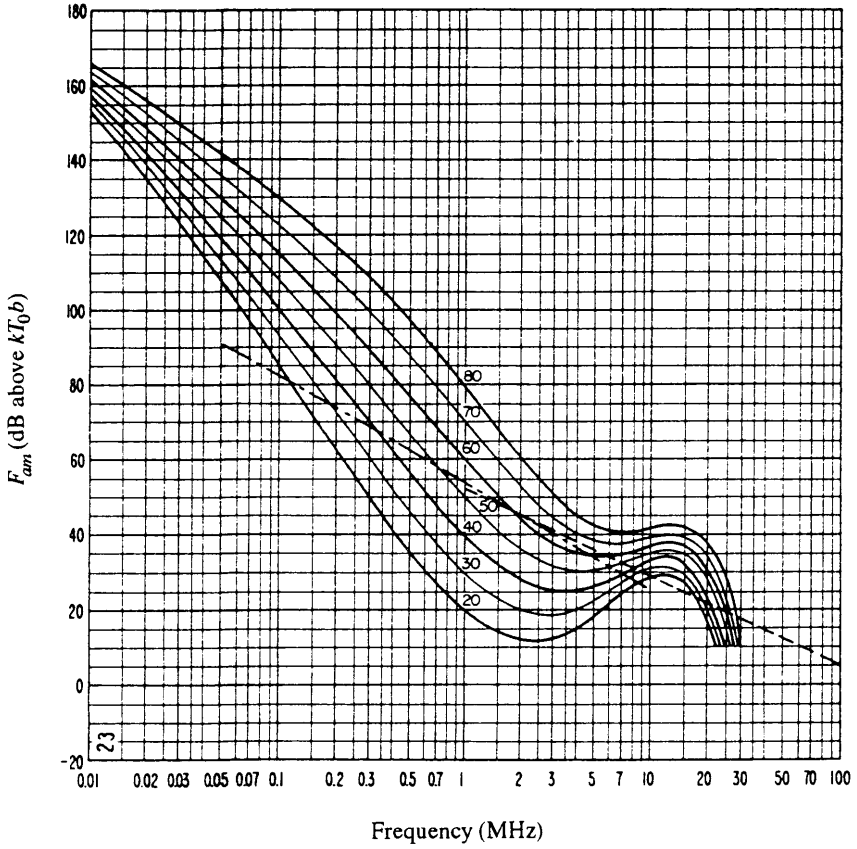

FIGURE 36b – *Variation of radio noise with frequency*
(Autumn; 1200-1600 LT)

See legend of Fig. 15b

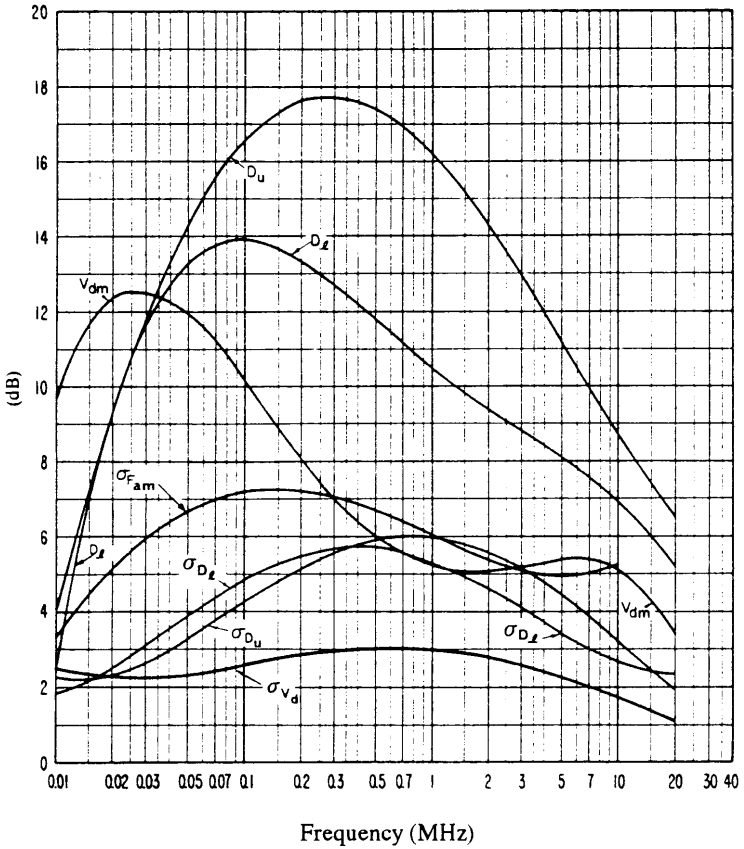

FIGURE 36c – *Data on noise variability and character*
(Autumn; 1200-1600 LT)

See legend of Fig. 15c

0372-36b

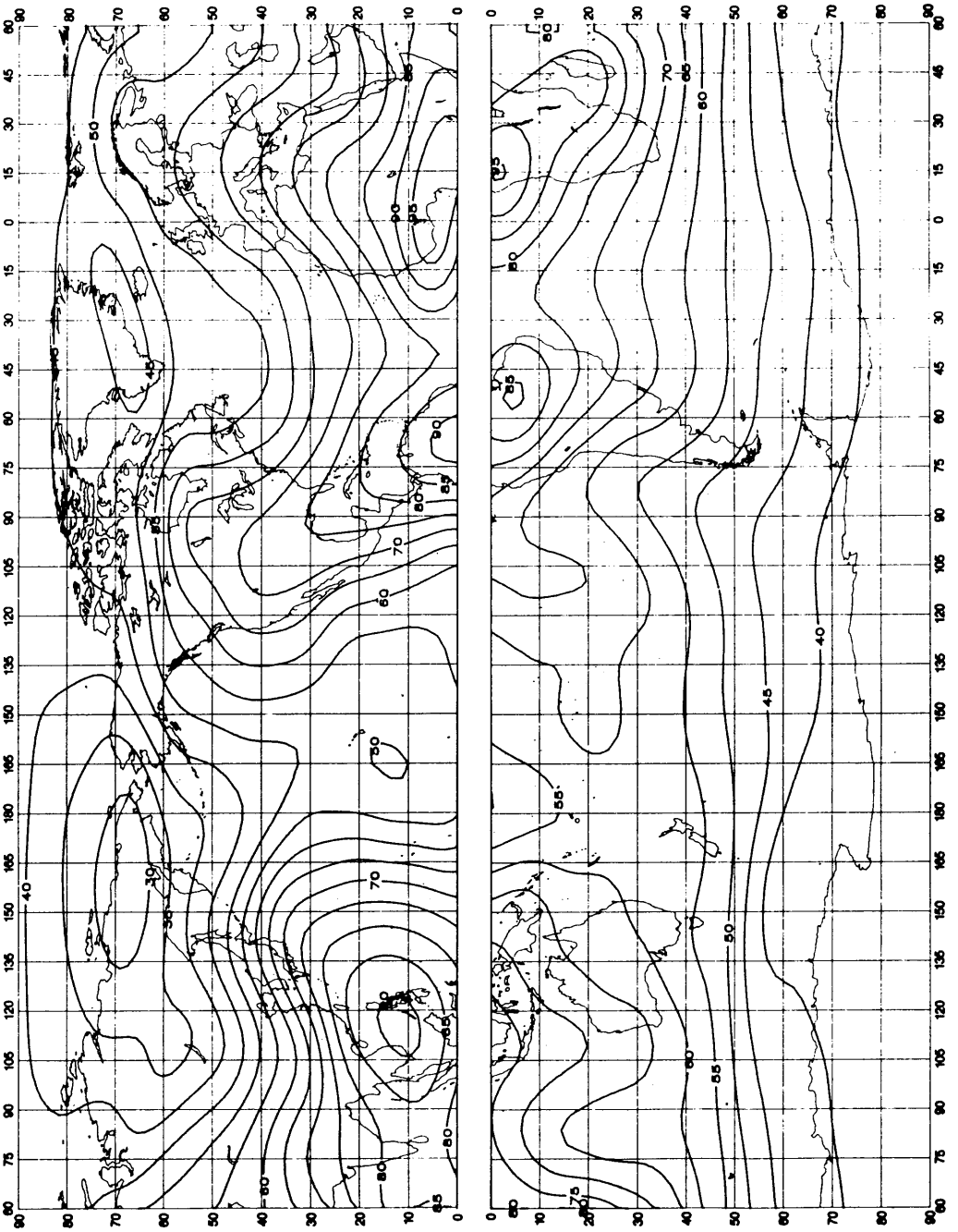

0372-37a

FIGURE 37a – *Expected values of atmospheric radio noise, F_{am} (dB above kT_0b at 1 MHz) (Autumn; 1600-2000 LT)*

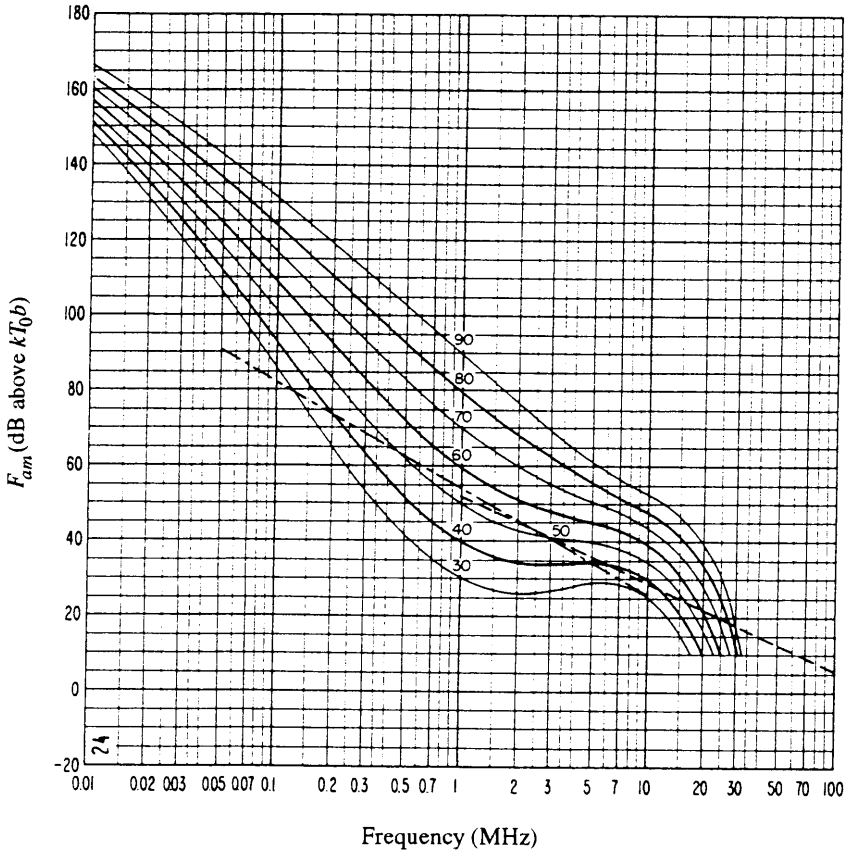

FIGURE 37b – *Variation of radio noise with frequency*
(Autumn; 1600-2000 LT)

See legend of Fig. 15b

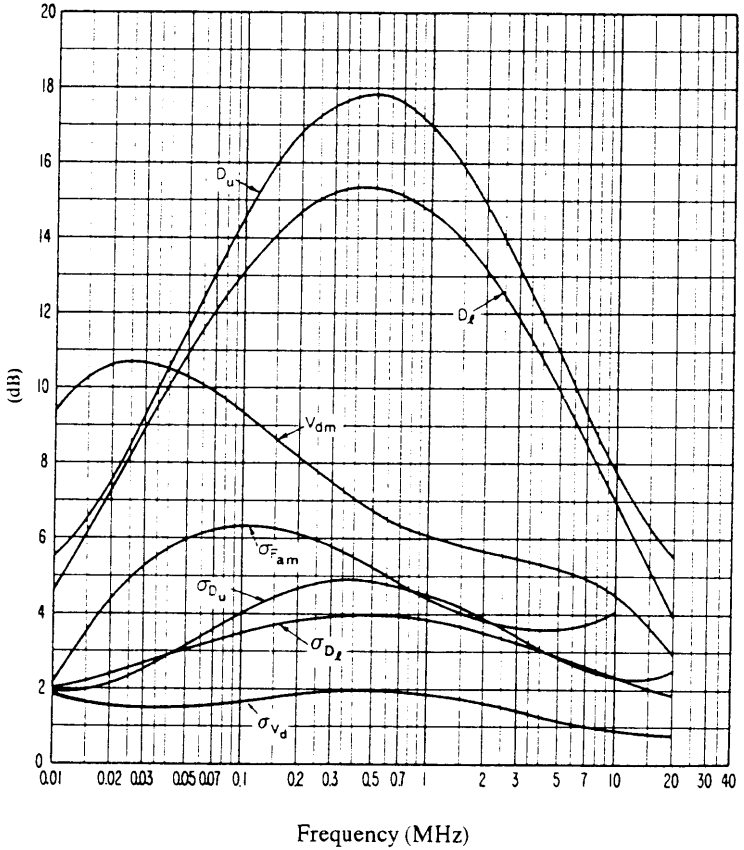

FIGURE 37c – *Data on noise variability and character*
(Autumn; 1600-2000 LT)

See legend of Fig. 15c

0372-37b

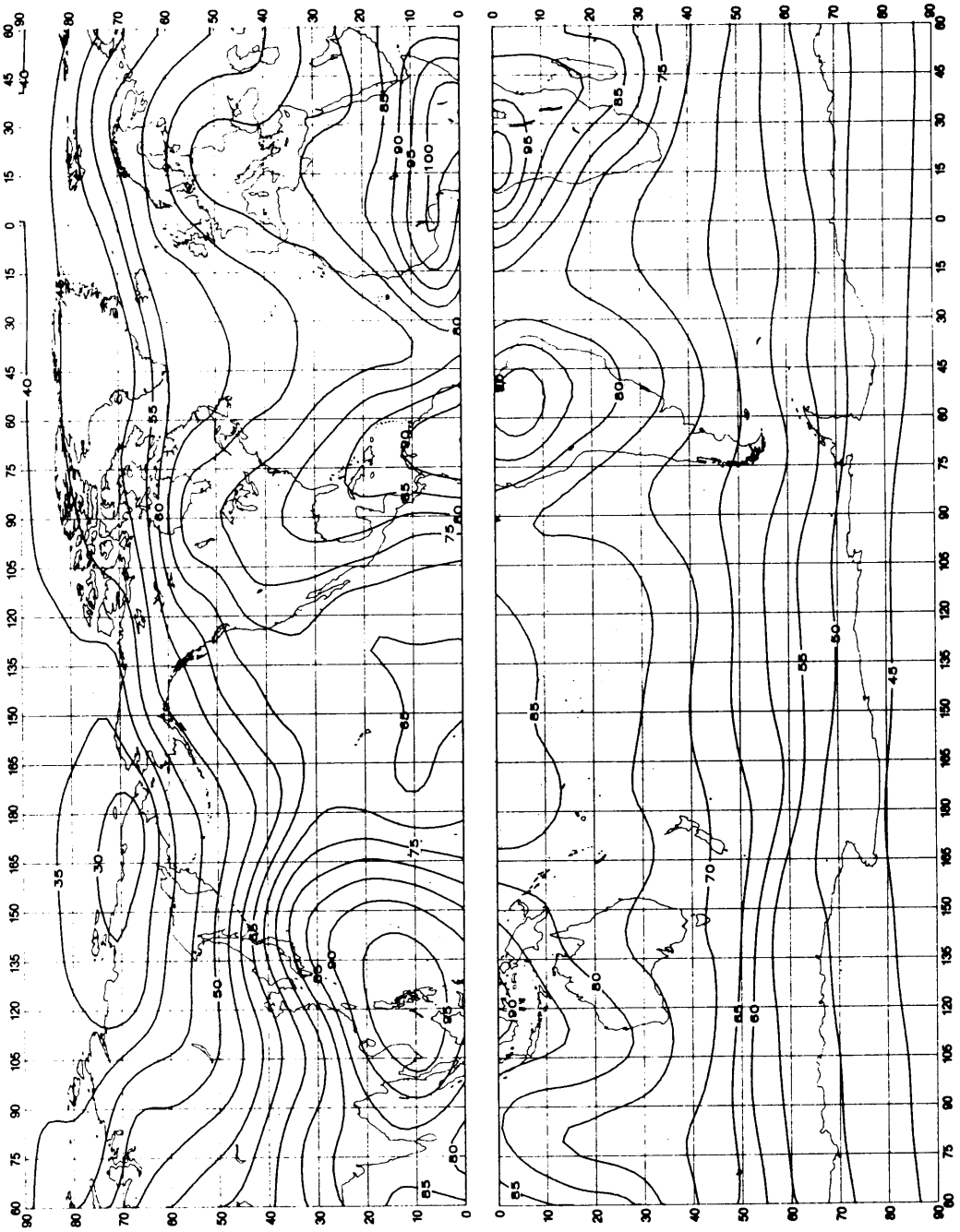

0372-38a

FIGURE 38a – *Expecied values of atmospheric radio noise, F_{am} (dB above kT_0b at 1 MHz) (Autumn; 2000-2400 LT)*

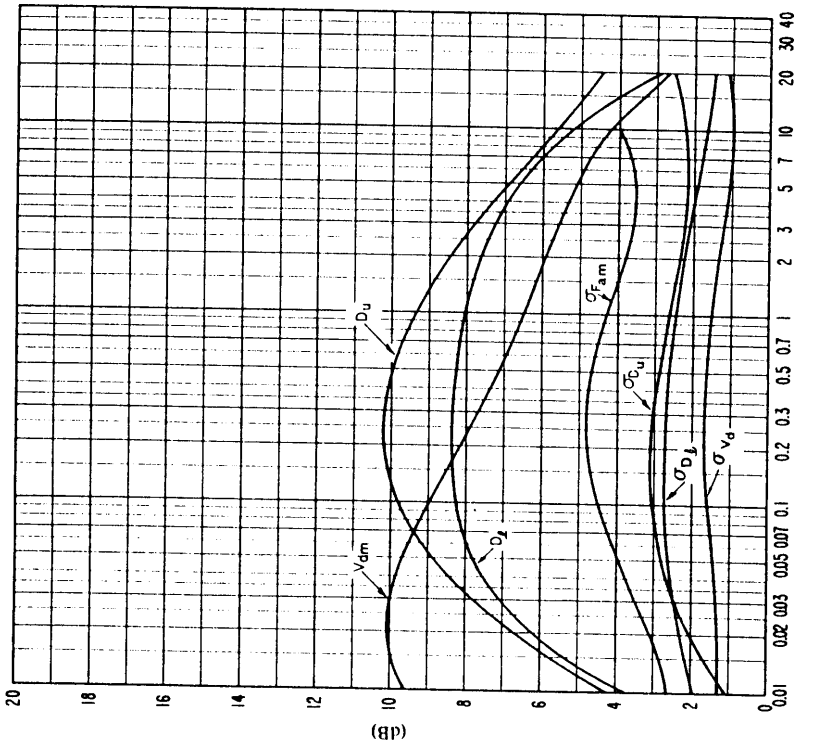

FIGURE 38c – *Data on noise variability and character (Autumn; 2000-2400 LT)*

See legend of Fig. 15c

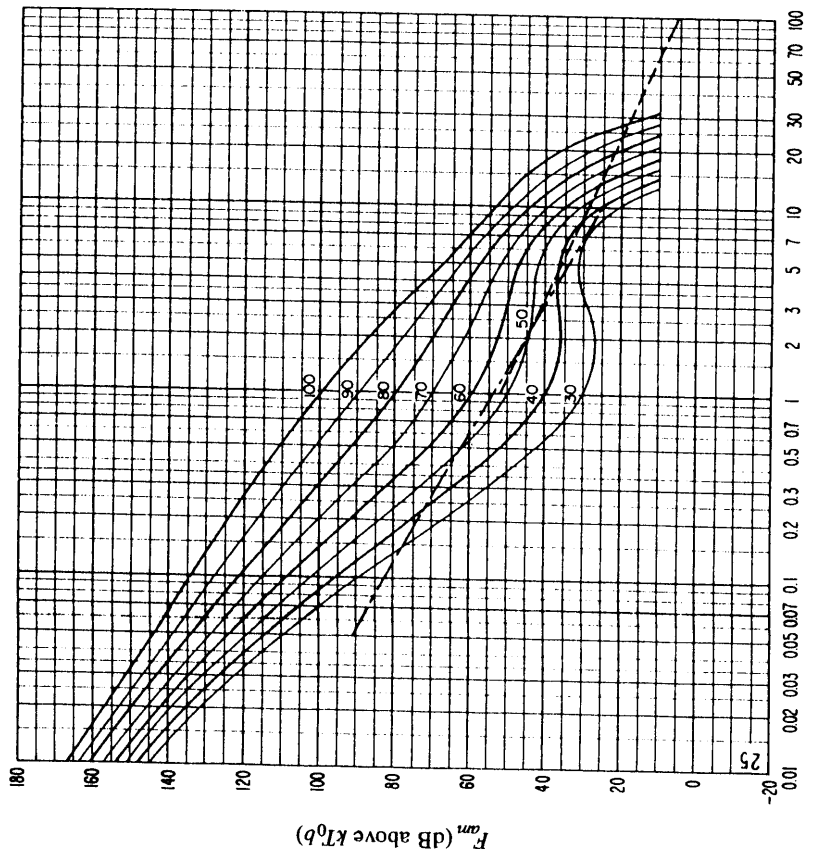

FIGURE 38b – *Variation of radio noise with frequency (Autumn; 2000-2400 LT)*

See legend of Fig. 15b

0372-38b

FIGURE 39

Amplitude probability distributions for atmospheric radio noise for various values of V_d

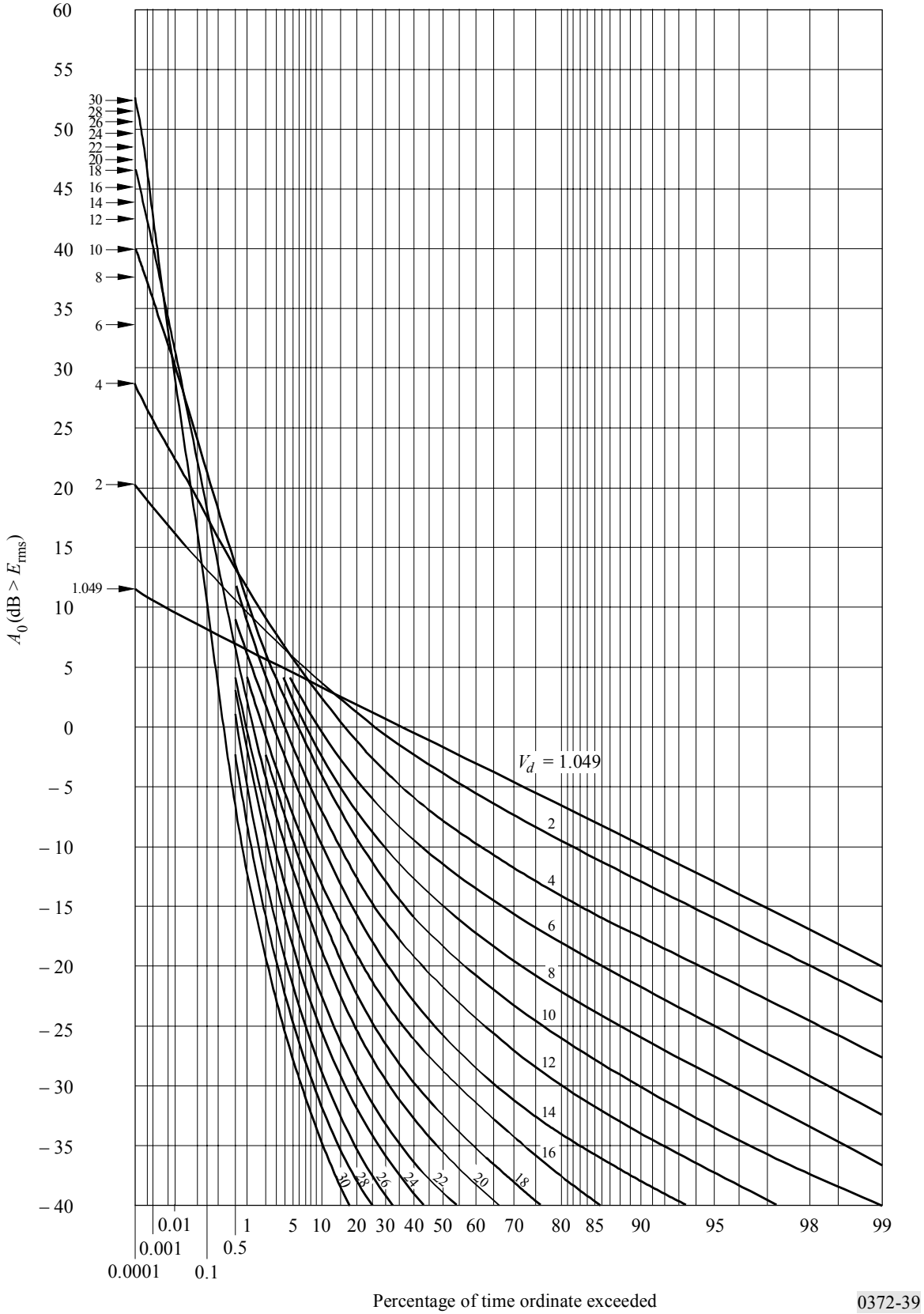

FIGURE 40

Translation of a 200 Hz bandwidth V_d, V_{dm}, to other bandwidths, b